



Task 13 Reliability and Performance of Photovoltaic Systems

S
P
V
P
S

Performance of Partially Shaded PV Generators Operated by Optimized Power Electronics

2024



What is IEA PVPS TCP?

The International Energy Agency (IEA), founded in 1974, is an autonomous body within the framework of the Organization for Economic Cooperation and Development (OECD). The Technology Collaboration Programmes (TCP) were created with a belief that the future of energy security and sustainability starts with global collaboration. The programmes are made up of six thousand experts across government, academia, and industry dedicated to advancing common research and the application of specific energy technologies.

The IEA Photovoltaic Power Systems Programme (IEA PVPS) is one of the TCPs within the IEA and was established in 1993. The mission of the programme is to “enhance the international collaborative efforts which facilitate the role of photovoltaic solar energy as a cornerstone in the transition to sustainable energy systems.” To achieve this, the programme’s participants have undertaken a variety of joint research projects in PV power systems applications. The overall programme is headed by an executive committee, comprised of one delegate from each country or organisation member, which designates distinct ‘tasks,’ that may be research projects or activity areas.

The IEA PVPS participating countries are Australia, Austria, Belgium, Canada, China, Denmark, Finland, France, Germany, Israel, Italy, Japan, Korea, Malaysia, Morocco, the Netherlands, Norway, Portugal, South Africa, Spain, Sweden, Switzerland, Thailand, Turkiye, and the United States of America. The European Commission, Solar Power Europe, the Solar Energy Research Institute of Singapore and Enercity SA are also members.

Visit us at: www.iea-pvps.org

What is IEA PVPS Task 13?

Within the framework of IEA PVPS, Task 13 aims to provide support to market actors working to improve the operation, the reliability and the quality of PV components and systems. Operational data from PV systems in different climate zones compiled within the project will help provide the basis for estimates of the current situation regarding PV reliability and performance.

The general setting of Task 13 provides a common platform to summarize and report on technical aspects affecting the quality, performance, reliability, and lifetime of PV systems in a wide variety of environments and applications. By working together across national boundaries, we can all take advantage of research and experience from each member country and combine and integrate this knowledge into valuable summaries of best practices and methods for ensuring PV systems perform optimally and continue to provide competitive return on investment.

Task 13 has so far managed to create the right framework for the calculations of various parameters that can give an indication of the quality of PV components and systems. The framework is now in place and can be used by the PV industry who has expressed appreciation towards the results included in the high-quality reports.

The IEA PVPS countries participating in Task 13 are Australia, Austria, Belgium, Canada, Chile, China, Denmark, Finland, France, Germany, Israel, Italy, Japan, the Netherlands, Norway, Spain, Sweden, Switzerland, Thailand, and the United States of America. The Solar Energy Research Institute of Singapore is also a participating member.

DISCLAIMER

The IEA PVPS TCP is organised under the auspices of the International Energy Agency (IEA) but is functionally and legally autonomous. Views, findings, and publications of the IEA PVPS TCP do not necessarily represent the views or policies of the IEA Secretariat or its individual member countries.

COVER PICTURE

Single-Family House in Dettingen, close to Konstanz, Germany (photo by Franz Baumgartner).

ISBN 978-3-907281-64-2: Performance of partial shaded PV generators operated by optimized power electronics

INTERNATIONAL ENERGY AGENCY
PHOTOVOLTAIC POWER SYSTEMS PROGRAMME

IEA PVPS Task 13
Reliability and Performance
of Photovoltaic Systems

**Performance of Partially Shaded PV Generators
Operated by Optimized Power Electronics**

Report IEA-PVPS T13-27:2024
November 2024

ISBN 978-3-907281-64-2



Authors

Main Authors

Franz Baumgartner, ZHAW Zurich University of Applied Sciences, Switzerland

Cyril Allenspach, ZHAW Zurich University of Applied Sciences, Switzerland

Contributing Authors

Ebrar Özkalay, SUPSI PVLab, Mendrisio, Switzerland

Matthew Berwind, Fraunhofer ISE, Freiburg, Germany

Anna Heimsath, Fraunhofer ISE, Freiburg, Germany

Christof Bucher, BFH, Burgdorf, Switzerland

David Joss, BFH, Burgdorf, Switzerland

Sara Mirbagheri Golroodbari, University Utrecht, The Netherlands

Wilfried van Sark, University Utrecht, The Netherlands

Alexander Granlund, RISE Research Institutes of Sweden, Sweden

Felipe Valencia Arroyave, ATAMOSTEC and Universidad Austral de Chile

Roland Bründlinger, AIT Austrian Institute of Technology, Vienna, Austria

Werner Herrmann, TÜV Rheinland, Cologne, Germany

Bert Herteleer, KU Leuven, ELECTA, Ghent, Belgium

Editor

Ulrike Jahn, Fraunhofer CSP, Halle, Germany



Table of Contents

Acknowledgements	7
List of Abbreviations	8
Executive Summary	9
1 Introduction	11
2 Shaded PV Systems and Power Electronics	13
2.1 Shaded PV Modules	13
2.2 Shading Tolerant PV Modules	14
2.3 String Inverter (SINV) Systems	17
2.4 Module-level Power Electronic (MLPE) Systems	18
2.5 Typical Shading Cases	21
3 Indoor Measurement Results	25
3.1 DC/AC String Inverter Efficiency	25
3.2 DC/AC Module Inverter	27
3.3 DC/DC Power Optimisers	27
3.4 DC/DC/AC System	31
3.5 Transient Power Electronic Measurement	32
4 Outdoor Measurement Results	38
4.1 Testing Set-up MLPE	38
4.2 Testing Set-up Shading Tolerant PV Modules	38
4.3 Shading with Single-axis Trackers in the MW Power Plant	41
5 Annual Simulations and Performance	43
5.1 Commercial Simulation Tools	43
5.2 ZHAW PVshade Simulations	43
5.3 Zenit Fraunhofer ISE Simulations	46
5.4 Simulation of Shading Tolerant Modules	48
6 Advantages and Disadvantages of MLPE Systems	50
6.1 Lifetime and Failure	50
6.2 System Costs and LCOE	52
6.3 Shading Induced Hotspot Effect	52
6.4 Safety and Hazards	54
6.5 Electromagnetic Emissions and Compatibility	57
7 Recommendations for PV Installers	59



7.1 Systems by Severity of Shading..... 59

7.2 Orientation and String-length Considerations 66

7.3 Improvement of One-axis Tracking 66

8 Conclusion 68

References 70

Appendix..... 76



Acknowledgements

This paper received valuable contributions from several IEA-PVPS Task 13 members and other international experts. Many thanks to:

The main authors would like to thank the colleagues who contributed mainly to the content of the following chapters to the group discussion:

Chap. 2.5 Ebrar Özkalay and Team of SUPSI PVLab, Switzerland

Chap. 4.3 and 5.4 Sara Mirbagheri Golroodbari and Wilfried van Sark, University Utrecht, The Netherlands

Chap. 4.4 and 7.3 Felipe Valencia Arroyave, ATAMOSTEC and Universidad Austral de Chile

Chap. 5.3 Matthew Berwind and Anna Heimsath, Fraunhofer ISE, Freiburg, Germany

Chap. 6.1 and 6.4 Christof Bucher and David Joss, BFH, Burgdorf, Switzerland

Chap. 6.5 Alexander Granlund, RISE Research Institutes of Sweden, Sweden

Many thanks to Werner Hermann and Bert Herteleer for the full document review with invaluable feedback.

The support of the work at the ZHAW by the Swiss Federal Office of Energy, Switzerland for the funded projects EFPVShade under contract no. SI/502247-01 2021 to 2022 and WebPVshade under contract no. SH/8100380-02-01-46 started in 2023 was an important key to the preparation of the chapters 3, 5.2 and 7.1 of this report.

For chapters 4.3 and 7.3, the support provided by the CORFO Technology Program 17PTECES-75830 ATAMOSTEC and the Centro de Desarrollo Energetico (CDEA), Universidad de Antofagasta, for facilitating the Labctur facilities to test our technology developments was highly appreciated.

This report is supported by the German Federal Ministry for Economic Affairs and Climate Action (BMWK) under contract no. 03EE1120B.



List of Abbreviations

IEA	International Energy Agency
PV	Photovoltaic
DB	Bypass Device
SI	Shading Index
SAE	Shading Adaption Efficiency
MPP	Maximum Power Point
DC/DC	Direct Current to Direct Current
DC/AC	Direct Current to Alternating Current
DC/DC/AC	Direct Current to Direct Current to Alternating Current
SINV	String Inverter
multistring-inverter	Converts each string with a single MPP tracker and finally to AC power
micro-inverter	Converts the DC power of one or very few PV modules into AC power
MLPE	Module Level Power Electronics
allMLPE	MLPE's for all elements of the PV generator in the string
indMLPE	Independent MLPE's placed at the most shaded elements in the string
hotspot	Localized heating within a PV module
hotspot-free	No localized heating will occur in such a PV module
PVshad	Simulation tool for performance analysis of shaded PV plants from ZHAW



Executive Summary

Inhomogeneous shading on the PV generator leads to disproportionately high losses. As the potential of PV generation on roofs or façades is to be increasingly utilised in the coming decades, these cases will occur more frequently. The aim here is to provide an overview of the challenges and state-of-the-art technical solutions for partial shading. Current developments in PV engineering show that maximum performance lies in the combination between optimised module placement, the use of modules that are tolerant of shading and optimised power electronics.

Shortly after the discovery of the solar cell, blocking or bypass diodes were used to solve the inhomogeneous currents of groups of solar cells arranged in series or parallel wiring. Even today, they are still the most efficient and robust solution for the majority of common shading PV applications.

Due to the very high rated outputs of the solar modules and the presence of only three bypass diodes, high temperatures can occur on a locally shaded solar cell. This forces heat outputs of up to 200W or 100W in the butterfly module connection through the associated activated bypass diode, which must be dissipated by the most shaded cell. If additional small-area defects occur in this affected solar cell, hotspot peak temperatures can occur, which can lead to permanent damage to the module or the risk of fire.

However, in order to prevent a third of the module output being lost in this case, four or more bypass diodes are now used in so-called shadow-tolerant PV modules. With a higher number of bypass diodes per module area, it is also possible to selectively bypass smaller, less efficient areas of the module, which leads to an increase in the module yield. The hotspot effects can also be comprehensively and robustly prevented by the small number of solar cells per bypass diode, provided the bypass diode is properly designed. The first manufacturers are beginning to place these shade-tolerant PV modules on the markets.

Today, planners can also select different power electronics systems for the next step in system integration towards grid feed-in, i.e. the connection of the individual modules in the string. This is the classic series connection of all modules in the string to the input of the DC/AC string inverter (SINV), which leads to the highest yields for weak and medium shading. This applies, for example, to light shading with a chimney or a ventilation pipe, where no more than one tenth of the modules in the string are reached by the shade at the same time during the six hours around midday, even when using standard modules with only three bypass diodes. (see Table 1)

With medium to heavy shading, the widely used DC/DC converters directly on the PV module (MLPE), often also called power optimisers, can be used profitably. However, the combination of shade-tolerant PV modules with conventional SINVs can often deliver comparable annual yields. However, if the optimisers are also used behind each module even with weak shading (allMLPE), they deliver less yield in total than the simple SINV, as their own DC/DC losses then have a negative impact compared to simple connectors. This only becomes apparent if the MLPE manufacturers' data sheet claims of 99% efficiency are not viable. The published measurements carried out in independent laboratories over the last four years are listed in this report, which suggest that losses are around 2% higher.

As the differences in yield between the power electronics variants SINV and MLPE are usually less than four per cent in annual yield for light to medium shading, the above-mentioned real MLPE efficiency at the specific operating points plays the decisive role in planning the most efficient system. However, as the commercial PV software planning tools currently use these MLPE manufacturer specifications which are over estimated, no meaningful system comparison can be expected for these shading categories. In this report the results of annual simulations performed by some sophisticated simulation tools that take these real MLPE losses into account are discussed.



Table 1: Comparison of annual electrical performance of PV system variants are given in terms of different degrees of shading and PV module types, standard modules with three bypass diodes or more and the choice of power electronics like SINV or indMLPE or allMLPE while + indicates better – less performance with 0 for no gains in performance expected.

Shading Scenarios			PV Module	Power Electronic Systems		
Shading degree	Objects	Modules affected	Type	SINV	indMLPE	allMLPE
Weak		<10%	Standard	+	+	-
			4+ Bypass diode	+	+	-
Medium		>10% and <40%	Standard	0	+	+
			4+ Bypass diode	+	+	+
Strong	Buildings, trees	>40%	Standard	-	0	+
			4+ Bypass diode	0	+	+

If there is very heavy shading in the system, so that more than 40% of the PV modules are shaded at the same time, e.g. by nearby neighbouring buildings or large trees, or if there are solar modules that have different orientations, and the strings are too short to use multi-string SINV, the allMLPE remains the most efficient system variant. It is also worth keeping an eye on future developments in power electronics, which may offer string inverters with more multi-string inputs. It could be helpful if shadow-tolerant PV modules that offer a higher DC voltage than today's standard modules come onto the market, so that the DC/DC boost converter internal to the SINV can be dispensed with and efficiency increased.

The long-term stability of the power electronics itself is also a highly relevant parameter to avoid expensive labour costs in the event of servicing, e.g. directly on the roof, when replacing the MLPE, which could possibly be more frequent due to the higher operating temperatures. PV designers can increase the annual yield by increasing the distance from the PV module to the shading object when using a SINV, without having to use an MLPE, which is one of the recommendations in the report.



1 Introduction

The share of solar energy in the total electricity generation and the density of photovoltaic modules on roofs and façades is growing worldwide. Planners often choose mounting locations for photovoltaic modules with considerable shading if they also want to maximize the use of solar energy in the building. At the same time, they are helped by the fact that the use of individual power electronics components at module level, Module Level Power Electronic (MLPE), has become very popular on the market in the last decade. MLPE promise more electrical yield and at the same time allow more details in the monitoring of individual PV modules. Thus by the use of this high-tech components, the current yield of each solar module on the roof is presented to the homeowner via a web tool, which is also very sales-promoting. End customers are happy to accept the slightly higher price compared to conventional string inverters (SINV) when they are told that these optimisers at module voltage level always enable maximum solar power production, even when there is shade. As a result, MLPE solutions have even become the market leader in the single-family house segment in some countries. At a trade fair in June 2024, a leading manufacturer reported over 126 million power optimisers delivered worldwide. They also offer protective functions in the event of a fault, e.g. if arcing occurs or higher temperature is sensed at the MLPE connector cables, the voltages are reduced to almost marginal values at the level of each individual module, thus avoiding any danger to persons. The manufacturers of MLPE components have thus been able to successfully build up stock market valuations in the billions, which also include the module inverters that have been known for some time, i.e. DC/AC converters and not DC/DC converters like the conventional MLPE.

However, do the marketing promises made by MLPE manufacturers and certain planners stand up to the facts that they always deliver the maximum yield and are therefore indispensable even for the smallest amount of shading?

When experts get to the bottom of this question, they find that MLPE manufacturers often only provide one or two efficiency figures in the data sheets, and some even refrain from declaring the efficiency of these power electronics components. Other experts, such as PV planners try to obtain solutions from commercial PV planning tools, all of which have precisely implemented this meagre data sheet information from the manufacturers. In the technical literature, there is a first publication from an independent research laboratory from 2010 on the indoor efficiency measurement of an MLPE DC/DC converter in the approved operating range. Over the past four years, the ZHAW has carried out a wide range of measurements on commercial MLPE in the indoor laboratory and published them as an independent research institute [3]. These results clearly show that the MLPE manufacturers specify weighted efficiencies exclusively at the optimum operating point, which, however, can certainly not be run in the annual cycle and is therefore not meaningful [14]. To assess the economic efficiency of decentralized power electronics components, researchers at NREL have produced an initial technical report, including annual simulations [2].

There are recognizable parallels to what the manufacturers of string inverters did two decades ago. At that time, they only published the highest efficiencies on their data sheets, but these only applied to a specific DC voltage and not to the entire permissible voltage window of the inverter. Deviations of up to three percent were the result. At that time, it also took years for the market, customers and planners to demand this data from manufacturers via the competition, then the standardization bodies followed suit by updating their documents [4].

But how can these differences in the annual yield of a given roof situation be precisely determined for the different PV power electronics systems commonly used today? In the systems, a distinction must be made between the conventional PV modules connected in series, which feed the input of the string inverter (SINV), and the use of MLPEs behind each PV module (all MLPE) or only for the PV modules



that are most heavily shaded (indMLPE). For this purpose, the exact loss models of these power electronics components must first be known to be integrated into an annual simulation. There are many powerful tools on the market for calculating shading ratios. However, they must have a high resolution, both locally, for each sub-cell in the module and with a temporal simulation interval of less than one hour, as the shadows often move more quickly across the individual cells.

Of course, every shading situation is different, just as the roofs and neighbouring buildings and shading objects can differ. If you want to measure each individual shading situation precisely, this requires much more effort, which quickly exceeds the conventional total plant planning time budgets, as higher measurement accuracies are required for shading in the immediate vicinity.

One method for comparing the annual performance is therefore based on the precise analysis of different typical shading situations, such as a pitched roof with a chimney, or with a dormer or with a ventilation pipe, or with combinations of these elements. This report presents the published work of this in journal papers, conference papers or student work, which also includes the loss models of the MLPEs measured in the laboratory. They show yield differences of mostly less than three percent with medium to slight shading. The distance between the PV modules and the shading object, such as a dormer, is also an important parameter for efficient PV planning. MLPE solutions are more efficient for strong shading or differently aligned solar modules. However, if new shade-tolerant solar modules are used in conjunction with conventional string inverters, each with the same orientation in a string, these solutions can also match MLPEs.

The discussion of the outdoor measurements, usually in the comparison of two different PV system variants, SINV versus MLPE, cannot be realised satisfactorily due to the unavailable accuracy of the measurements. The reason are the uncertainties of the nominal power of the modules, the wind and temperature conditions, or the unrealistic choice of the shading object or the number of modules in the string or the efficiency of the power electronics components used are themselves critically scrutinized. Nevertheless, they can help to narrow down the range of yield differences to invalidate the speculative figures from MLPE marketing, which usually show double-digit annual yield differences.

For the annual yield, the questions of MPP tracking by the MLPs or the SINV with partial shading are also important. Measurements of commercial MLPE components show good MPP tracking of less than one minute settling time when starting up in the morning. However, even in laboratory tests in conjunction with other optimisers and communication with the inverter, they usually fail to find the MPP as an absolute MPP at high current and low module voltage, which unnecessarily limits the maximum annual yield.

On the research side, new complex power electronics integrated in the module have been investigated, which comprise one or only a few solar cells per power electronics component, which are also briefly presented here. Shade tolerant PV modules could also have yield advantages for utility scale power plants, as some researchers have recently suggested [5]. This concerns shading by the front row or the neighbouring tracker in horizontal mechanical solar trackers.

The dominant question regarding the economic efficiency of the different PV system variants SINV, MLPE or SINV with shade-tolerant modules must in any case also consider the history of the probability of failure of the power electronics at these high temperatures on the roof as well as the costs for the craftsmen when replacing the modules. More realistic, independently determined data and facts of total cost of installation and typical operation and service costs of MLPE versus SINV solutions are expected to be published in the near future.



2 Shaded PV Systems and Power Electronics

2.1 Shaded PV Modules

Shading may change solar cell current by a few tens of percent and voltage by only a few percent. Therefore, the solar cells in the PV generator would have to be connected in parallel, but this is ruled out because of the module currents of a few 100 amps if all cells are in parallel. Consequently, over the last half century, PV modules have been produced primarily as a series connection of solar cells. In principle, other causes of different currents can also occur such as manufacturing tolerances, microcracks or different local semiconductor or optical losses, but also different contact resistances over the operating time can generally lead to differences in the current/voltage characteristics of the same cell type.

The unequal module currents in the series connection are commonly bridged by Bypass Devices (BD) - see Figure 1. Robust diodes, single FET's or elaborate DC/DC converters are used as BD. Low number of cells in a string protected by a BD leads to less power losses e.g., at partial shading and lower hotspot temperatures in the solar cell which is operated in the string not as a generator anymore [69]. However, very low numbers of solar cells connected in series (Figure 6) can lead to additional losses if the forward voltage of the BD is too high and several such sectors have an activated BD [6,7].

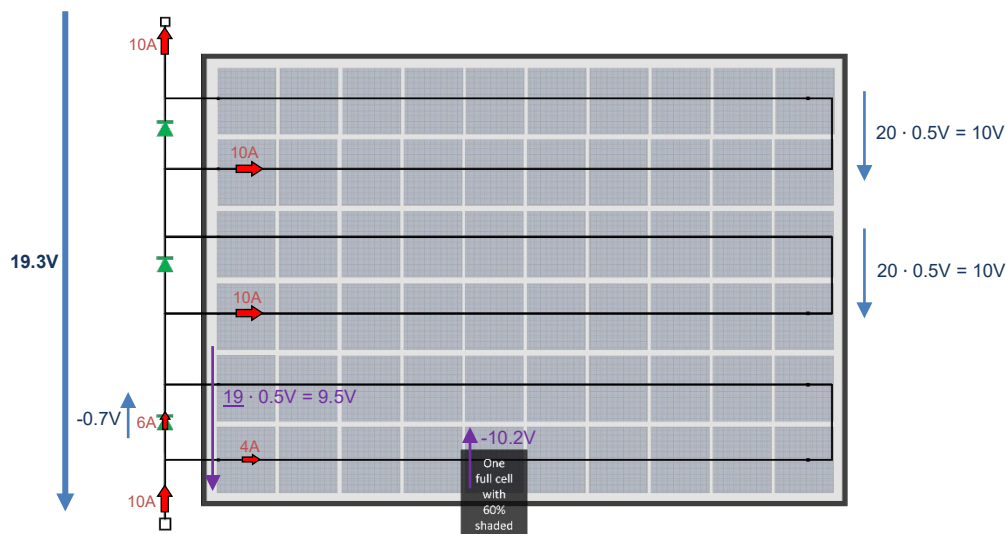


Figure 1: Conventional full cell PV module internal circuitry including bypass diodes (in green). For the case that one full cell is shaded by 60%, the ensuing current paths and magnitudes are visualised in red, the arising, internal substring voltages are shown in purple and the resulting voltages in blue (PV module voltage in bold letters) [8].

The heating power of a single shaded cell is proportional to the remaining current in the string, which is limited to the remaining short circuit current of the shaded cell, if no junction breakdown due to reverse biasing happens. The power is calculated by the product of this current multiplied by the number of the generating solar cells reduced by one and their voltage and added by the voltage drop of the protecting BD. With sixty or more six-inch full cells protected by three BD, local heat outputs of well above 100 W will be achieved. Excessive heat effect can prevent a successful passing of the hotspot test for the IEC 61215 type test of PV modules or minimise the safety margin. This can occur when the total heat power dissipates on a small area of the cell. To prevent hot spot effects from irreversibly damaging the encapsulation and/or lamination filling materials of the module, the area of the cell is now halved or further



reduced (see discussion at the end of Chap. 6.3). This has led to the half-cell modules commonly used today, which also allow tighter electrical performance sorting in the module production process as well as lower series resistance. (Figure 2).

In order to prevent reverse current in parallel connecting strings blocking BD, they were first introduced in space application in the first decade after the invention of the solar cell [9].

2.2 Shading Tolerant PV Modules

During the last decade different electrical wiring layouts of shading tolerant utility-scale photovoltaic modules were investigated and compared in terms of, shading tolerance, and costs. In [5] an optimum number of 12 series connected silicon half-cells was found for the Cross Fox wiring concept, which again was connected in parallel with similar substrings and protected by four bypass diodes in the PV module.

Nowadays PV module products enter the markets which consist also of parallel connected strings in series-connected small size solar cells without blocking diodes as shown in Figure 4. In their advertising information, these manufacturers give the impression of over 60% additional yield compared to other products, but do not mention the measurement setup and thus deceive the customer into believing that they have an annual additional yield of this magnitude [10].

Similar marketing approaches were used by DC/DC power electronic optimiser manufacturers in the last decade, where customers were promised up to 30% additional yield, but this is usually wrong by a factor of ten for the annual balance of typical systems [11].

Today other shading tolerant module wiring concepts are mentioned with less cells used per BD, like in Figure 5 with four to six BD and in Figure 6 with only one BD for each solar cell. In Chap. 7.1 detailed shading simulation shows higher annual performance for this type of modules (Figure 62) with less cells per BD.

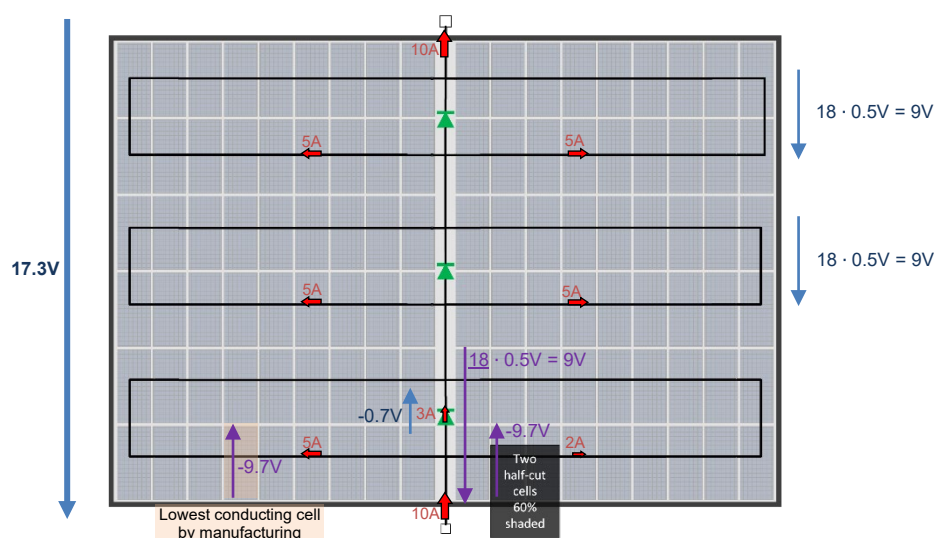


Figure 2: Half-cut cell PV module internal circuitry including bypass diodes (in green). For the case that two half-cut cells are shaded by 60%, the ensuing current paths and magnitudes are visualised in red, the arising, internal substring voltages are shown in purple and the resulting voltages in blue (PV module voltage in bold letters) [8].

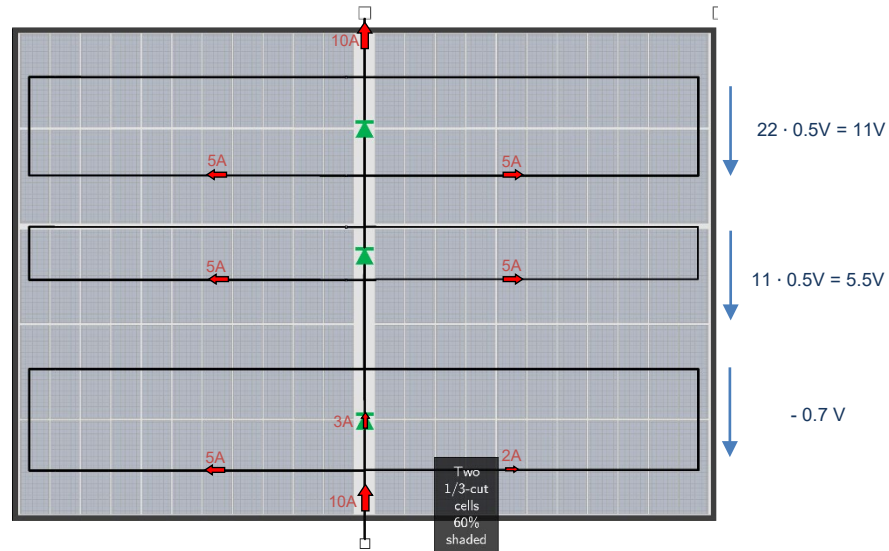


Figure 3: Third-cut cell PV module internal circuitry including three bypass diodes (in green). For the case that two third-cut cells are shaded by 60%, the ensuing current paths and magnitudes are visualised in red. The arising voltages are identical to the ones of the half-cut cell module for the displayed shading scenario, and are therefore not displayed.

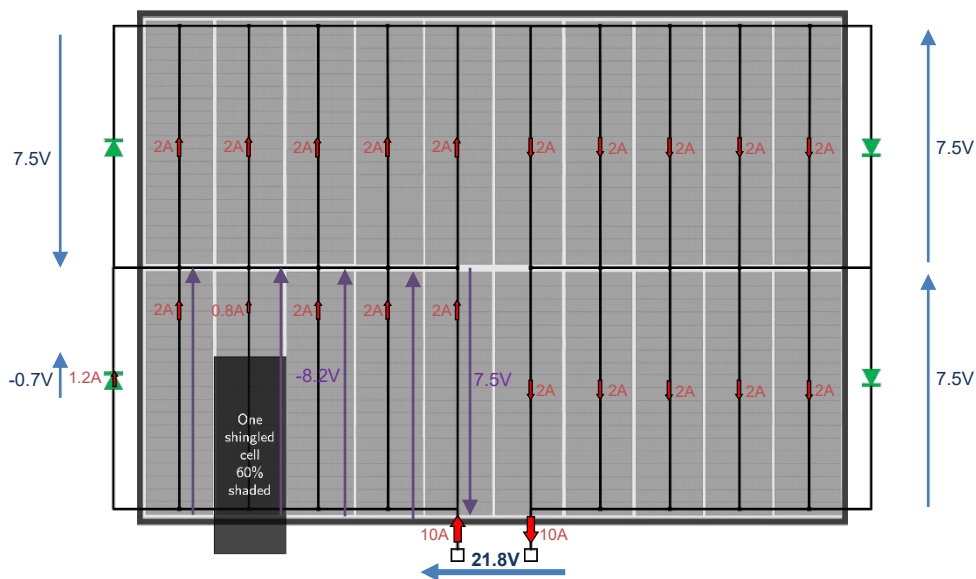


Figure 4: Internal circuitry of a PV module consisting of four series-connected segments of five shingled solar strips in parallel, whereby a bypass diode (in green) is installed in each quadrant [10]. For the case that one shingled solar strip is shaded by 60%, the ensuing current paths and magnitudes are visualised in red, the arising, internal substring voltages are shown in purple and the resulting voltages in blue (PV module voltage in bold letters).

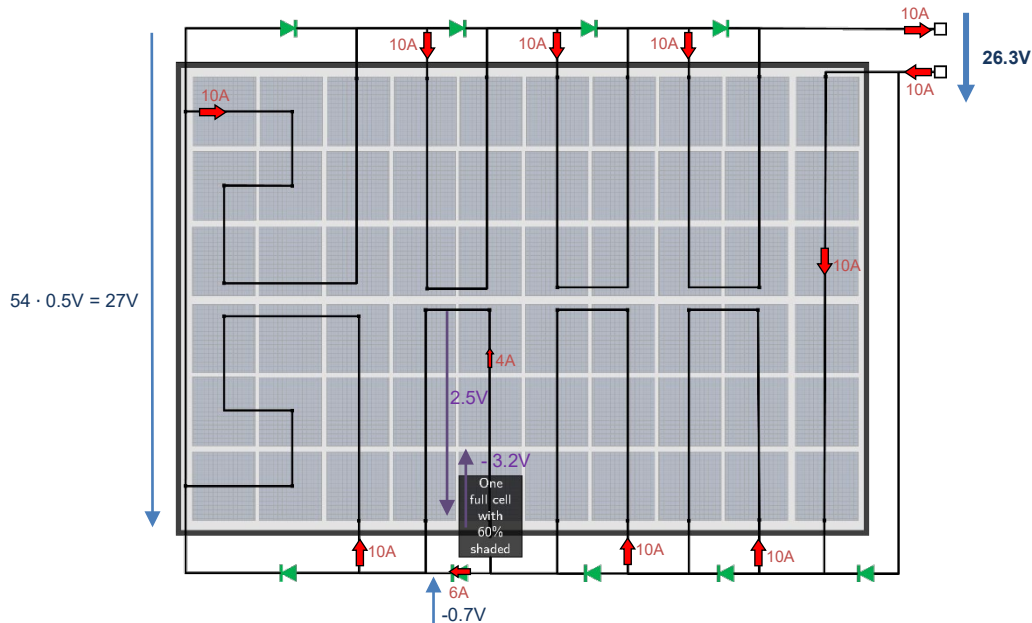


Figure 5: Internal circuitry of a PV module with 9 substrings, each equipped with a bypass diode (in green) see patent from 2009 in [7]. For the case that one full cell is shaded by 60%, the ensuing current paths and magnitudes are visualised in red, the arising, internal substring voltages are shown in purple and the resulting voltages in blue (PV module voltage in bold letters).



Figure 6: Internal circuitry of a hotspot-free PV module with a bypass diode (in green) installed at each PV cell [17]. For the case that one shingled solar strip is shaded by 60%, the ensuing current paths, as well as their magnitudes are visualised in red and the resulting voltages in blue (PV module voltage in bold letters).

Interdigitated back contact (IBC) solar cells offer the potential to implement a built-in bypass diode in the solar cell wafer, by tuning the lateral gap between the p and n contacts. The gain in annual yield of 7 to 21% for four different shaded modules on a typical Dutch solar rooftop were analysed by simulation, relative to typical commercial IBC PV modules, consisting of 96 5-inch IBC solar cells and three Schottky



bypass diodes. For reduced lateral gaps of 6 and 9 μm , cell efficiency drops by 0.6% and 0.2% for all cells, while the annual module gain improved by 21% to 2.1% for that heavily shaded solar module due to the local bypass of the shaded cells within the module. In 2024, an IBC module with efficiencies of above 24% was introduced to the markets, which offers such an integrated improved bypass function in each solar cell. Unfortunately, the manufacturer has not yet provided more precise information in the data sheet on the range of the forward voltage of the cell in the bypass mode, which poses a challenge in cell production to keep this range small [18]. It is assumed that the PV modules in Figure 4 are additionally equipped with three BD per sector as usual to reduce the forward voltage to the forward voltage of a single BD if, for example, one third of the cells are shaded.

2.3 String Inverter (SINV) Systems

Around 1991, solar modules were increasingly mounted on roofs that were electrically connected in series. The electrical power was fed into the AC grid by a DC/AC power conditioner PV inverter. With the subsequent development and improvement of power electronics, it proved to be efficient to dispense with a transformer and to have the DC voltage at the input of the string inverter (SINV) slightly above the peak voltage of the grid voltage, see Figure 10. This made it possible to avoid unnecessary losses in the DC/DC converter. Bypass diodes built into the module took over the function of reducing losses caused by partial shading, which could also be caused subsequently by bird droppings or leaves.

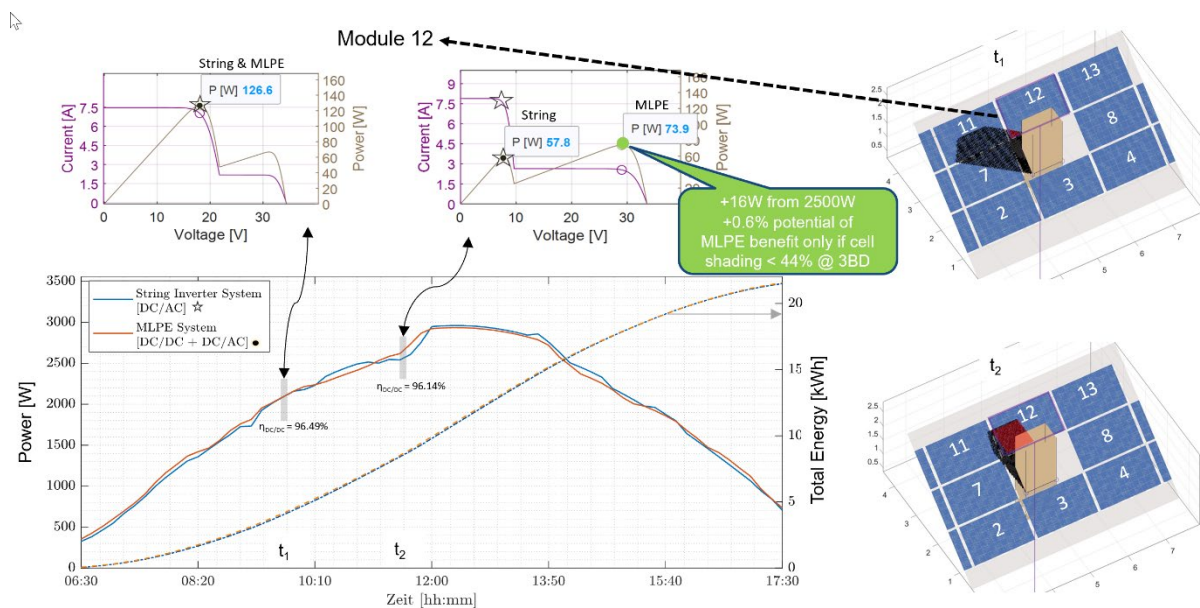


Figure 7: During the course of the day, the shadow of the chimney moves over module number 12 and produces different current-voltage characteristics at the two times t_1 and t_2 shown, which are shown at the top with different possible local and absolute power maxima. Below is the current power and the cumulative energy yield of the two possible SINV and MLPE system configurations, which were calculated with the ZHAW PVShade software considering the actual losses of the power conditioners [19].

These BD fulfilled the task quite well with partial shading, as seen in Figure 7. If several modules with typically three BD are connected in series, the SINV finds the absolute maximum power at high string current. If a shaded module in one of the three substrings (Figure 1 to Figure 3) cannot carry this current



due to limited short-circuit current because of the solar cell that is most heavily shaded there, the bypass functionally takes over the remaining current by BD. In this case of activated BD, the shaded part of the module therefore contributes nothing to the resulting power at the module terminals, as around a third of the module voltage is then missing, as seen in the top left-hand image in Figure 7.

As solar modules became cheaper and cheaper, PV roof systems became larger and soon occupied different sloping roof surfaces of a building. However, the concept of a simple series connection to the input of the same SINV failed. The first concepts of a multi-string PV inverter with different DC/DC inputs and a common DC/AC converter were developed 30 years ago in Switzerland [20]. Different electrical string values, which could arise e.g. due to different orientations or shading, were thus operated at their optimum absolute MPP (Maximum Power Point). However, the output of these DC/DC converters was connected in parallel to the input of the DC/AC converter. A few years later, SMA successfully launched a similar product on the market. The DC/DC and DC/AC converters are integrated in one device, which is now the standard for most SINV manufacturers. The multi-string inverter concept is currently also available for PV outputs of several 100 kW, with a dozen MPP trackers in one device in order to be able to operate different string characteristics, which can also be the result of massive temporary shading, e.g. on large roofs [20].

In recent years, SINV manufacturers have also introduced improvements to the control strategy that increase the yield of a partially shaded string and usually also reduce the hotspot effect, which is discussed in section 6.3.

2.4 Module-level Power Electronic (MLPE) Systems

However, the function of the bypass diode in the module described above has its limits in terms of optimum performance for a module. It has led to the market launch of new decentralized system components, see Figure 8 which will be explained below from the perspective of the performance of the overall system.

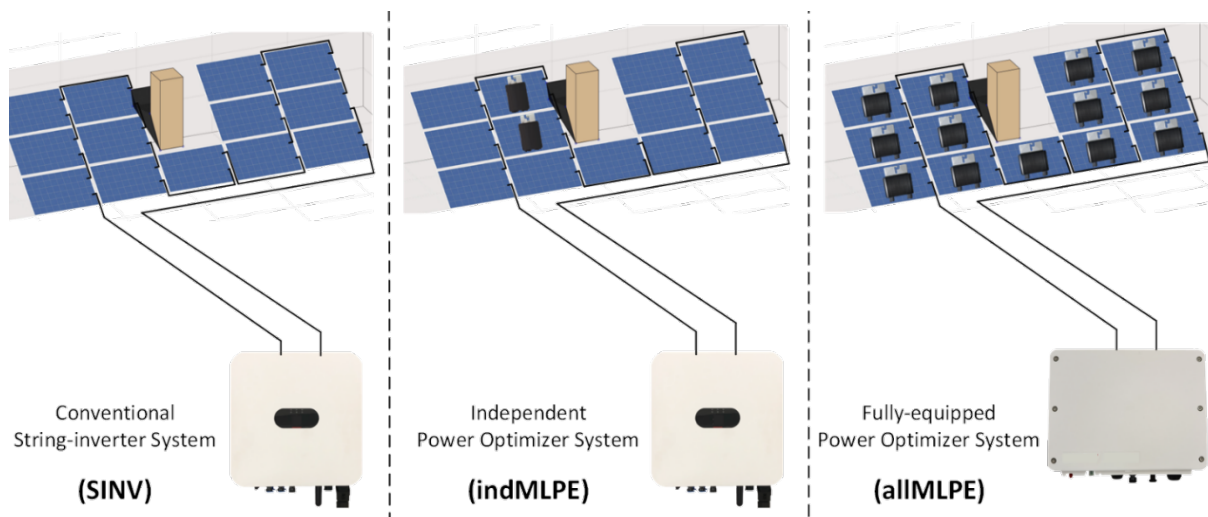


Figure 8: PV system interconnection for three different PV system configurations, a conventional string inverter system (SINV), a partially equipped power optimiser system (indMLPE) and a fully equipped power optimiser system (allMLPE) of a residential rooftop system consisting of 13 PV modules with partial shading by a chimney [1, 16, 22]

To do this, we want to analyse the shading of a single cell in the system as shown in Figure 7 in more detail. If the absolute available irradiation on the most shaded cell does not fall by more than 44%, the



maximum module power can be found at a high voltage and low current, as shown in the Figure 7 (right) if three BD are used. However, the SINV will not carry this low string current, as otherwise the total string power would collapse and therefore the SINV MPP tracker will find an operating point at high current but poor power yield from this one cell shaded module, i.e. at 21 V for module no. 12 in the above case at time t_1 . However, to gain the absolute maximum power of this module at a low shading of less than 44% of a single solar cell, a DC/DC converter must be used to decouple the module output from the string coupling (see the two figures below). The high input voltage is then supplied to the DC/DC converter and a reduced output voltage is supplied to the string. This means that less power generation is available there compared to the unshaded modules.

However, the total power loss of all DC/DC wall-mounted converters, these decentralized Module Level Power Electronic MLPE components, must also be considered in the final power balance. Especially with high irradiation and hardly any shading, more losses occur with the MLPEs than with an efficient SINV alone. At the time t_2 shown in Figure 7, there is a potential of 16 W more power with MLPE, which corresponds to only 0.6% of the string power. However, if the sum of all MLPE losses, including those of the unshaded modules, is more than this 0.6%, which is usually the case with commercial MLPEs, the MLPE system configuration can still not be more efficient here. With this closer look, it becomes clear that only about 1-2% of losses with MLPE is the decisive factor in order to provide a reliable statement on the comparison of the annual yield of SINV and MLPE if there is only low to medium shading.

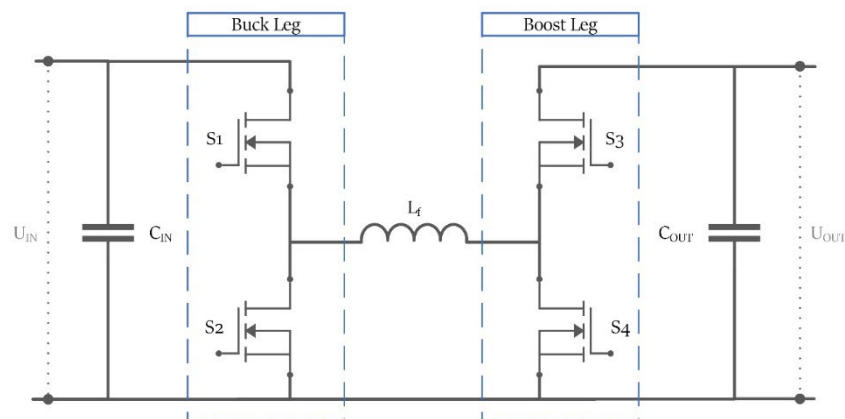


Figure 9: Simplified circuit of a 4-switch buck/boost-converter (commonly used for Power Optimisers in fully equipped MLPE systems), with indication to the switches that are actively operated either during buck- or boost-mode [22].

DC/DC converters can be used as a common circuit concept as MLPE, often as a buck/boost converter, which can generate both a higher and lower voltage at the output, if necessary, as shown in Figure 9. The MLPEs using boost stages must ensure via communication that the DC input voltage of the DC/AC converter can be set and does not reach unauthorized maximum values. For such an allMLPE System Figure 10 shows that for this MLPE and DC/AC System product a constant 360 V DC voltage at the DC/AC input is performed during operation.

This means that if all modules deliver the same power, i.e. there is no partial shading, and twelve MLPEs are used, different from the top view left in Figure 10, one of each PV module will have 30 V at the output of each MLPE, as shown in Figure 10 right. Let us assume that the individual MPP trackers of each MLPE can set the individual operating point of the MPP voltage at the PV module at 30 V because all modules are unshaded and oriented in the same direction. Then the DC/DC converter must set a voltage ratio of 1, input voltage similar then output voltage, so it would be superfluous in this case. However, as



soon as one PV module is partially shaded and the associated MLPE sets a different operating point, combined with a lower power, this DC/DC output voltage in the series circuit will also have to be lower than the neighbouring unshaded PV module MLPs. Then, in an automatic control algorithm, all MLPEs must readjust their output voltages so that the total DC voltage remains constant at 360 V, as this market-dominant manufacturer has realized (see actually measured performance of the MLPE control in Chap. 3.5).

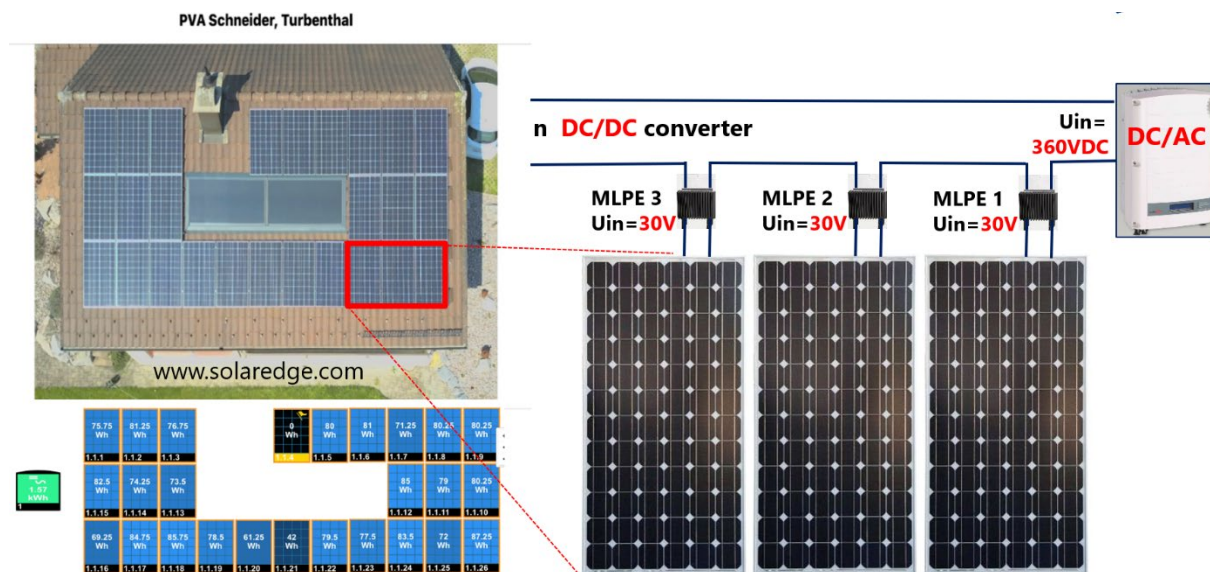


Figure 10: Commonly used allMLPE system as series connection of module level buck/boost DC/DC converters/Power Optimisers powering the DC/AC converter of the same manufacturer at a constant DC voltage. [22].

If the system variant in Figure 8 with few indMLPEs is used, and for the most heavily shaded modules only, buck converters whose output voltage is always lower than the voltage of the connected module are generally used. Some manufactures call this power optimiser 'independent' because they do not need complex communication with the inverter, like the allMLPEs. In addition to the topology, the efficiency of all PV power electronics depends on the power transistors. In the future, the use of SiC GaN high bandgap materials, especially for DC/DC converters, will make it possible to increase efficiency by a further 1%-point [23].

As explained in Chap. 5, the independently performed laboratory measurements of commercial MLPEs have led to strong deviations from the data sheet values, which also depend strongly on the respective operating point, the voltage transformation ratio and the power. A detailed analysis is therefore possible for each case, but general recommendations can still be made in the Chap. 7.1 depending on, for example, the degree of shading or distances from the shading objects to modules.

For three decades micro inverters have been on the markets, with gaining market share in recent years, stimulated also from some regulations in the US. They also will find the absolute optimum module power, because they are typically connected to each PV module, if the MPP voltage range is well-matched. Costs and complex electronics on the roofs at elevated temperatures are still challenging for the development of their products to guarantee a long service life.



The system variants known today in PV power plants for the interconnection of modules or cell arrays and the use of the associated power electronics components will be summarized as: (a) Central inverter, (b) multi-string inverter, (c) Micro-inverters, (d) Cascade inverters, (e) DC parallel optimisers, (f) DC series optimiser, and (g) PV reconfiguration [21]. Within this large repertoire of PV power concepts, the three system variants outlined in Figure 8 have currently established themselves on the roof of buildings with shading, and hardly any micro module inverters, which are common in the USA. With differently oriented PV modules on the roof in the same string or very strong shading, all MLPE with DC/DC converters behind each module have established themselves in order to generate the maximum annual performance. However, the new shading tolerant PV modules coming onto the market allow the use of a conventional inverter without MLPE with similar yields, provided that the module orientation is the same, and the combination with multi-string inverters if acceptable string lengths are possible.

The multi-string inverter concept without MLPE is currently also available for PV outputs of several 100 kW, with a dozen MPP trackers in one device in order to be able to operate different string characteristics, which can also be the result of massive temporary shading, e.g. on large roofs [24]. The global market leader in PV inverters also has a 150-kW multistring-inverter with 7 MPP trackers in its current product portfolio. One manufacturer recommendation is the combination of that device with MLPE DC/DC buck converter with 1100 W each for two or three PV modules. Due to the missing boost concept of the MLPE, the voltage at the individual DC/DC inputs can fluctuate, e.g. in case of partial shading. According to the data sheet, additional losses in the DC/AC system of around 0.2% are to be expected if this DC voltage drops from the optimum value of 480 V to 400 V, for example [25].

2.5 Typical Shading Cases

Various studies have been carried out on measures that can be taken at module and system level to reduce the yield losses that can be caused by shading [26 - 31]. Although there are different shading scenarios for evaluating these measures, it is difficult to identify standard shading scenarios due to the random nature of shading. The most common shading cases for modules and systems in open fields and built environments are summarised in Table 2. These influences of shading can be directly mitigated by the PV system design such as tilt angle selection for snow, whereby for most influences such as snow or bird droppings, only an adjustment or cleaning process can reduce the shading.

Table 2: Summary of the most common shading cases for PV modules and systems in open field and built environments.

	PV System in Open Field	PV System in Built Environment
System Design	Row-to-row Rear-side shading of bifacial modules	Construction (e.g. buildings, walls, etc.) Vertical roof objects (e.g. chimney, ventilation pipe, etc.) Box shaped structures (e.g. dormer, HVAC unit, etc.)
Environment Conditions	Snow Soiling Trees and other vegetation	
Others	Droppings Leaves Module assembly components in close proximity	



The shading conditions experienced by field-mounted and residential PV systems can vary depending on the operating conditions. In order to achieve the maximum yield from field-mounted modules, module spacing, and various factors are designed for optimum operation. However, they may be subject to shading due to system design (i.e. row-to-row shading (i) left in Figure 11, or from the rear side shading for bifacial modules from cable lines, transverse or longitudinal rails from the mounting frame, or switch cabinets attached to the mounting frame, as well as special “solar trees” with shadow of a wing of the Helioplant etc., Figure 11 right) and (ii) environmental factors (e.g. snow, soiling, etc., see Figure 12).

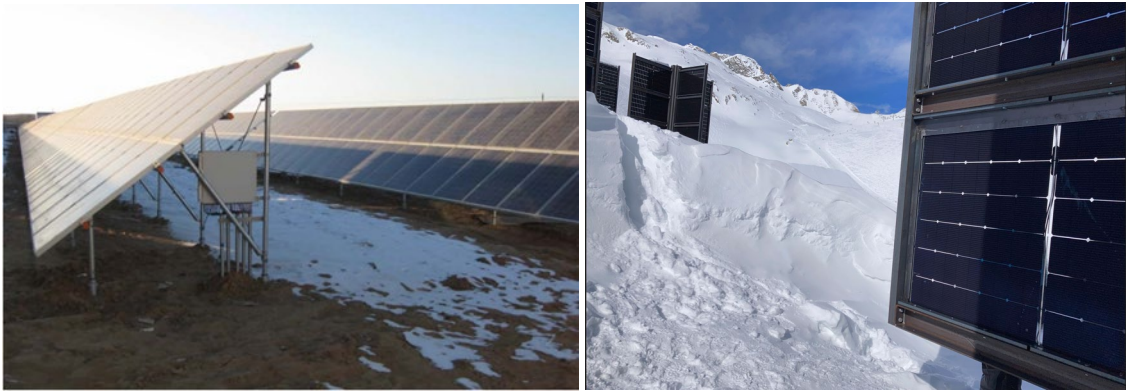


Figure 11: Row-to-row shading. Left image obtained from [31], right a Helioplant solar tree [70].



Figure 12: Shading due to (a) snow and (b) soiling. Images from [32].

Unlike field-mounted PV modules, modules in a built environment are exposed to an increasing variety of shading cases, as it is not always possible to operate them in the optimal conditions. In fact, as shown in Figure 13, the shading factor increases as the system capacity decreases [33]. Larger PV systems installed in the built environment are usually found on the large roofs of commercial buildings, such as warehouses and barns. These structures typically have fewer shading elements compared to their sizes and are often situated on larger land. On the other hand, smaller PV systems are installed on residential buildings, including single-family homes, where the number of shading elements is greater than the size of the roof.

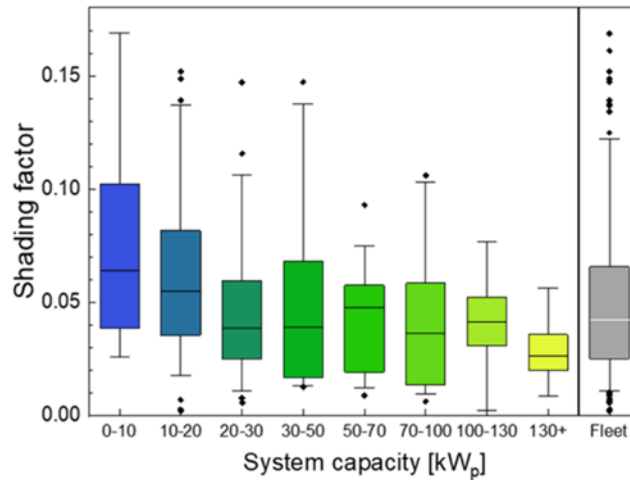


Figure 13: Shading factor as a function of system capacity for 55 residential PV systems in Switzerland. Image from [33].

Modules in a built environment can be exposed to shading situations related to the system design, such as (i) construction (e.g. buildings, walls, etc., see Figure 14a), (ii) vertical roof objects (e.g. chimneys, ventilation pipes, etc., see Figure 14), and (iii) box-shaped structures (e.g. dormer, HVAC unit, etc., see Figure 14c). Apart from these, snow, soiling, trees (see Figure 15a), and vegetation (see Figure 15b) caused by environmental conditions are also among the shading cases. In addition, modules mounted on façades can be subjected to shading from various nearby objects, such as self-shading (see Figure 16), other buildings, and trees, due to their abnormal orientation in an urban environment. Moreover, both in the field and in the urban environment, PV modules can be exposed to small shadows, such as bird droppings and leaves (see Figure 17).



Figure 14: Shading due to (a) another building, (b) the chimney and (c) the dormer [19]. Images from [34].



Figure 15: Shading due to (a) trees and (b) vegetation. Images from [34] and [31], respectively.



Figure 16: Self-shading of BIPV façade PV modules. Image from [35].



Figure 17: Shading due to dropping. Image from [31].



3 Indoor Measurement Results

3.1 DC/AC String Inverter Efficiency

An essential influencing factor of the performance of PV systems is the amount of power losses that occur in the PV power electronic devices. Most important drivers of power losses in PV power electronics are switching losses, ohmic losses in semiconductors and inductors, core losses by the filter coils, as well as static losses for the supply of the internal circuit. The main power electronic device, which is used in all grid-connected systems is the PV DC/AC inverter, whereas nowadays in most systems the string inverter type is used. Until the beginning of the 2010s, many PV inverters still integrated a transformer, which was used for the voltage ratio adjustment and served as galvanic isolation of the electrical in- and outputs. These days mainly transformer less designs are used, which offer higher efficiencies, due to the absence of the significant core and winding losses of the internal transformer (see Chap 2.3).

Since 1999, the performance measurements for DC/AC inverters in photovoltaic systems have been standardized by IEC 61683 [36], or DIN EN 50530, while a second edition of IEC 61683 is planned for publication in 2024 [37]. The results of the performance measurement of PV inverters are to be included in the manufacturers datasheet as standardized by IEC 62894 [38], or DIN EN 50524. While IEC 62891 describes the method for the MPPT efficiency measurement procedure [39], IEC TS 63156 provides additional methods for evaluating the expected overall energy efficiency for a particular location [40]. Standardization for the testing equipment used in performance measurement of power conditioner performance is described in IEC TS 63106-1 and IEC TS 63106-2 [41, 42]. The effects of the input voltage on the efficiency of solar DC/AC inverters were described by F. Baumgartner [43] and colleagues. With the cooperation of other specialist groups, this led to the inclusion of standardized testing of efficiency at three different input voltage levels within the IEC 61683 also listed in today's inverter datasheets [36].

The mentioned influence and its modelling are described in further detail in Pearsall [4, pp. 162-163], where the two standardized methods of the average weighted efficiency of solar inverters are described.

The weighting factors in Equation (1) reflect typical irradiance frequency distributions/histograms over the year, with the CEC efficiency reflecting high insolation conditions (e.g. California & Southern USA, but also Spain & Portugal), whereas the EU efficiency better reflects conditions in and around Germany. Firstly, the protocol developed by Sandia National Laboratories and BEW [44], which was adopted by the California Energy Commission and implemented by IEC 61683 [45, p. 12, 2], the CEC efficiency is described in Equation (1).

$$\begin{aligned} \eta_{CEC} = & 0.04 \cdot \eta_{10\%P_{Rated}} + 0.05 \cdot \eta_{20\%P_{Rated}} + 0.12 \cdot \eta_{30\%P_{Rated}} \\ & + 0.21 \cdot \eta_{50\%P_{Rated}} + 0.53 \cdot \eta_{75\%P_{Rated}} + 0.05 \cdot \eta_{100\%P_{Rated}} \end{aligned} \quad (1)$$

Second, the European weighted efficiency, which was developed by EU JRC/ISPRA and implemented in IEC 61683 is introduced [36] as stated by the Equation (2).

$$\begin{aligned} \eta_{EURO} = & 0.03 \cdot \eta_{5\%P_{Rated}} + 0.06 \cdot \eta_{10\%P_{Rated}} + 0.13 \cdot \eta_{20\%P_{Rated}} \\ & + 0.1 \cdot \eta_{30\%P_{Rated}} + 0.48 \cdot \eta_{50\%P_{Rated}} + 0.2 \cdot \eta_{100\%P_{Rated}} \end{aligned} \quad (2)$$

In summary, for a comprehensive evaluation of the PV inverter efficiency, the laboratory measurements of power losses should not only include a variation of operating power, but also a variation of input voltage. The effects of these parameters on the efficiency are visualized by Figure 18, which shows the efficiency of the Huawei SUN2000 3.68KT-L1 single-phase inverter.

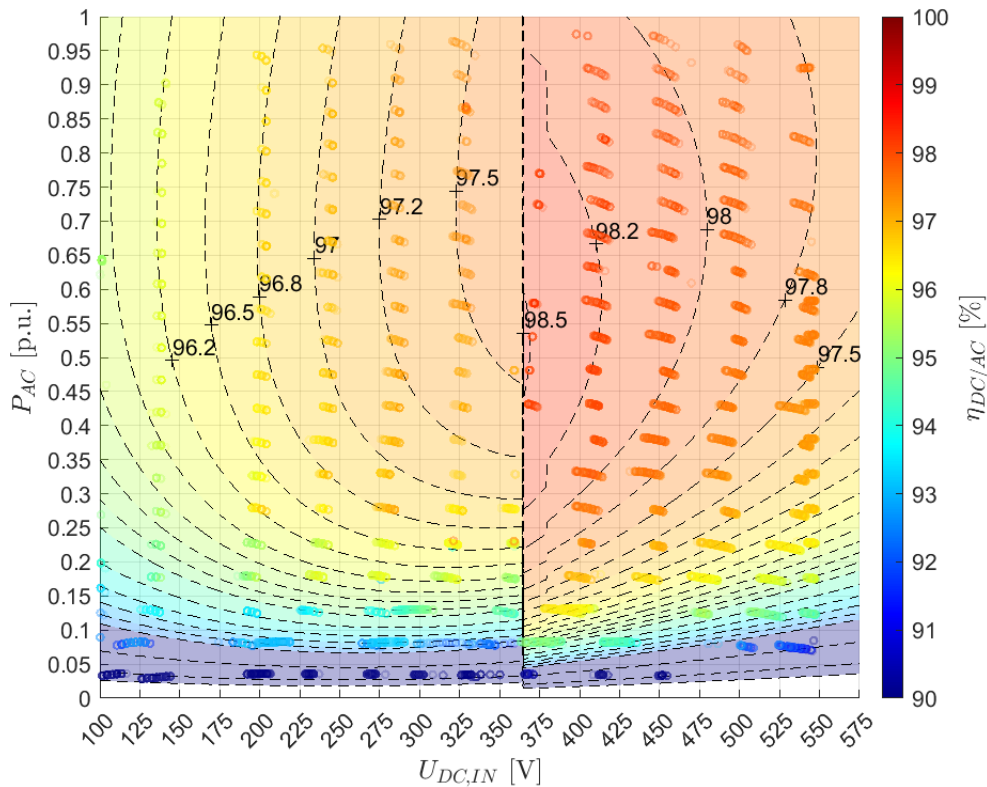


Figure 18: Efficiency mapping of the triple-mode power loss model (individual power loss calculation for buck, boost and passthrough mode) as a function of P_{AC} [p.u.] and $U_{DC,IN}$ [V] with colouring based on corresponding DC/AC conversion efficiency for the Huawei SUN2000-3.68KT-L1 - based on 20'300 points of measurement [22].

It is noticeable that the highest efficiency with $98.6 \pm 0.2\%$ ($k=1$) is reached at the rated input DC voltage of 360 Volts, which aligns with the optimal input voltage for the DC/AC-conversion by single-phase inverters connected to 230/400 V (50 Hz) electrical grids as visualized by the Equation (3).

$$U_{IN,1PH,opt,230V} = \hat{U}_{1PH} \cdot k_{safety} = U_{Grid,RMS,L1-N} \cdot \sqrt{2} \cdot k_{safety} \approx 230V \cdot \sqrt{2} \cdot 1.1 \approx 360 V \quad (3)$$

$$U_{IN,3PH,opt,230V} = \hat{U}_{3PH} \cdot k_{safety} = U_{Grid,RMS,L1-L2} \cdot \sqrt{2} \cdot k_{safety} \approx 400V \cdot \sqrt{2} \cdot 1.1 \approx 620 V \quad (4)$$

In contrast to the values at the optimal input voltage, the efficiencies during operation at higher or lower input voltages are at least 0.2% lower. This is the case due to the reason that the transistors in the upstream DC/DC conditioner within the string inverter do not need to be active at rated input voltage, which in turn reduces the losses in the device. While the efficiency measurements of the DC/AC string inverter show only a slight reduction above the rated input voltages, the efficiency is markedly lower with lower voltage (i.e., boost-mode operation) with a maximum of $97.6 \pm 0.1\%$ ($k=1$).

Slight partial shading of a PV generator would automatically activate e.g. the two bypass diodes of the two affected substrings of the PV module; in order to maintain the high current of the string for maximum string power, this leads to a change in the operating point in Figure 18. Accordingly, the efficiency of the DC/AC inverter, for example, would increase slightly by approx. 0.1% with the shading if the DC input voltage drops from 450 V to approx. 425 V due to the shading when a standard PV module is used (Figure 1). However, this power gain would only correspond to about one tenth of the power lost directly at the module due to shading.



3.2 DC/AC Module Inverter

For the operation of individual PV modules or tiny PV systems, micro-inverters can be used. (see Chap. 2.3) These devices offer the same capabilities as a string inverter, but were developed for low power PV applications, i.e., for one or a few PV modules, usually with a total power of below 2 kWp. If they are applied to individual PV modules, they offer module-level control, which can offer improved yield in conditions with partial shading, due to the reason that each module of the system is operated at its individual maximum power point without influencing the operation of other PV modules, because they are connected in parallel on the AC line.

In Figure 19, the indoor measured DC/AC efficiency of the Enphase IQ7+ is visualized as a function of output power of the AC-side, P_{AC} , relative to rated power and the input voltage $U_{DC,IN}$.

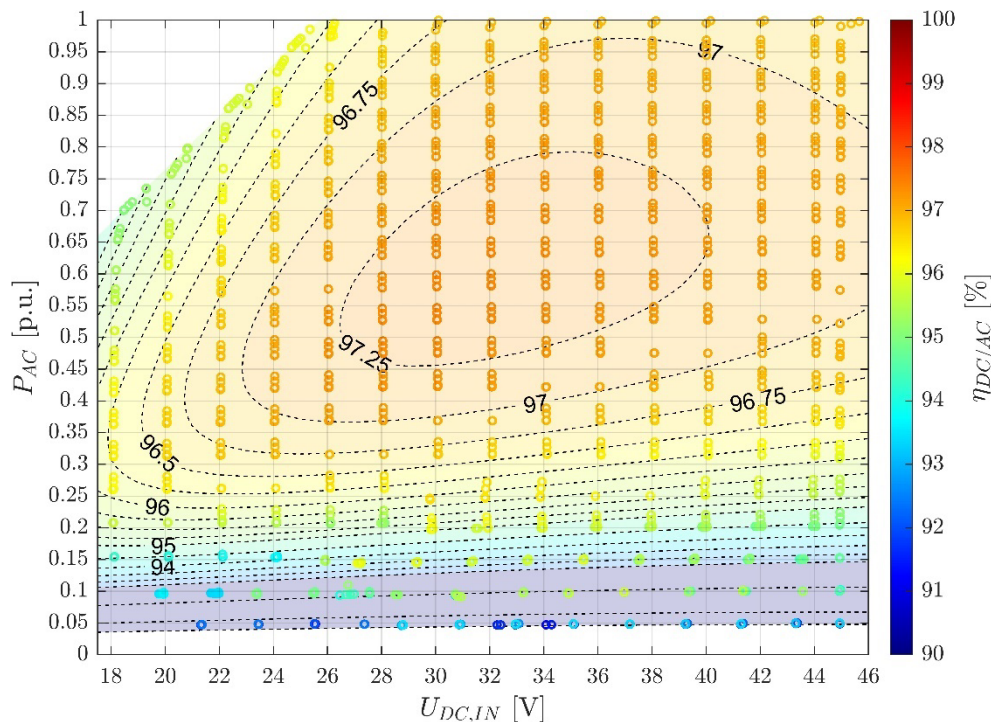


Figure 19: Efficiency mapping of the power loss model (only boost mode applicable) as a function of P_{AC} [p.u.] and $U_{DC,IN}$ [V] with colouring based on corresponding DC/AC conversion efficiency for the Enphase IQ7+ (2020 Edition) - based on 4'200 points of measurement at ZHAW.

Notably, for many operating points the DC/AC efficiency of the Enphase IQ7+ is lower than the measured efficiencies of the string inverter Huawei SUN2000-3.68KT-L1 visualized in Figure 18, with a difference of up to 1.25% for the maximum efficiencies of both devices. The main reason for this is the operation of the module-inverter at around 1/10th of the usual input voltages of the string inverter, indicating an operation in boost-mode of the internal DC/DC conditioner at a much higher duty cycle (i.e., longer “on time of power-electronic switches”), which causes an increase of losses in the converter.

3.3 DC/DC Power Optimisers

In 2010, power optimisers were first commercially introduced on the PV market by SolarEdge. Within the last 14 years, these DC/DC converters have increasingly been installed in PV systems around the



globe, mostly but not limited to residential systems and offered as a tool to counter the effects of shading by manufacturers such as SolarEdge, Tigo Energy, Huawei, and some other companies.

In contrast to the standards mentioned for the performance of DC/AC solar inverters, a standardization does not currently exist for the performance testing and measurement of solar DC/DC conditioners (i.e., power optimisers). The first independent measurements of commercial DC/DC power optimisers were conducted and published by Bründlinger et. al. in 2011 [1].

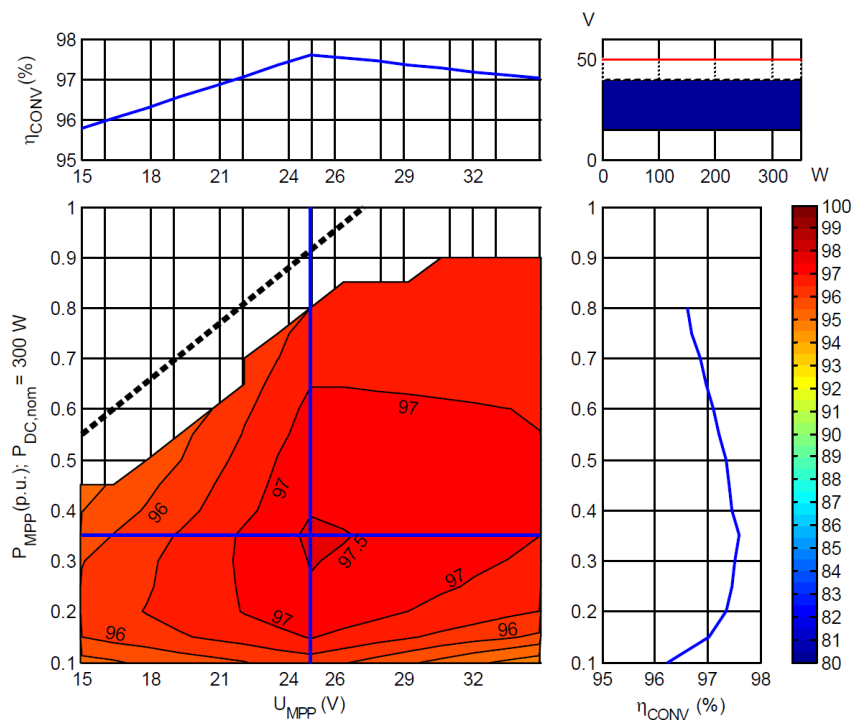


Figure 20: Conversion efficiency plot of the Power Optimiser PO01 (model of 2011) as function of MPP input power and output voltage; output voltage was set to 25 V [1].

Nowadays, the datasheets of power optimisers generally show two numbers, the maximum efficiency and the weighted efficiency. Common values for the mentioned numbers range from 98.5 to 99.5%. Between 2021 and 2023, indoor measurements of commercial power optimiser models were conducted by the Institute of Energy Systems and Fluid-Engineering at the Zurich University of Applied Sciences in Winterthur, which was part of a research project funded by the Swiss Federal Office of Energy (SFOE) [12-16]. The maximum measured efficiencies of up to 99.6% ± 0.4 ($k=1$) confirmed the existence of the highest efficiencies given by the manufacturer's datasheets. However, the efficiencies stated in the datasheet were only measured at the input/output equilibrium, at which no switching losses occur [19]. As visualized in Figure 21, the efficiencies during the buck or boost operation of the DC/DC-converter are at least 1% lower than in the previously mentioned mode of operation. Accordingly, prevailing datasheets of power optimisers show distinctively higher efficiency values than are usually encountered in real-life conditions, where others like a buck-converter manufacturer, give no efficiency values.

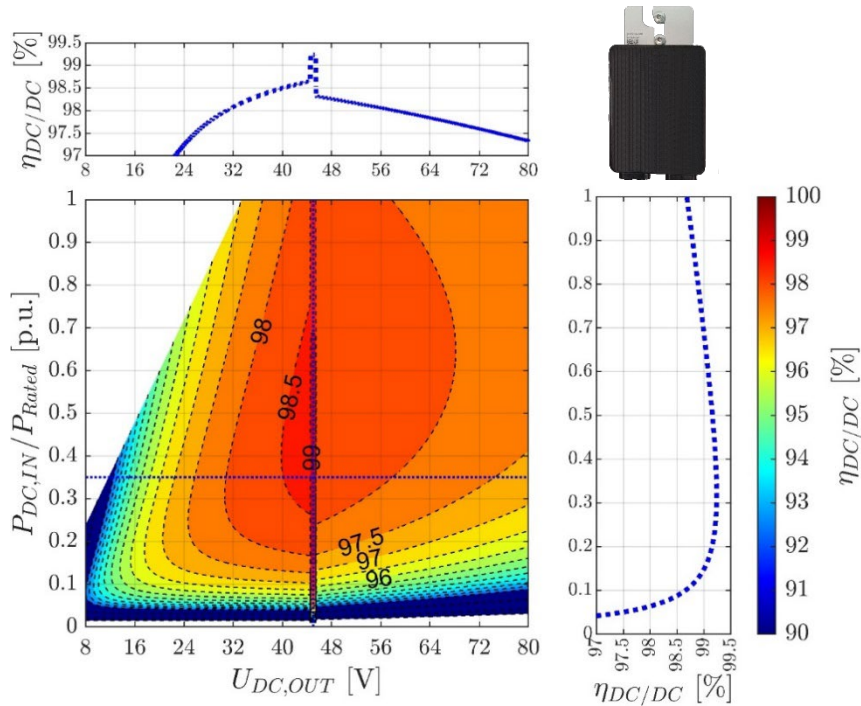


Figure 21: DC/DC efficiency mapping of the triple-mode power loss model (individual power loss calculation for buck, boost and passthrough mode), as a function of the relative DC input power, $P_{DC,IN}/P_{Rated}$ [p.u.], and DC output voltage, $U_{DC,OUT}$ [V], for the SolarEdge S500B (2023 Edition) - based on 157'900 points of measurement at ZHAW see Figure 26. Input voltage was set to 45 V.

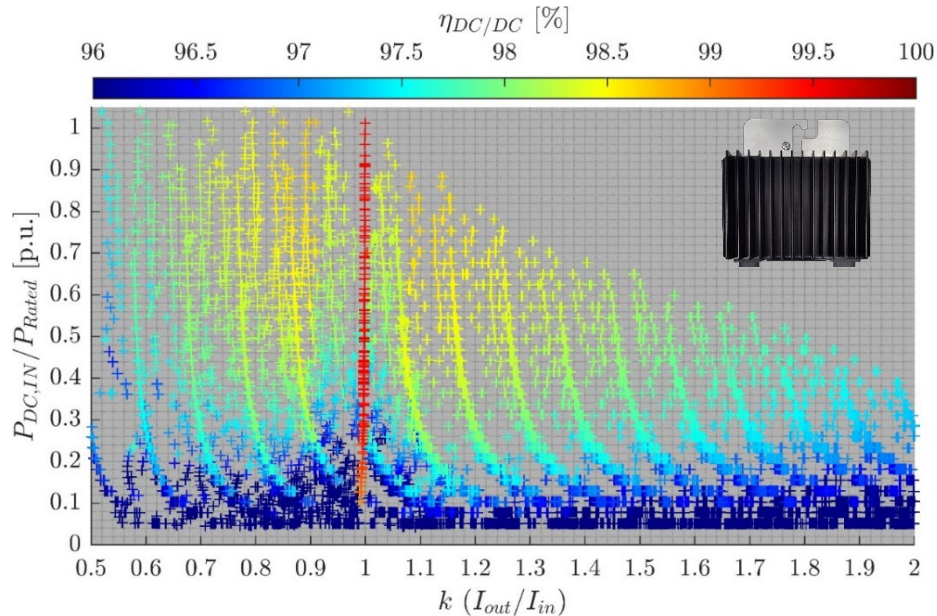


Figure 22: SolarEdge S500B static DC/DC efficiency $\eta_{DC/DC}$ measurement at ZHAW with a constant input voltage, U_{IN} starting at 20 V up to constant 80 V in 5 V intervals as a function of the output to input current ratio I_{OUT}/I_{IN} , k_i and P_{IN} .

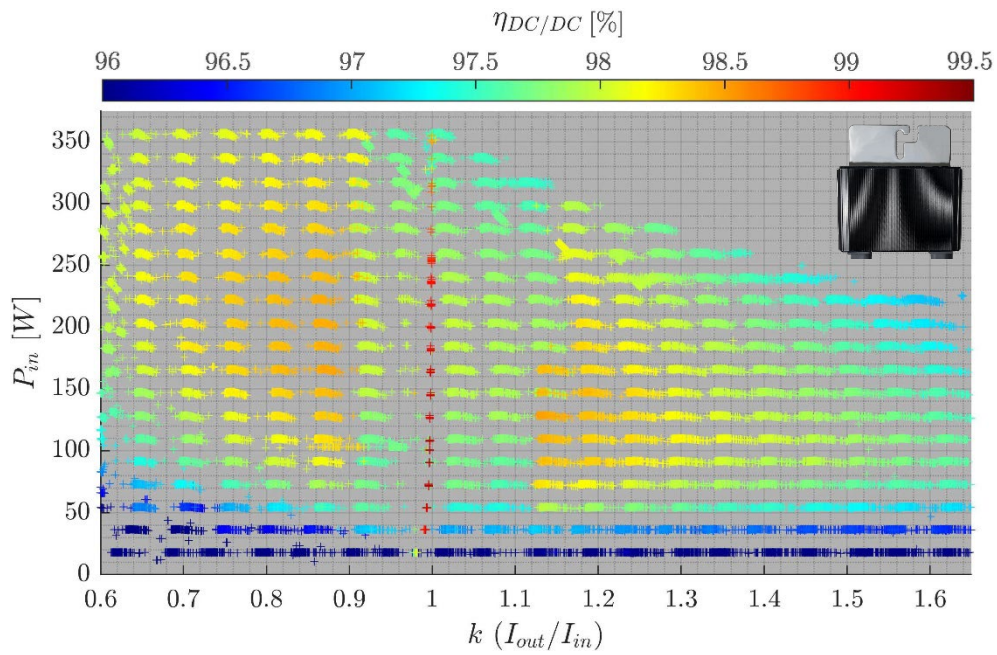


Figure 23: SolarEdge P370 static DC/DC efficiency $\eta_{DC/DC}$ measurement at ZHAW with a constant input voltage, $U_{IN} = 35 \text{ V}$ as a function of the output to input current ratio I_{OUT}/I_{IN} , k_i and input power, P_{IN} [14, 46].

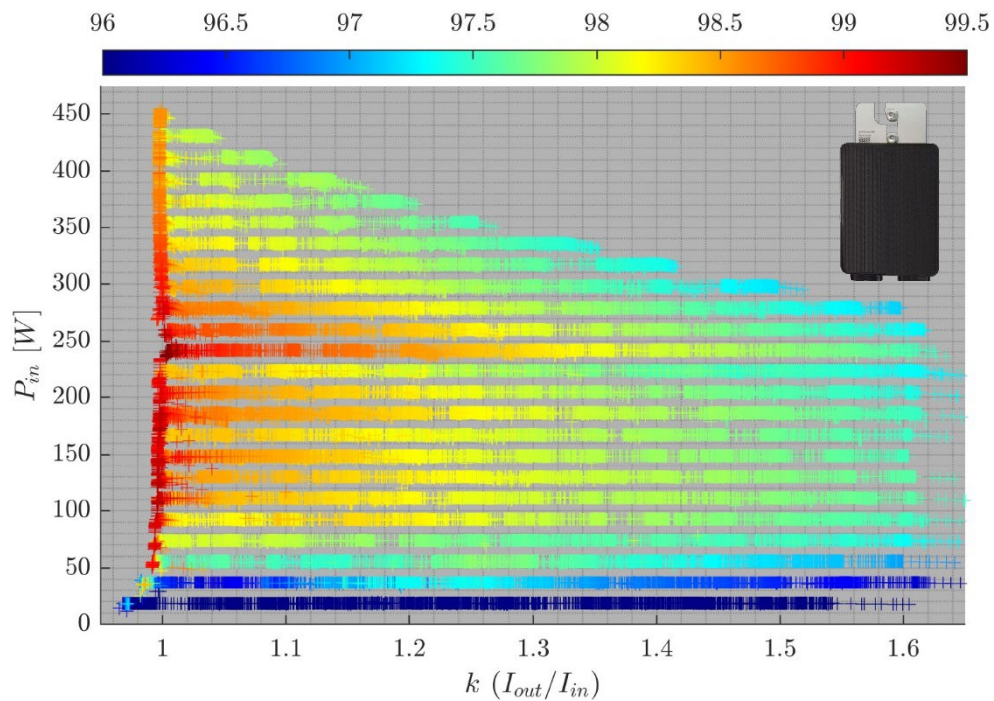


Figure 24: Huawei SUN2000-450W-P static DC/DC efficiency $\eta_{DC/DC}$ measurement at ZHAW with a static input voltage, $U_{IN} = 35 \text{ V}$ as a function of the output to input current ratio I_{OUT}/I_{IN} , k_i and input power, P_{IN} relative to P_{Rated} [22].

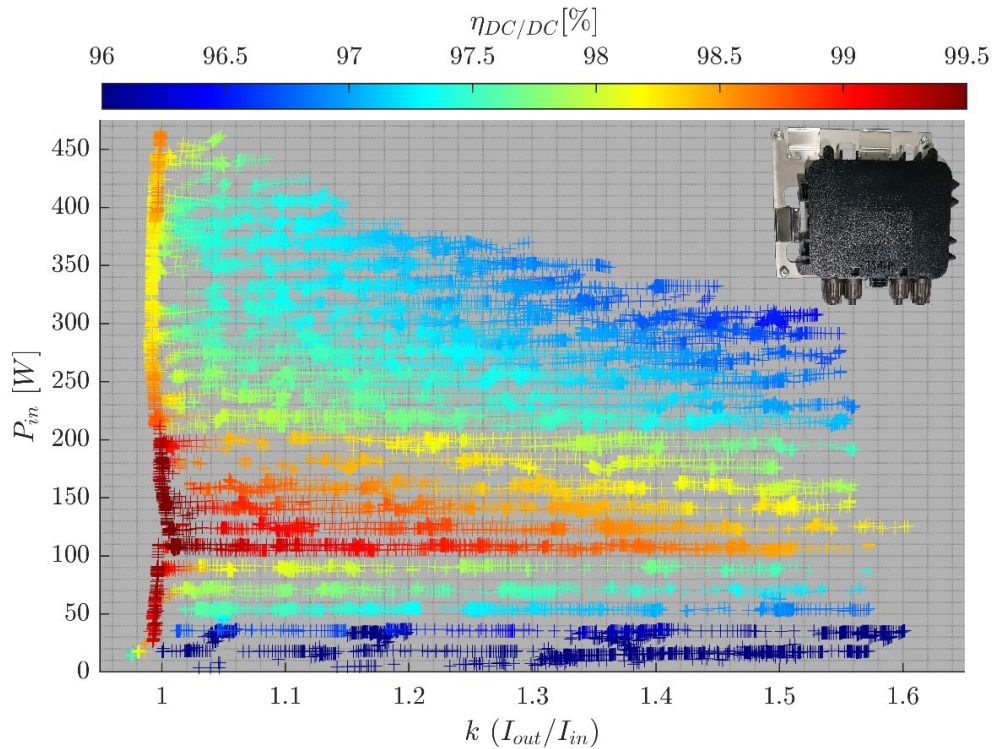


Figure 25: Tigo TS4-R-O static DC/DC efficiency $\eta_{DC/DC}$ measurement at ZHAW with a constant input voltage, $U_{IN} = 35V$ as a function of the output to input current ratio I_{OUT}/I_{IN} , k_I and input power P_{IN} relative to P_{Rated} [22].

3.4 DC/DC/AC System

At the ZHAW indoor laboratory, ten workstations are equipped with several types of MLPE by different manufacturers, which are powered by Keysight E4261A-J01 solar array simulators (SAS) and measured with a Newtons4th PPA1530 power analyser at the electrical input and output terminals. During testing, the desired operating points of the PV modules are entered into the SAS devices, which calculate respective IU-curves for the given inputs to each MLPE. Accordingly, the SAS generate DC-currents and voltages for the device-under-test based on photovoltaic IU-curves with a resolution of 4,096 points. For a comprehensive overview, the electrical topology of the indoor laboratory setup is visualized in Figure 26. Further descriptions of the setup are given in "Performance analysis of shaded PV module power electronic systems" and "Performance of New Photovoltaic System Designs" [13, 19, p. 26, 46].

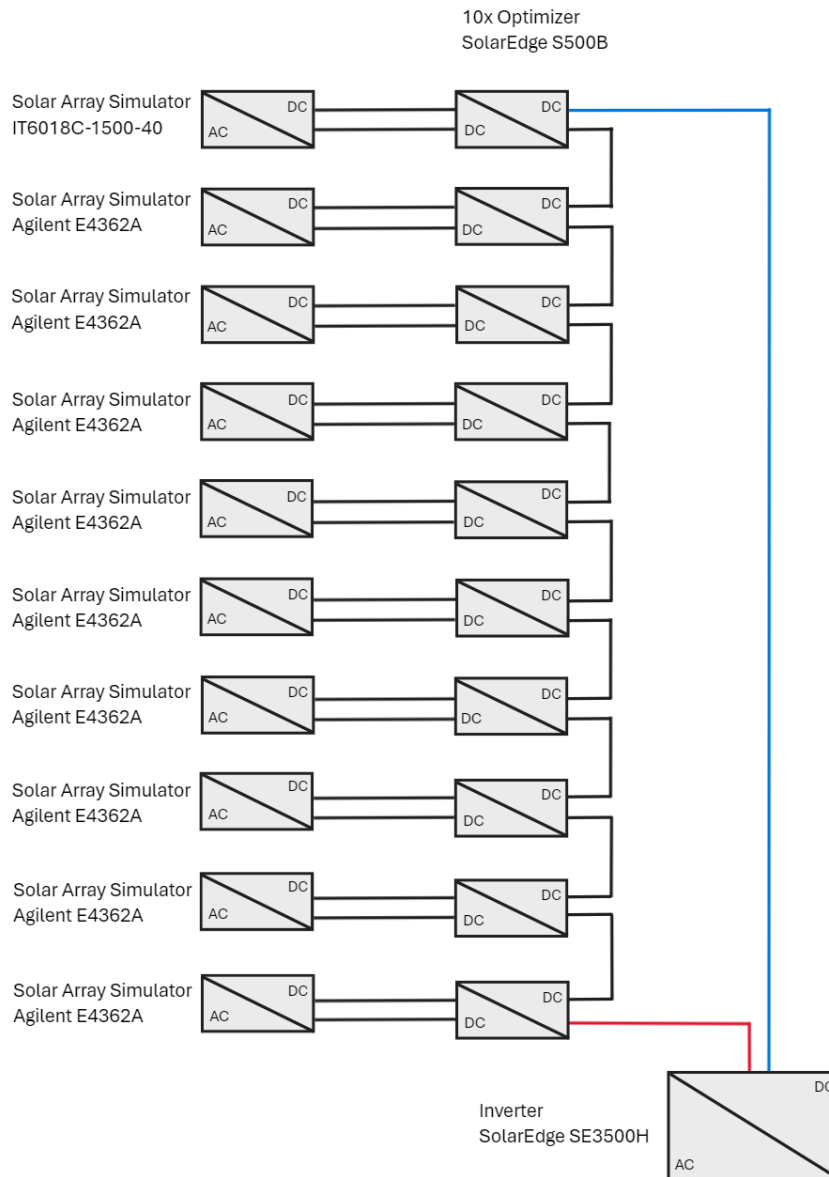


Figure 26: Indoor Laboratory with module-level power electronic setup and topology at the ZHAW School of Engineering in Winterthur, Switzerland, which is used for the precise efficiency measurements of PV power electronics [49].

3.5 Transient Power Electronic Measurement

In contrast to traditional methods of power production (e.g., coal power plants), the electricity generation by photovoltaic systems is not constant, but greatly dependent on environmental and meteorological factors. Accordingly, changes in irradiance or temperature affect the operation of PV generators and must therefore be considered for estimations of the PV system operation. Accordingly, transient power electronic measurement is an essential part in estimating performance in real-life conditions or to accurately model a PV system for dynamic analysis.



While IEC 62920 describes the methods of transient measurement including tests for electromagnetic compatibility in DC/AC inverters, IEC 62891, the MPPT efficiency measurement procedure is described, wherein the testing of the performance of solar power electronics for changes in irradiance is mentioned [39, 47]. On the other hand, transient measurements are also performed to analyse the operation and behaviour of components in the internal circuit and therefore, improve the modelling of power electronic devices. In Figure 27, the transient measurement of the input/output voltages, as well as currents of a SolarEdge P370 power optimiser in buck-mode operation is visualized for a duration of 10 μs .

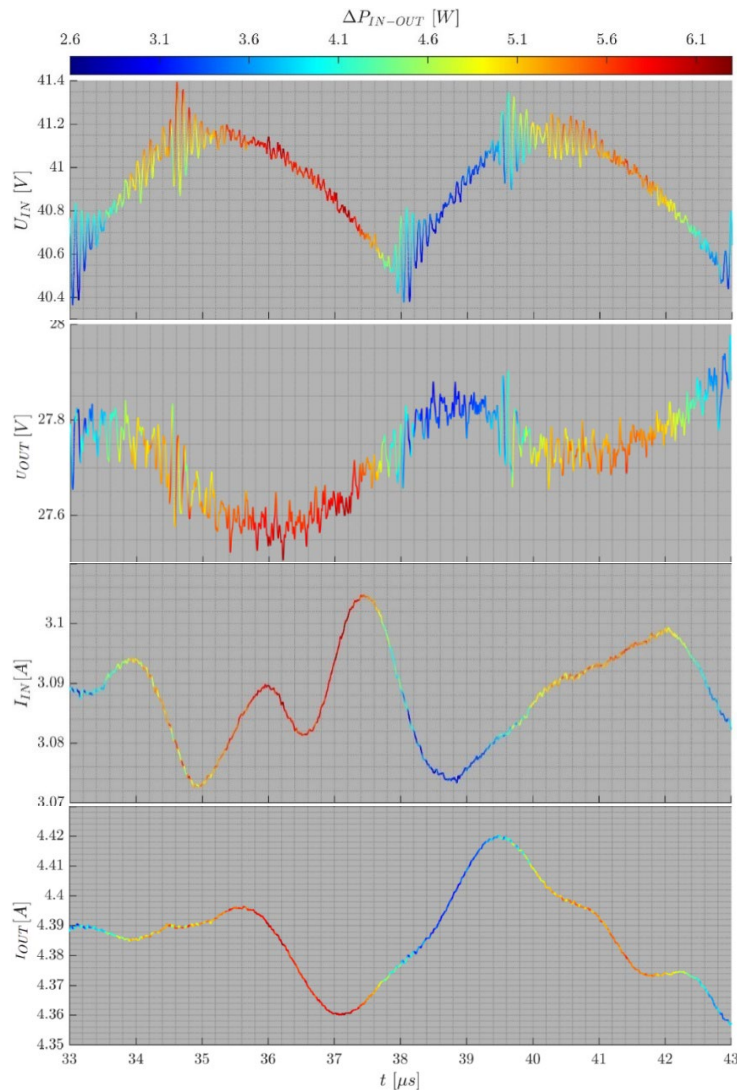


Figure 27: Transient measurement of the SolarEdge P370 in-/output voltage and current in a time scale of 10 μs in 0.2 μs divisions during the pulse-width modulation in buck-mode operation [22].

In detail, the figure shows the pulse-width modulation of the DC/DC converter during steady state conditions in buck-mode operation. Notably, the input voltage remains within ± 500 mV of 40.9 V and a high-frequency noise of up to 0.5 V is visible, which is possibly caused by switch node ringing. In short, although the noise translates to the output, the process still provides a nearly constant output voltage of 27.75 V ± 250 mV and current of 4.39 A ± 30 mA.

Another testing sequence was conducted to measure the MPPT behaviour of the Huawei 450 W-P when a change of partial shading occurs (shown in Figure 28). During the 9 minutes of testing, the module first encounters a sudden partial shading, afterwards, the severity of partial shading of 1/3 of the PV



module is gradually decreased by 10% (i.e., stepwise increase of 600 mA) until the partial shading is entirely removed. In general, the MPPT manages to find and stay at the individual local maximum power point well. Furthermore, in the case that a MPPT multi-peak scanning is initiated by the Huawei PV inverter - visible by the yellow-coloured points in the figure between 4 to 5.5 A and 25 to 22 V -, the MPPT correctly decides on the global MPP at a higher voltage and finishes its search within 1.1 seconds. In contrast, this indicates that the MPPT of the Huawei 450W-P is only capable of a local MPPT (similar to optimisers by other manufacturers) and cannot find the global MPP of the module without initiation by the connected PV inverter. In other words, due to the reason that Huawei inverters are currently only programmable to execute a MPPT multi-peak scanning not less than every five minutes, the power optimiser will periodically track a suboptimal power point and therefore, not optimize the system performance. In the least favourable case, the interval of the multi-peak scanning is set to 10 minutes or more, which could significantly reduce the annual PV system performance when the plant is subjected to frequent shading.

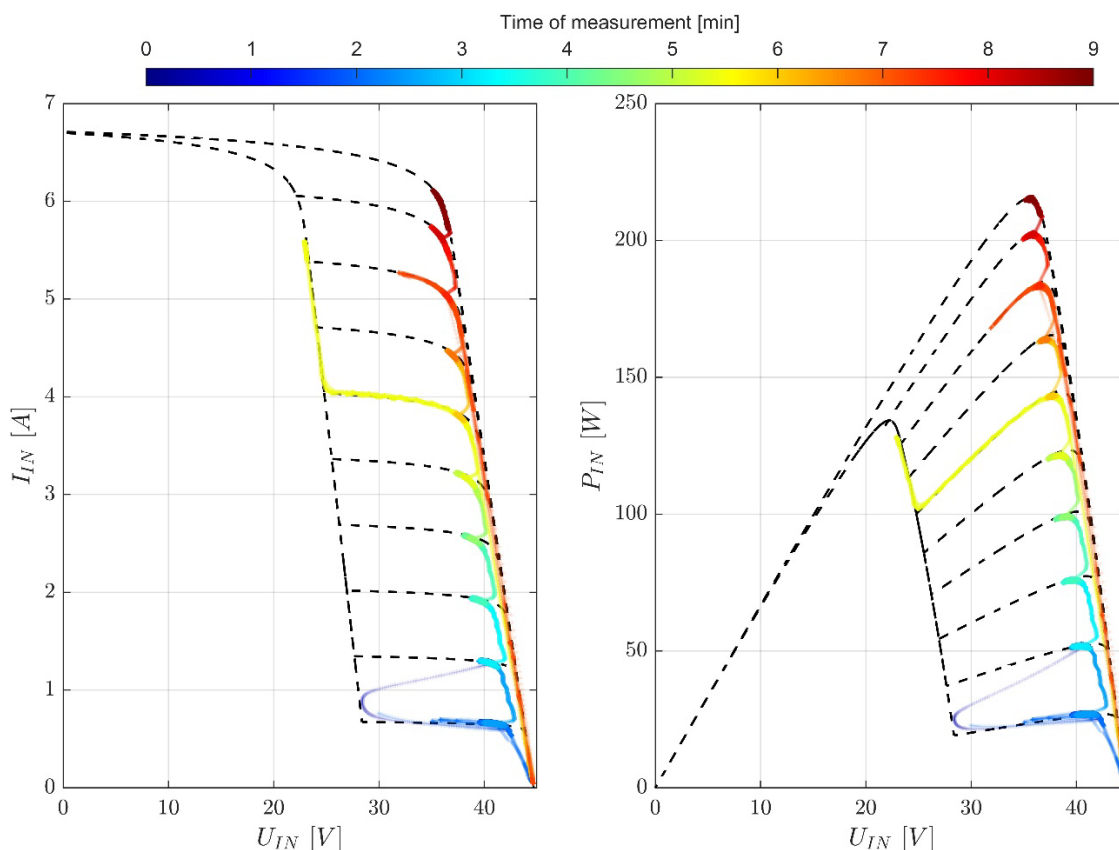


Figure 28: Plot of the 9-minute transient test of the Huawei 450W-P with measurement values in colour, which corresponds to the measurement time, and corresponding UI-curve and PU-curves in black, which were programmed in the solar-array simulator. During the measurement, the effect of a passing shadow on the module was simulated, whereby 1/3 of the PV module was first shaded by 90% and then, the shading was decreased in 10% increments until no shading remained [22].

In 2024, two dominant MLPE products on the market were tested for their ability to demonstrate operation at the absolute maximum performance under changing partial shading conditions, as a product name promises power optimisers [48]. The results documented below are sobering. They pursue a different control objective, but do not always detect the maximum MPP.

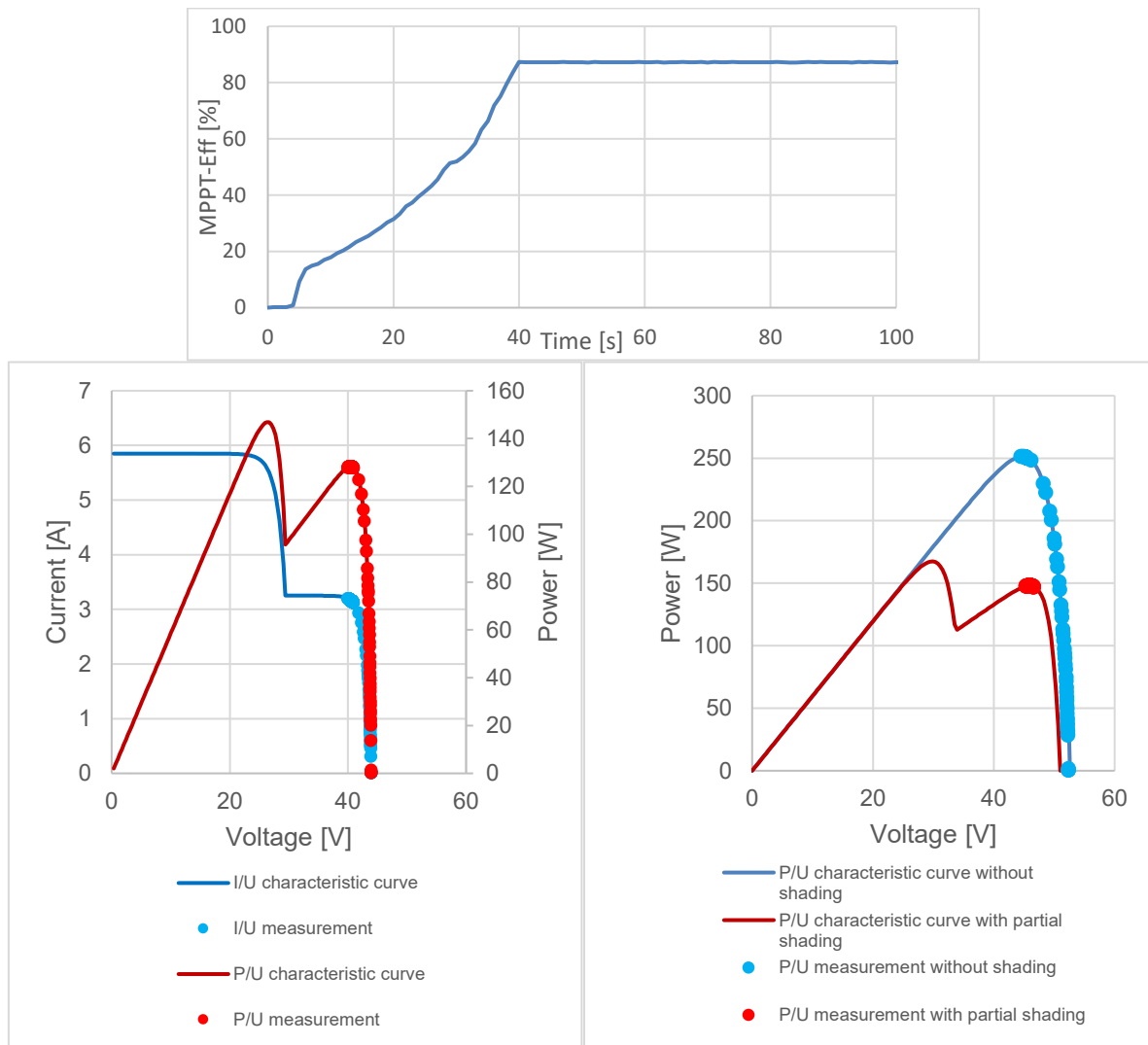


Figure 29: MPP Tracking measurement results of the SolarEdge S500B performed at the ZHAW IEFELaboratories [48].

The measurement results in the indoor ZHAW Laboratory (Figure 26) clearly show a very similar behaviour of the two commercial products in Figure 29 and Figure 30 on top, starting up to find the MPP from the open circuit point. The first local maximum is reached very quickly. The 10% to 90% rise time is 33 seconds for the SolarEdge S500B and 19 seconds for the Huawei SUN2000-450W-P. However, both products fail to find the absolute maximum power at approx. 27 V and a higher module current over a period of one hour and thus only reach less than 90% of the available power of the partial shaded PV module. Although the Huawei SUN2000-450W-P tried to find a new MPP every 5 minutes and was briefly successful, as the second image in Figure 30 shows, it then left the optimum operating point again and returned to the secondary lower MPP.

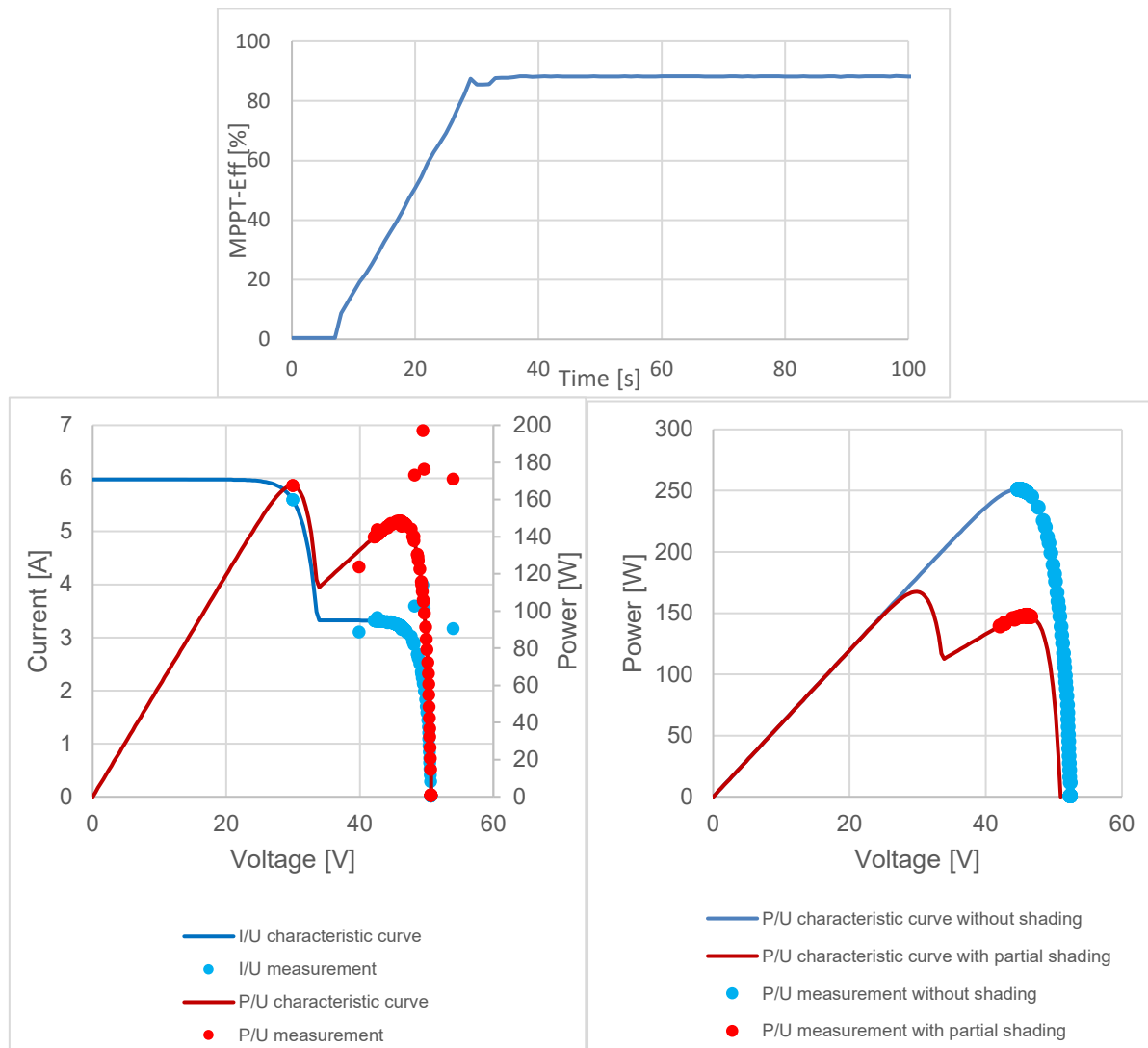


Figure 30: MPP Tracking measurement results of the Huawei SUN2000-450W-P performed in the ZHAW IEF E Laboratories [48].

After the work in [22] showed the same persistence in the secondary lower minimum with the gradual reduction of shading (Figure 28), a further test was subsequently undertaken. The unshaded PV module was suddenly subjected to a 50% shading of a single solar cell of the 60 full cells, which are connected in the module array with the usual three bypass diodes (Figure 1). The result was the same for both products, namely that only the local MPP is found and maintained, but this does not correspond to the function of a power optimiser, as potential solar power is not used (see the right-hand images in Figure 29 and Figure 30). This systematic behaviour, which is not shown in the data sheet and probably not known even to experienced PV planners, could have another cause. It could be an intentional system setting of these products under investigation that the MPP with the lower current is held and thus the activation of the bypass diode is deliberately suppressed, which in these cases corresponds to a loss of power. On the other hand, the possible occurrence of hotspots can be avoided, but this must always be communicated on the data sheets. The customer should be able to decide whether he wants to buy an optimiser type with the feature algorithms to find the maximum MPP despite the hotspot, as he uses half-cell modules, or not and then choose the current algorithms. As described in Chap. 3.1 for the SIN V, the annually weighted efficiency for power electronics, which is now established as the standard and only applies to the limitation of the unshaded PV generator, has so far been completely lacking for partial



shading. F. Baumgartner is currently developing a technical specification for some typical shading cases for the IEC, see Table 4 with an international working group within TC82 SG5. The aim is that, similar to the standard for SINV [45], see Chap. 3.1, efficiency measurements of the specific product are made on SINV or MLPE based on indoor laboratory, with different power, but now also different current/voltage ratios within the PV generator, due to the specific partial shading. As suggested in [19, 48], these are also measured with weighting factors [14, 22], the others are averaged like those in [45] to the annual weighted efficiency, one value per shading case. In future, these shading efficiencies could also be used on the data sheets as a figure per shading case for comparing products.



4 Outdoor Measurement Results

4.1 Testing Set-up MLPE

In an outdoor test, a typical shadow of a streetlight pole, a flagpole, power pole was modelled with a wooden pole, as shown in Figure 31 using standard crystalline silicon modules equipped with three bypass diodes [50].

For the SINV without an optimiser, the SMA SB3.6-1AV-40 was used. Two MLPE setups were installed, one with the buck converter Tigo TS4-R-O as MLPE A and the same type of the previous SMA inverter. The second MLPE B system comes from SolarEdge with optimiser P300 and inverter SE HD Wave 3,6. The three systems have each fourteen PV modules of the same type.

The results of MLPE gain of 3.1% for MLPE A and 4.2% to SINV with modern MPP tracking (SMA ShadeFix see Chap. 6.3 in Ref [64]) on this cloudy day of 8.5.2019 with moving clouds. On the other hand, the SINV offered 2% more yield relative to MLPE A and a gain of 1.3% to MLPE B on the clear sky day of 23.4.2019. The annual yield of SINV and MLPE B did not differ by more than 0.05%, while MLPE performed 2.45% worse.

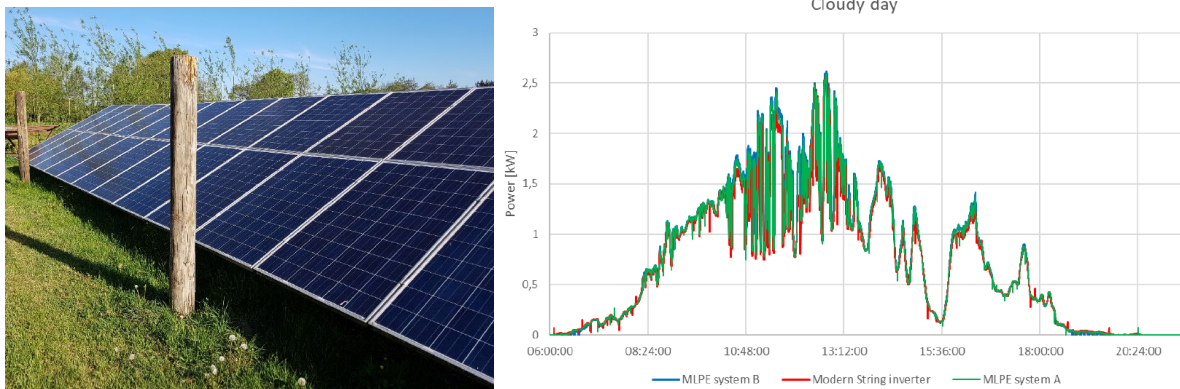


Figure 31: Outdoor comparison of yield data of SINV and MLPE with the same pole shading of each string as performed by the University of Southern Denmark [50].

In general, such a small difference in yield must be critically analysed for side effects. For example, this is the nominal PV power of the two systems and their module degradation over the measurement period, as well as other local winds and thus the resulting cell temperature conditions. However, the outdoor test clearly shows that the difference between the different system variants is not greater than 3%.

4.2 Testing Set-up Shading Tolerant PV Modules

At partial shading of cells, hotspots emerge, due to the activation of the bypass diode and due to the power dissipation of up to around 100 W in the most shaded cell in standard modules, which depends on many factors as described in Chap. 2.2. To protect the encapsulation material beside that cell, the heating power is reduced by cell and module design. For example, by smaller cell area like half-cells and thus lower current, or lower number of series connected cells per BD as shown in Figure 5 [5]. However, BD do not prevent cell heating from occurring, but could avert the potential damage if the hotspot temperature has moderated limits below the maximum temperature of 100°C.

Finding this hot spot sub circuit and then operating it at lower current values to avoid the hot spot, was the focus of the following research project of University of Utrecht [76, 53, 54]. A smart PV test module



was developed with several sub cell circuits equipped, each with an individual DC/DC converter to lower the shaded cell current, as shown in Figure 32. Furthermore, the smart module requires an electronics circuit to be mounted at the back of the panel to realise the converter and the active hot spot detection technique.

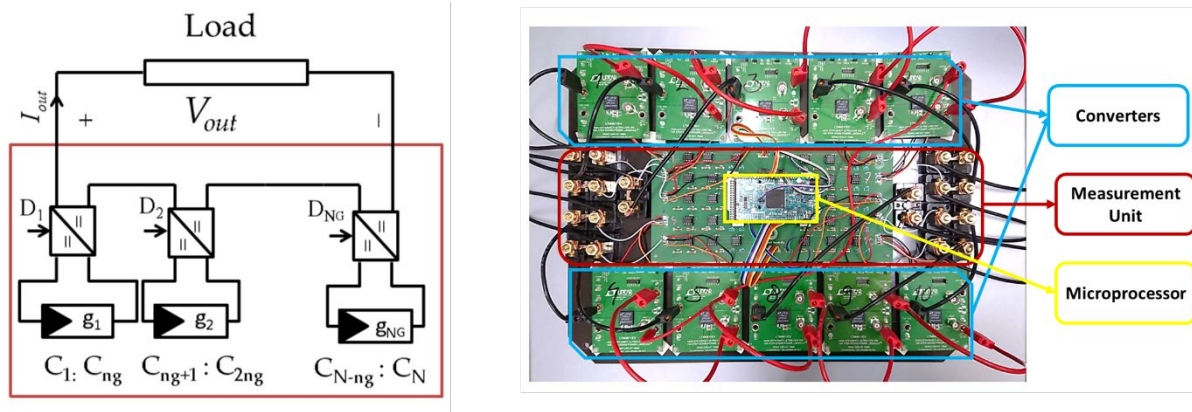


Figure 32: Design of groups of cells in the smart module and electronics design [53].

Experimental results have shown that when a PV cell string is under a maximum power point tracking control, hot spotting in a single cell results in an increase of capacitance and DC impedance. This may be used to detect the hot spot in real time by implementing appropriate tools to measure both I-V curve and capacitance in the cells. To obtain a fair comparison, the test module design is divided into two sections, a smart, and a conventional section which is equipped with two BD. In the smart section (see Figure 33), each group of six cells is connected to one DC/DC converter and all converters are connected in series to their output side. This smart module implements a sweep method MPPT algorithm per group of cells and has been simulated, prototyped on the module level and practically outdoor tested within a short time frame [53, 54].



Figure 33: Cell sectors in the smart module, pole and bird droppings shading scenarios [53].

Different shading patterns are applied in the testing. Furthermore, a test run is conducted without any shading. To be able to compare the results of both halves of the module it is imperative that both halves receive the same shading pattern. This rules out the possibility of using natural fouling sources during the tests because this would result in a random and most likely different pattern for both halves [56]. At the start of testing each pattern the panel is cleaned to minimize the effect of natural fouling build-up. The following shading patterns are tested during this research: (i) A pole shadow as shown in the middle of Figure 33; (ii) A heterogeneous non-transparent pattern to represent the effect of bird droppings in the right photograph of Figure 33, or moss growth etc.; (iii) A homogeneous semi-transparent pattern, a mosquito curtain is placed across the entire panel.



Measurement results

The results showed a significant increase in the output power under partial shading conditions, compared to a conventional panel. The measured irradiance in the plane of the module and the temperature of the module throughout the testing day are shown in Figure 34. Some intermittent cloud coverage occurred during the testing day which results in the fluctuations in irradiance. Furthermore, the temperature of the module also changed throughout the day. These changing conditions make the data and results not suitable for direct comparison between different test conditions. However, the data recorded from both halves during each test are compared in Tab. 3 since both halves were operating at the same conditions at that time.

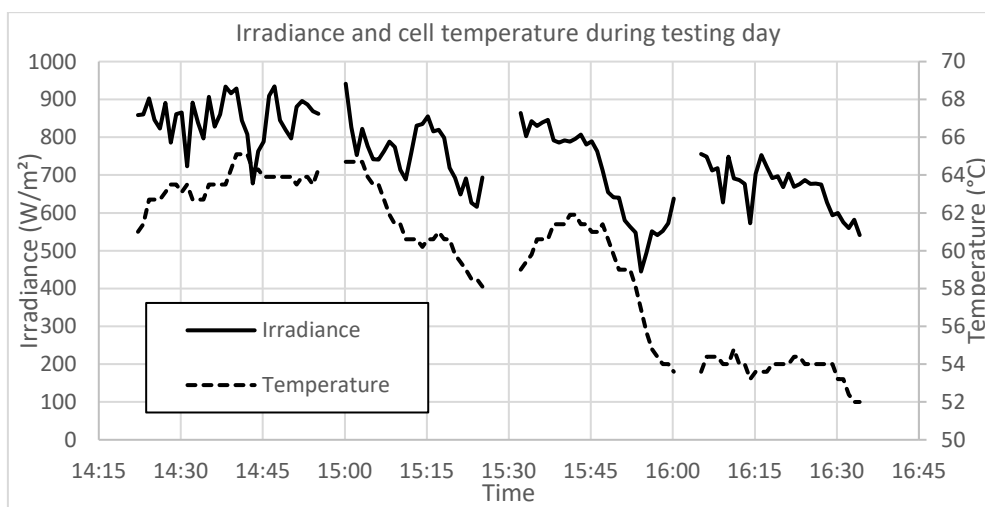


Figure 34: Irradiance in the module plane and average cell temperature during the testing day [54].

During analysis, it was found that group one did not function correctly due to circuit breakage, resulting in lower power output. Consequently, group one was excluded from the results, and only groups two to five were considered. In the latter two tests (bird droppings and homogeneous shade), group five showed significantly higher efficiency, likely due to a measurement error from a faulty voltage divider, rather than actual performance differences. This error led to excluding group five's efficiency from the smart half's average. The smart module's output power was highest during the test without shade, indicating high module temperature also contributed to decreased efficiency.

Table 3: Average efficiency of the module sectors during the tests (see Figure 34).

	G1	G2	G3	G4	G5	Smart	Conven-tional	Ratio Smart/conv.
No shade	3.4%	5.7%	6.3%	4.6%	5.8%	5.6%	5.2%	108%
Pole shade	4.6%	6.9%	8.3%	6.0%	6.7%	7.0%	5.3%	131%
Bird droppings	5.7%	8.0%	7.5%	7.2%	11.3%	7.6%	5.8%	132%
Homogenous fouling	4.2%	5.3%	7.0%	7.0%	10.1%	6.4%	4.4%	146%



During the four tests, the cells of the module were grouped as shown in Figure 33, and IR images were taken at the start and end of each test. These IR images of the test pole shade and bird droppings are shown in Figure 35 and Figure 36 and used the same temperature colour scale. In the bird droppings test, a hotspot developed on the conventional side but not on the smart side in Group 5. Measurement points M1 and M2 in Figure 36 showed a temperature difference of 4.1°C (53.1°C vs. 49.0°C). No other tests resulted in hotspot formation and thus confirms the functionality of the smart module concept.

Chap. 5.4 compares the results of a simulation model based on the solar irradiation measured in the above outdoor test and the electrical design of the smart module for the investigated shading.

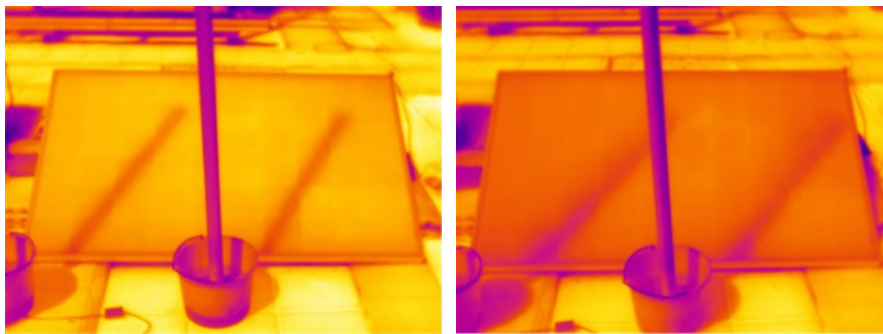


Figure 35: IR image of pole shadow left beginning and right the end of this interval [53].

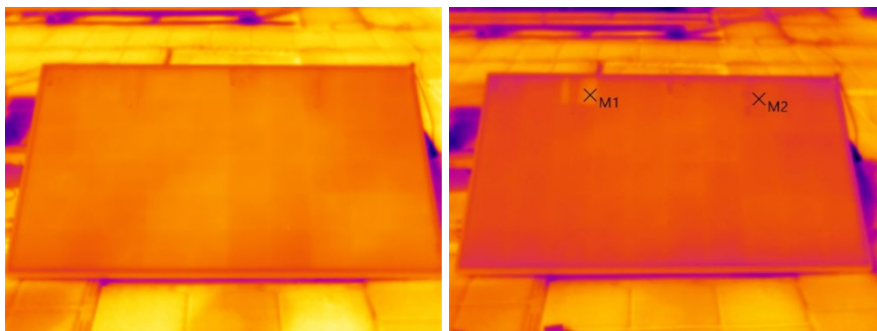


Figure 36: IR image of bird droppings shadow left beginning and right the end of this interval [53].

4.3 Shading with Single-axis Trackers in the MW Power Plant

Previous studies have shown [67] that partial shading in photovoltaic power plants using mechanical trackers is still a non-solved issue. Therefore, changes in the algorithms should be implemented to accommodate them to local conditions so as the loss of associated energy gets reduced. To deal with this inconvenience, the facilities managed and operated by ATAMOSTEC in the Atacama Desert were used to test new tracking algorithms to prevent partial shading among the single axis tracking structures often used in the implementation of photovoltaic power plants. Specifically, the Lalcktur power plant was used for this purpose. Lalcktur is a 1 MWp photovoltaic power plant composed of four power blocks of 250 kWp each with a single tracking system. In this plant, 48 Refusol string inverters, each one of a rated power of 15 kW, three Huawei string inverters with a rated power of 60 kW each, and two more Huawei string inverters, one with a rated power of 30 kW and the other one with a rated power of 40 kW,



were installed and monitored to provide evidence if there are differences in the power generated among the strings and power blocks of the plant.

The current tracking system is shown in Figure 37a and the distribution of the inverters throughout the facility in Figure 37b. The terrain where the plant was installed is not completely flat. In fact, the power blocks at the bottom of Figure 37b are in a higher altitude than those in the top of the same Figure. Consequently, during the morning and the afternoon the bottom power blocks partially shade the top power blocks, reducing the power/energy generated by these.

Chap. 7.1 shows by what factor the performance could be increased by developing a new tracking algorithm that avoids partial shading.



a)



b)

Figure 37: The Lalcktur power plant used to test the new tracking algorithm. a) Tracking system implemented and distribution of the modules on one of the power blocks. b) Aerial view and distribution of the inverters within it.



5 Annual Simulations and Performance

5.1 Commercial Simulation Tools

The commercial PV planning tools that professional planners use for PV power plant design have also been developed to correctly simulate the shadow cast by shading objects over the PV generator. Initially, some were content to simply calculate the percentage reduction in annual irradiation per PV module. However, if the exact mounting position, portrait or landscape and the correct position of the bypass diode and the orientation of the protected substrings in the module can be entered, it should also be possible to correctly simulate the current-voltage characteristic of each module and thus of the string, as has been possible for years with PVsyst, for example [2].

However, since these tools today have implemented the data sheet specifications of the manufacturers of the power electronics components, which is usually excellent for the simple SINV including the DC voltage dependency, this cannot be confirmed for the MLPE. The current 2024 versions of PVsyst, PVsol or PVCASE have implemented the overrated data sheet efficiencies of weighted DC/DC optimisers of typical 99%, which does not correspond to reality as explained in detail in Chap. 3.3. PVsyst has started to implement efficiencies lower than the typical 99% official datasheet values for DC/DC converter conversion factors other than 1 in the software. However, the resulting values are still about 1.5% too high compared to the figures in Chap. 3.3. In addition, MLPE manufacturers are expected to provide all customers with transparent, correct and independently verified parameters. Chap. 5.2 compares a simulation tool developed at the ZHAW with realistic efficiencies of the power electronics components at the respective operating points with the annual performance simulation of commercial PV planning tools, with considerable deviations. In addition, two other PV shading simulations from research institutions are also presented in this chapter.

A good agreement between the comparison of SINV and MLPE system designs for the same shading situation of a tilted roof with chimney could be confirmed for the annual performance between the results of the tools from ZHAW PVShade and those of the ISE Zenith.

5.2 ZHAW PVshade Simulations

A part of the research of the ZHAW PV shading and MLPE analysis include the comparison of the annual simulation results of the conventional string inverter system (SINV) and the fully equipped power optimiser system (allMLPE). With the irradiance measurement data of Kloten, Zurich, various shading scenarios (with either thirteen 400 W Modules for the chimney case, twelve 350 W modules for the Tree 1 and Dormer (L) cases, or ten 350 W modules for the rest mounted in landscape position, details see [22]) were evaluated for the previously mentioned PV system configurations, which are presented by Table 4. The cases are arranged by severity of shading, described by the shading ratio see Eq. 3. The results include the energy production of the PV plant without shading and losses, the shaded PV system without losses on the DC side (sum of individual MPPs of all PV modules), as well as of the allMLPE system and SINV system with losses (details see [22]). Finally, the MLPE gain [%] is given including losses, which shows the additional relative energy by the allMLPE system compared to the SINV.



Table 4: Annual ZHAW PVshade simulation results of eight shading cases equipped with full cell PV modules for the two power electronic system setups allMLPE and SINV systems are shown [22]. See illustration of the cases in Appendix Figure 66. Definition of $SI_{DC,max}$ see Eq. 3.

Cases	No:	Shading Severity	Shading index $SI_{DC,Max}$ [%]	Simulated annual yield [kWh]				MLPE Gain [%]
				no shading & no loss [kWh]	no losses [kWh]	allMLPE [kWh]	SINV [kWh]	
Dormer (s)	1	Low	0.9	4410	4368	4207	4247	-1.0
Vent. Pipe	2	Low	2.9	4410	4282	4122	4129	-0.2
Chimney	3	Low	3.6	6337	6109	5904	5858	0.8
Tree 1	4	Medium	5.0	5295	5029	4862	4802	1.3
Tree 2	5	Medium	6.0	4410	4145	3987	3926	1.5
Building	6	Medium	7.9	4410	4062	3905	3802	2.7
Dormer (L)	7	Heavy	9.1	5295	4812	4643	4435	4.7
Roof Edge	8	Heavy	12.7	4410	3847	3693	3621	2.0

The numerical measure that was used to define the severity of shading, was the Shading Index $SI_{DC,Max}$, which is a formulation based on the Shading Index SI by NREL and defined as described by Equation (5) [56].

$$SI_{DC,Max} [\%] = \left(1 - \frac{\sum_{t=0}^{T=1yr} \sum_{i=1}^{k=nModules} P_{Mod,i,MPP,shaded}(t)}{\sum_{t=0}^{T=1yr} \sum_{i=1}^{k=nModules} P_{Mod,i,MPP,unshaded}(t)} \right) * 100 \quad (5)$$

In general, the greater the impact of shading, the higher is the performance of the allMLPE relative to the SINV system. Notably, the “Roof Edge” case contradicts the mentioned generalization, which is due to the reason that the partial shading of each PV module is identical for most instances during the year. This specific condition decreases the improvements by the module-level control of the power optimisers in comparison to the central control by the conventional string inverter system without MLPE, which indicates that with increasing variance in power of every PV module, also the annual energy gain of the module-level power electronics becomes greater.

For the results of partially shaded PV systems, a high-resolution shading analysis tool for simulations of PV systems was used, which has been developed at ZHAW IEFÉ and continuously improved since 2019. In detail, the simulation tool was created within the Mathworks Matlab environment [57] and is based on Carigiet [58], whereby the simulated PV system, including shading objects are modelled in 3-dimensional space, based on existing systems and the shading situations are calculated for each position of the sun during the year with any temporal resolution. Global horizontal irradiance data provided by MeteoSwiss, the Swiss meteorological service [59], are used and transposed to the PV plane for each time stamp using the transposition model by Ineichen and Perez [60]. The shadings on the PV module plane are calculated in such a way that there is no rasterization of the module plane, resulting in the highest possible resolution. Accordingly, the accuracy of the shading is only dependent on how accurate the convex shading object is modelled. Furthermore, based on the shading situation at each time step, the reduction of direct irradiance is determined for each solar cell in each PV module. Finally, the reduced direct irradiance together with the diffuse light, the ambient temperature, and the electrical configuration of the PV modules in the string are used to calculate the I-V curves.



As shown in Chapter 6.4, Figure 47, when using SINV, a higher string power in the global MPP can be achieved by slightly reducing the module current using the MPP algorithm. This is achieved because the slightly shaded module does not activate the bypass diode in the series connection and thus a higher string voltage is possible, which in some rare cases can bring yield benefits. In the yield calculation of the ZHAW PVshade tool, this finding of the optimal global MPP is always included in the SINV annual yield analysis.

To evaluate the overall accuracy of the ZHAW PVshade tool and to assess the correctness of the shading simulation and MLPE performance by commercial tools, a comparison to PVSyst and PVSol was realized for the partially shaded PV systems visualized in Figure 38.

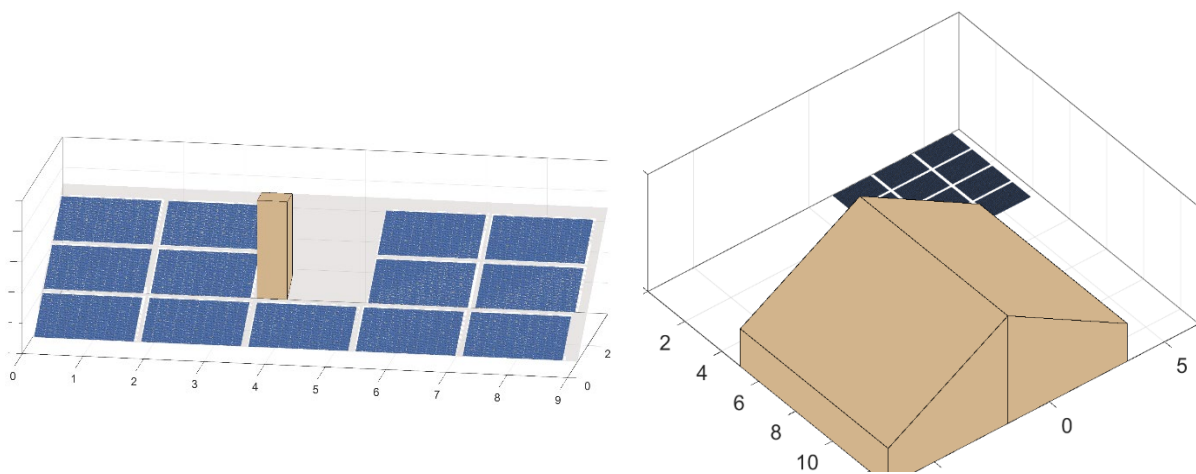


Figure 38: PV simulation cases for weak (left) and heavy shading (right), which were simulated with the same meteorological data, PV modules, as well as power electronic components in PVSyst, PVSol and the ZHAW PVshade tool [22].

In Table 5, the simulation results of ZHAW PVshade, PVSyst and PVSol for the two shading cases are shown based on their degree of shading, namely Shading Index ($SI_{DC,Max}$). The so-called Shading Adaption Efficiency (SAE) was introduced [19] to compare the individual performance to the three system concepts. It gives the ratio of output AC power versus the maximum available sum of aggregated DC power from each of the k PV modules in the string if all of them are operated in their individual absolute MPP. The SAE could have an efficiency of less than 100% with partial shading of a SINV string, even with a lossless DC/AC inverter. In contrast, a lossless MLPE would achieve a value of 100% for SAE for both DC/DC and DC/AC in this hypothetical case.

The SAE may also be defined on the DC output of the string and not on the AC output, as discussed in Chap. 7.1 and Figure 56 to Figure 59.

$$h_{SAE} = \frac{P_{ac}}{\sum_{i=0}^k P_{mod,i}} * 100 \quad (6)$$



Table 5: Comparison of the annual simulation results of the ZHAW PVshade simulation tool, as well as of the commercial tools, PVSyst and PVSol, presented as Shading Adaption Efficiency (SAE) and annual MLPE yield gain, for the same setup and system configuration of two different shading cases [14, 22]. The PVSyst indMLPE results are approximated, as the tool was not capable of modelling MLPE systems with partially installed power optimisers at the time of the analysis.

Case	Shading Index $SI_{DC,Max}$ [%]	SINV SAE [%]	allMLPE MLPE gain [%]				indMLPE MLPE gain [%]			
			SAE [%]	PV shade	PV- Syst	PV- Sol	SAE [%]	PV shade	PV- Syst	PV- Sol
Weak Shading	2.8	96.0	96.6	+0.6	+3.3	+4.3	96.6	+1.0	(+1.6)*	+2.1
Heavy Shading	9.0	94.4	96.5	+2.2	+7.2	+14.6	96.1	+1.8	(+4.1)*	+12.1

It is noteworthy that the differences in the MLPE gain between PVSyst and PVshade are in the range of 2.3% - 5% of additional annual yield gain by PVSyst. Accordingly, the difference is similar to the difference in the datasheet efficiency values of the power optimisers (max. 99.5% and weighted eff. 99 %) and the general efficiency values in the regular operation points of approximately -0.5 to -2.5%, or lower for a power of less than 60 W measured in the indoor laboratory at ZHAW. Today's commercial PV tools generally only include one value for all MLPEs in the system, the weighted efficiency according to the MLPE data sheet, and do not take into account the much higher losses at the actual individual operating points.

On the other hand, the great differences between PVshade and PVSol (up to 12.6% in annual MLPE gain) or between PVSyst and PVSol (up to 8% in annual MLPE gain) are only partially caused by an overestimation of MLPE performance. Mainly it is based on the incorrect calculation of shading and its effects on the PV modules by PVSol. In detail, the severity of shading is not evaluated individually at each PV cell with consideration to the substring configuration by PVSol as it is done in PVshade or for the maximum shaded PV cell within each substring by PVSyst, but only as a fraction of the entire PV module area. Accordingly, shading of a PV system is only roughly estimated with a substantial margin of error and thus, the commercial tools today are not usable for PV systems affected by shading for detailed PV design recommendations.

5.3 Zenit Fraunhofer ISE Simulations

The tasks undertaken at the Fraunhofer ISE revolve around the usage and adaptation of the PV power plant yield analysis tool Zenit© [61], a custom developed Python environment capable of being flexibly adapted to unique power plant scenarios. Zenit offers comprehensive capabilities for simulating photovoltaic (PV) power plants. It provides detailed PV module modelling, capturing the performance characteristics of various PV technologies under different environmental conditions. Users can design and configure different types of PV systems, including ground-mounted, rooftop, and building-integrated setups. The tool calculates energy yield based on local solar irradiance data while considering factors like shading, tilt angle, and module orientation.

Zenit also allows for detailed performance analysis of PV power plants, assessing efficiency, energy production, and degradation over time. It can simulate interactions between PV systems and other



energy components such as storage units, grid connections, and other renewable sources. Economic analysis features evaluate investment costs, operational expenses, and financial returns. Additionally, Zenit supports scenario analysis to explore the impact of various design choices, operational strategies, and environmental conditions on PV power plant performance, making it a valuable resource for planning and optimizing renewable energy projects.

As a first step, the complex shading scenario of the task was modelled in Zenit's ray-tracing environment with the aim of calculating cell-resolved light distribution values and a resulting shading rate. The Case 3 chimney example, in Tab. 3 and Figure 53 and Figure 14, was selected as the most relevant for initial development and subsequent analysis work, and a sample rendering of the simplified rooftop/chimney scene is depicted in the following Figure 39. For calculating the effective shading rate of individual modules, incident irradiation at every cell is taken from a ray tracer output and divided by an unshaded reference value. As a next step, the residual power of the modules is estimated by a calibrated set of "critical part" lookup tables, which are in essence a collection of inputs derived from PV module simulations as detailed in [5]. The use of lookup tables is motivated by the desire to strike a balance between computational efforts and accuracy.

With light availability, its distribution, and residual power values as inputs, a subsequent yield calculation as a function of shading conditions can be derived for heterogeneous light scenarios. For the electrical configuration considering MLPE across the board, an annual yield of 5949 kWh was attained, whereas the string inverter layout resulted in 5884 kWh, showing a roughly 1.1% boost in yield attained by an all MLPE system. Compared with the results from the ZHAW PVshade simulations in Table 3 (5904 kWh, 5858 kWh, and 0.8%), a high degree of both absolute and relative overlap is apparent, despite the significantly different methodologies employed. This speaks for applicability of both tools in such complex shading scenarios.

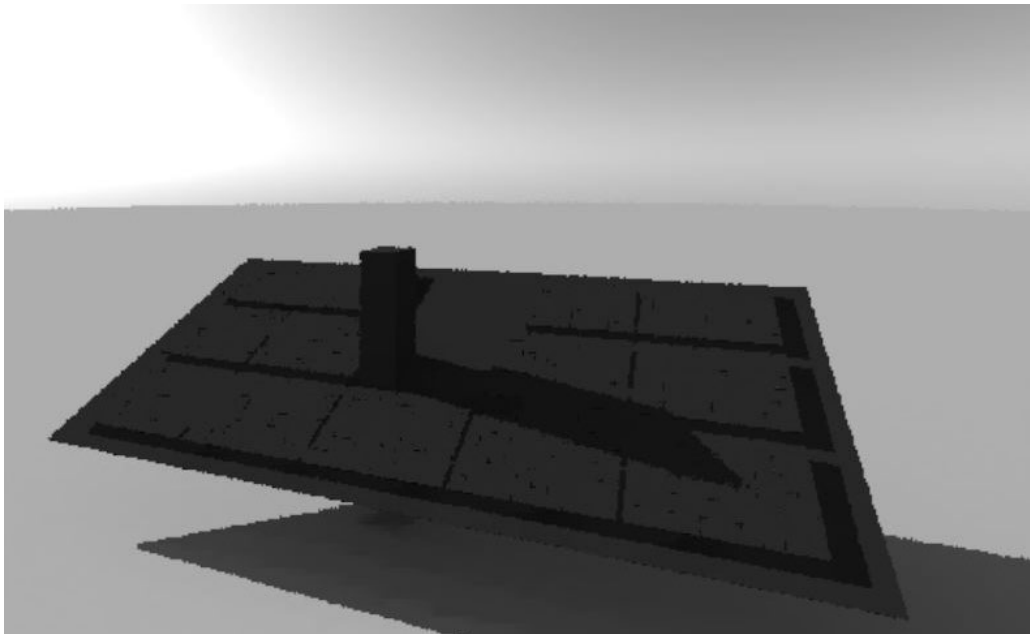


Figure 39: Single timestep rendering of the cell-resolved light simulation in the Case 3 rooftop chimney analysis.



5.4 Simulation of Shading Tolerant Modules

In Chap. 4.3 outdoor measurement results of standard PV modules and a smart test module are discussed under different shading conditions. The research group developed a simulation tool for this smart module (Figure 32) and validation with this test results (Figure 33) will be discussed here in detail [54]. If the result is promising, the smart module designed in future could be improved, e.g. by choosing the optimum number of solar cells per substring.

A model for the complete smart module considering the groups designed before has been modified allowing to include temperature difference effects between different cells. The temperature variation in this model is a function of both ambient temperature and heat arising from electronics elements. Measured data are implemented in the model and a comparison between the developed smart module and a standard series-connected module available in the market is made.

For modelling the smart module, a surface of the 60-cell module is considered to consist of 600,000 pixels, which means that each solar cell has 10,000 pixels (ignoring inter-cell distances for simplicity). The irradiation level on pixel p is called G_p and is given in Equation 6:

$$G_p = \begin{cases} G_{p,GHI} & \text{if it is not shaded} \\ G_{p,s} & \text{if it is shaded} \end{cases} \quad (6)$$

where $G_{p,GHI}$ is the global horizontal irradiance (GHI) at the pixel and $G_{p,s}$ the irradiance at the pixel under the shaded condition.

To calculate the irradiation level on each cell Equation 7 is used, which is based on experimental results from a study by Sinapis et al. [55].

$$G_c = (F_{unshaded} \times G_{GHI}) + (F_{shaded} \times G_{dif}) \quad (7)$$

where $F_{unshaded}$ is the unshaded fraction of cell, F_{shaded} is the shaded fraction of cell, G_{GHI} is the global horizontal irradiance, G_{dif} is the diffuse irradiance at the cell C . The cell with the lowest short-circuit current in each serially connected group N_i , which is usually the most shaded cell, determines the output current of that group.

In this study two different realistic shading conditions are considered: (1) Random shadow, which might result from the effect of dust, bird droppings, snow, etc.; and (2) pole shadow, which is caused by a static obstacle during daylight, and which is mostly caused by pole shapes, chimneys, dormers, or a part of the building on the roof. Also, these shading conditions can be combined.

The recorded irradiance data from the experiments are shown in Figure 40, with three 15-minute time frames used for shading experiments. From Figure 41 to Figure 43, different shading patterns and their impact on groups of PV cells for various architectures can be seen. Figure 41 shows a combination of pole and random shadows, while Figure 42 only shows pole shadow effects. Table 6 presents the output power for the three-time frames. In time frame 1, the series-connected architecture performs poorly due to bypass diodes, significantly affecting both current and voltage. Cells under darker shadows are bypassed, resulting in very low current due to shading. Each time frame represents a 15-minute period with constant irradiation variables.

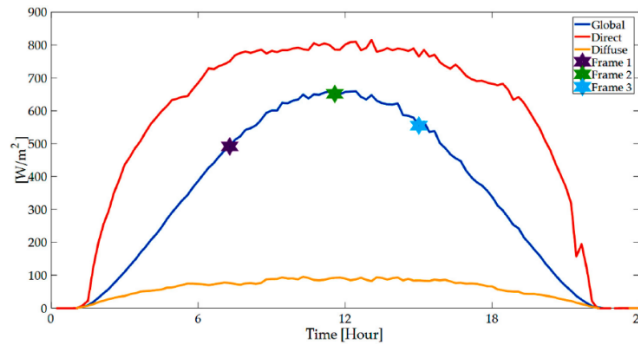


Figure 40 Global, Direct and Diffuse irradiation levels during the experiments (see Fig. 31)

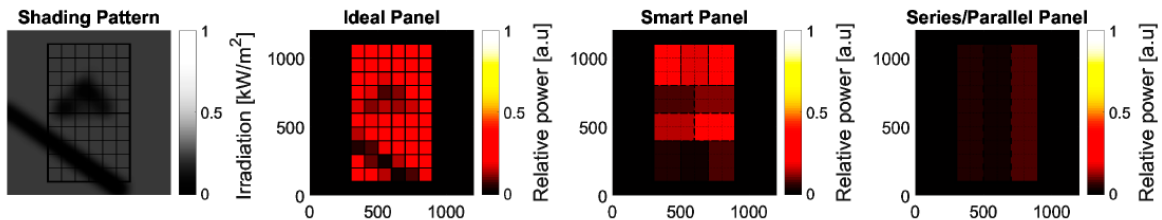


Figure 41 Combined pole and random shading patterns and effect of that on different architectures at time frame 1

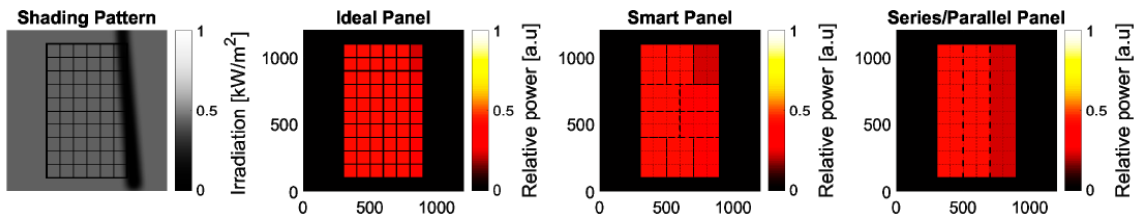


Figure 42 Pole shading pattern and effect of that on different architectures at time frame 2

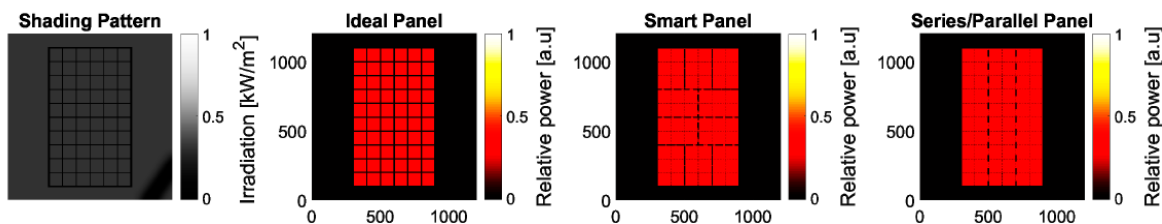


Figure 43 Pole shading pattern and effect of that on different architectures at time frame 3. Note that the shade is not cast on the panel.

Table 6 Output power in the three time frames indicated in Figure 40.

Architecture	Frame (1) [W]	Frame (2) [W]	Frame (3) [W]
Ideal Architecture	48.35	84.23	116.54
Smart Architecture	18.49	69	108.85
Series Connected Architecture	0.84	30.95	112.35
Parallel Connected Architecture	4.51	62.97	113.42



6 Advantages and Disadvantages of MLPE Systems

6.1 Lifetime and Failure

The comparison of 1526 inverters without optimisers with 237 inverters with optimisers operating residential and small commercial systems in Switzerland shows a failure rate around twice as high for the system with optimisers (Figure 44), [62]. This is not due to the low reliability of the optimisers, but to their high number. Figure 45 shows that a single optimiser has a very low failure rate. Figure 47 shows that around 20 optimisers together have the same failure rate as an inverter.

The comparison of optimisers and inverters must be viewed with caution, as like is not compared with like. In some points the comparison favours the inverters, in some points the comparison favours the optimisers. The following points are emphasised in the paper:

- The comparison considers an energy-relevant fault, which typically must be rectified by a specialist, as a failure. While the system with optimisers continues to run (a defective optimiser typically bypasses the PV module), the system without optimisers usually switches itself off. However, an inverter can often be repaired, whereas an optimiser must be replaced.
- Systems with optimisers also require an additional inverter. Figure 44 and Figure 45, which attest to the high reliability of the optimisers, do not consider the additional failure rate of the inverters.
- The number of optimisers in a system has a significant influence on the failure rate (Figure 46). If a system only has very few optimisers, the reliability should not be significantly impaired compared to a system without optimisers.

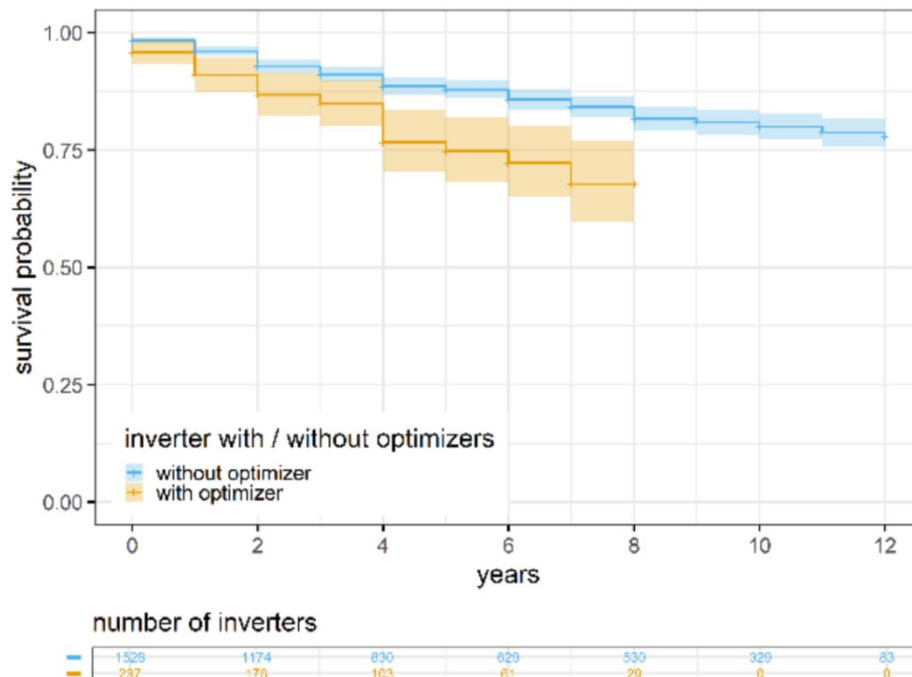


Figure 44: Survival probability for systems with and without optimisers [62].

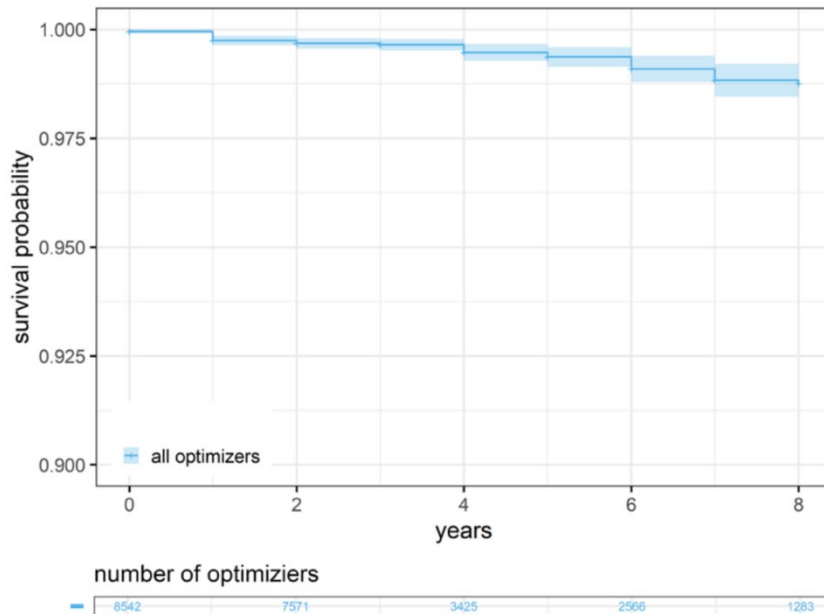


Figure 45: Survival probability of all optimisers (without inverter) [62].

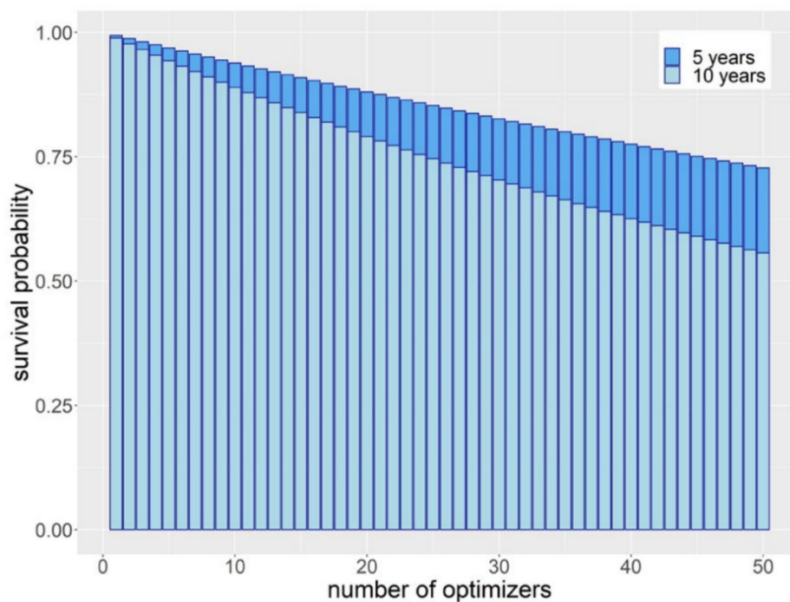


Figure 46: Survival probability after 5 and 10 years for a given number of optimisers (without inverter) [62].

Manufacturers promise improvements in terms of reliability and service life. For example, SolarEdge states that the number of components in the power optimisers will be reduced from generation to generation, thereby increasing reliability. The warranty period of 25 years also corresponds to the typical



warranty of a PV module. For the benefit of the end customer, future independent studies on the reliability of MLPE and SINV should provide meaningful failure rate data. These studies must closely consider the specific generations of the products, not just the manufacturer.

6.2 System Costs and LCOE

A cost analysis in [49] showed additional costs of 5% for the hardware for the MLPE system on a typical detached house in Switzerland compared to SINV. This means that the MLPE system would have to generate an additional annual yield of 5%, which only applies to the small market share of heavily shaded PV roofs (see Chap. 5.2 Table 3 and Figure 62). This does not consider the additional time required for the additional installation of the MLPE behind the PV module, its identification at the exact installation location and its integration into the data system. Of course, this exact allocation of the power optimiser to be replaced helps in the event of servicing, but the total costs, especially the working time on the roof and the possible implementation of fall protection, are significantly more expensive, as compared to the installation time for replacing a SINV in the building. Still, it can maximize the absolute annual yield of the power plant.

6.3 Shading Induced Hotspot Effect

In the IEA report PVPS Task 13 “Quantification of Technical Risks in PV Power Systems”, numerous errors resulting from the hotspot due to shading were specified as follows: glass breakage, burn marks, bypass diode failures, arcing or fire as well as an acceleration of the module aging process, resulting in higher degradation rates [63]. In most cases, they found an annual yield loss of up to 5% and in very few cases of massive shading due to improper module placement (see page 104 in [63]) even 20-30%.

This means that there can be two competing interests in the PV plant design, on the one hand the avoidance of hotspot effects in order to prevent the damage described above or the use of control strategies for MLPEs that have the avoidance of hotspots as their main objective. If the former is pursued, then the module operating points that provide the absolute MPP are not approached, as they would result in a hot spot with an activated bypass diode, e.g. with high module currents, see Chap. 3.5. If these operating points are therefore avoided, these possible yield gains cannot be achieved with these module types.

Due to the current-voltage characteristics of the state-of-the-art solar module equipped with three bypass-diodes, see Figure 1, which is only affected by very slight shading, specifically with of one single solar cell, typically less than approx. 14% depending on the number of series connected PV modules, the SINV can increase the electrical power when regulating to a higher string voltage. Allenspach has demonstrated a more complex and realistic practical shading situation in detail in [22], as shown in Figure 47 for the different PV power electronics topologies SINV, indMLPE and allMLP.

This simulates a PV roof of 20 PV modules producing 280 W at 35 V MPP voltage for the unshaded modules each at this solar irradiance condition. Three of the modules are shaded by a dormer reducing the current at MPP in the shaded part of the submodule string to 7.1 A and two of them shaded by a ventilation pipe to 4.1 A. The operating point SINV 1 of a string inverter will only find the MPP at a string voltage of 560 V at only 4400 W on the output of the DC string if tracking the string current in the same range than the unshaded case before.

Another MPP tracking algorithm will search and find the operation point SINV 2 for the string inverter at a higher voltage of 694 V and at a much higher DC string power of 5028 W without using a MLPE. This higher DC voltage is possible due to the improved MPP control algorithm SMA ShadeFix described in [64]. The allMLPE solution will result in a maximum of 5257 W DC power at a fixed DC input voltage of 670 V at the final DC/AC converter due to the buck/boost MLPEs behind each PV butterfly module. The



indMLPE can produce a slightly smaller DC power of 5221 W, with a much smaller number of buck MLPEs.

In summary, the allMLPE and indMLPE systems can improve the DC power of the PV plant in this shading moment by 4.6% and 3.8% respectively. However, due to the additional losses by the conversion of the specific commercial MLPE devices, the performance increase is finally thinned out especially for the allMLPE solution in advantage for the indMLPE on the AC side.

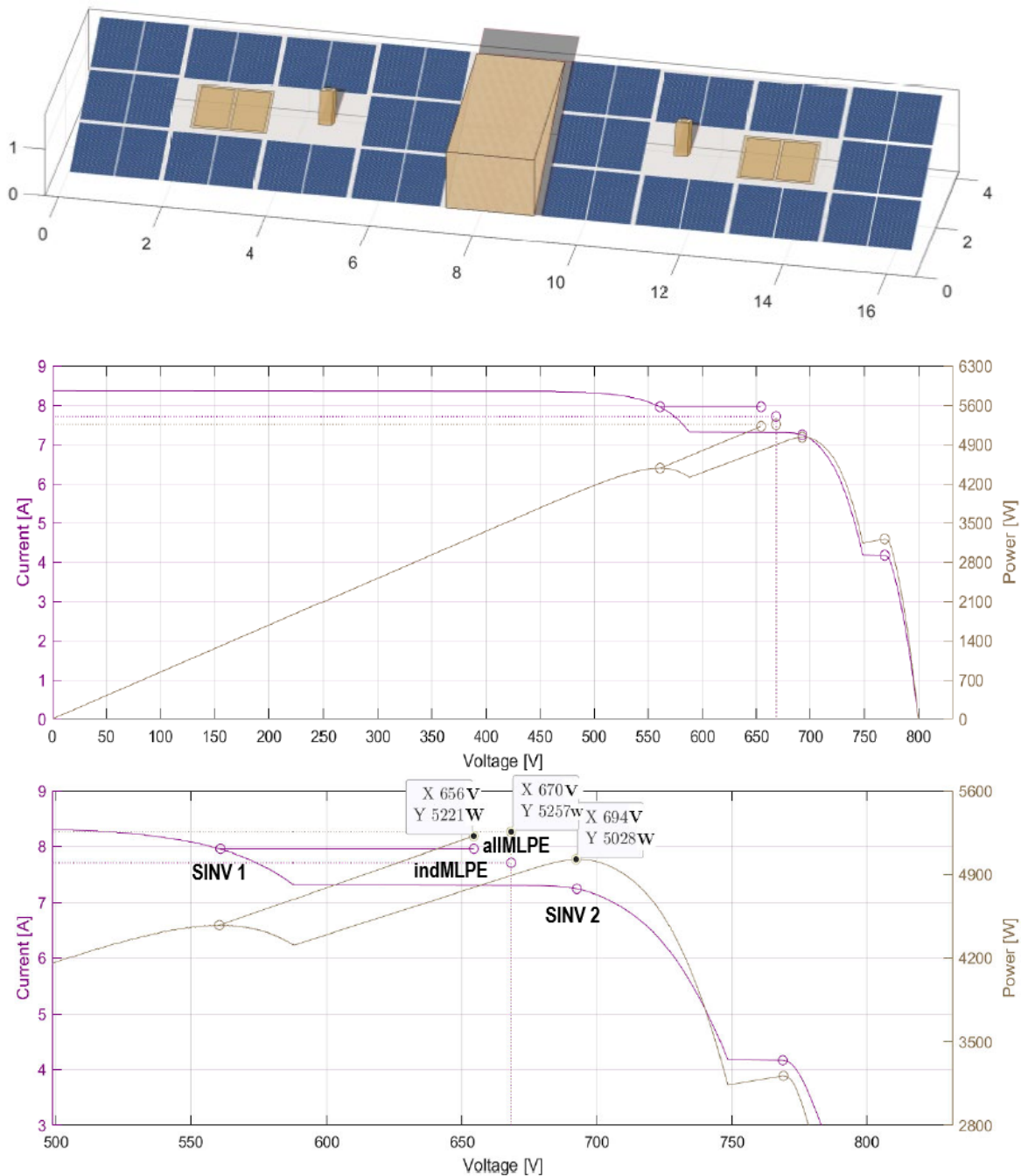


Figure 47: Illustration of solar roof with dormer and two ventilation pipes as shading objects and their current voltage characteristics of the string current and power voltage characteristics with several marked local and absolute MPP's for the different PV power electronic system topologies SINV, indMLPE and allMLPE [22].



Some of the commercial power optimisers and micro inverters products will fail to activate two bypass diodes due to insufficient input voltage range. If their MPP control algorithm will be insufficient to find that maximum power point, or systematically not operate at this high module current, the risk of hot spots can be reduced, as discussed before in this chapter.

In the past, for full-cell modules with high currents, this activation avoidance of the bypass diode was a target-oriented control strategy for the DC/DC optimiser to avoid critical hot spot effects. However, with the introduction of half-cell modules (see discussion in Chap. 2.1), the heating power when the bypass diode is activated has been halved in one fell swoop. This will reduce the critical temperature only in the case of localization of the fault and heat development on a small square millimetre of the cell surface, compared to the performance of full cell modules. This means that a hot spot no longer leads to critical temperature increases for half-cell modules. However, if the heating power is distributed over the full area of the entire cell, as there is no localized punctual failure, the resulting temperature will hardly differ between full and half-cell modules, as the same heating power is available per surface. In the literature, lower hot spot temperatures are determined for half-cell modules based on simulations [71], while the opposite was found by recent experimental field measurements on bifacial half-cells due to hot spot mirroring effects [72]. In the past, the control strategy of DC/DC manufacturers for full-cell modules was not to optimise performance if there was a risk of hotspots, but this should be reconsidered for today's half-cell modules or shading-tolerant modules.

6.4 Safety and Hazards

The following chapters are based on ongoing research by the PV laboratory at the Bern University of Applied Sciences (BFH). They have not yet been published.

6.4.1 Maximum System Voltage

The following measurements and tests were carried out using a SolarEdge system as an example. Up to 50 modules or power optimisers can be connected in series. In the hypothetical case that all 50 power optimisers with the same fault pattern were defective (input = output), string voltages of up to 2500 V could occur. Such voltages are not only above the defined system limits for which the products were specified, but they would also certainly damage components. It is the task of the optimisers to prevent this scenario.

The BFH investigated this situation and carried out test measurements to see whether the bus voltage could rise above the nominal value and how the system would react. This behaviour was provoked by connecting an artificial DC voltage source in series with the optimisers. However, this increase in bus voltage was limited and compensated by the inverter. The system switched off immediately if the maximum system voltage was about to be exceeded. However, the inverter did not send an error message notification, so it may not be possible to trace the reason for the switch-off.

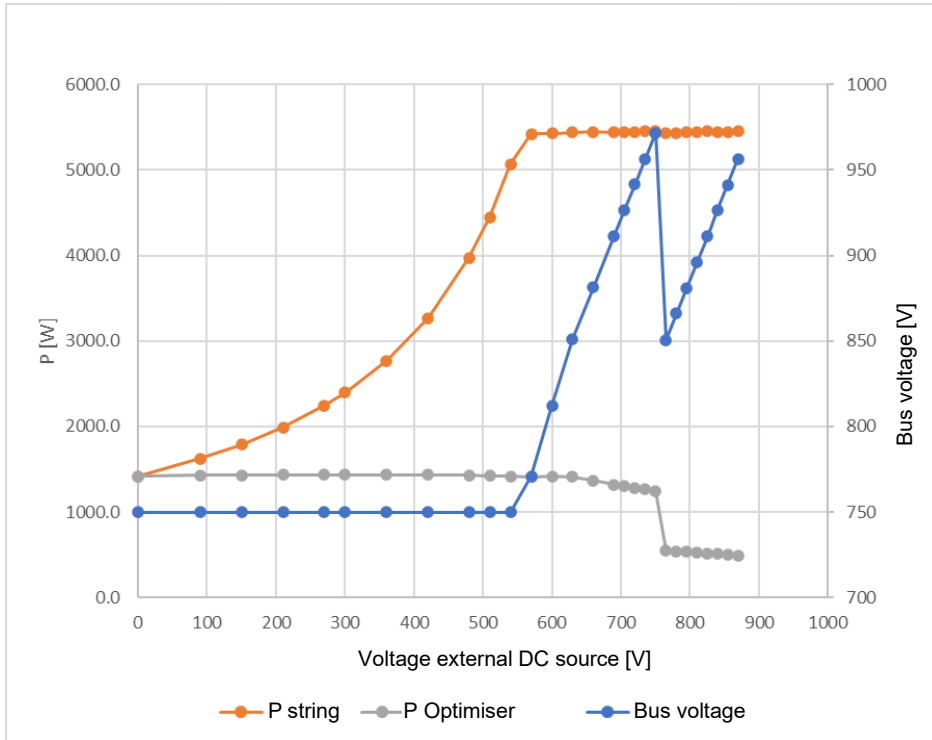


Figure 48: Increase in system DC voltage and power in a SolarEdge system by an artificial, external voltage source. The voltage limitation below the maximum system voltage limit functions reliably in a two-stage process. The system is switched off when about 850-900 V.

6.4.2 SafeDC at System Level

In a second test, the contact protection of the system is tested. Based on the SafeDC functionality, the system is expected to reduce the optimiser output voltage and thereby the string voltage to a safe value in the event of a fault. According to SolarEdge [65], the SafeDC mechanism only works if

- a) the inverter is switched off
- b) the AC mains supply is interrupted and
- c) the ambient temperature of the power optimisers rises above 85°C.

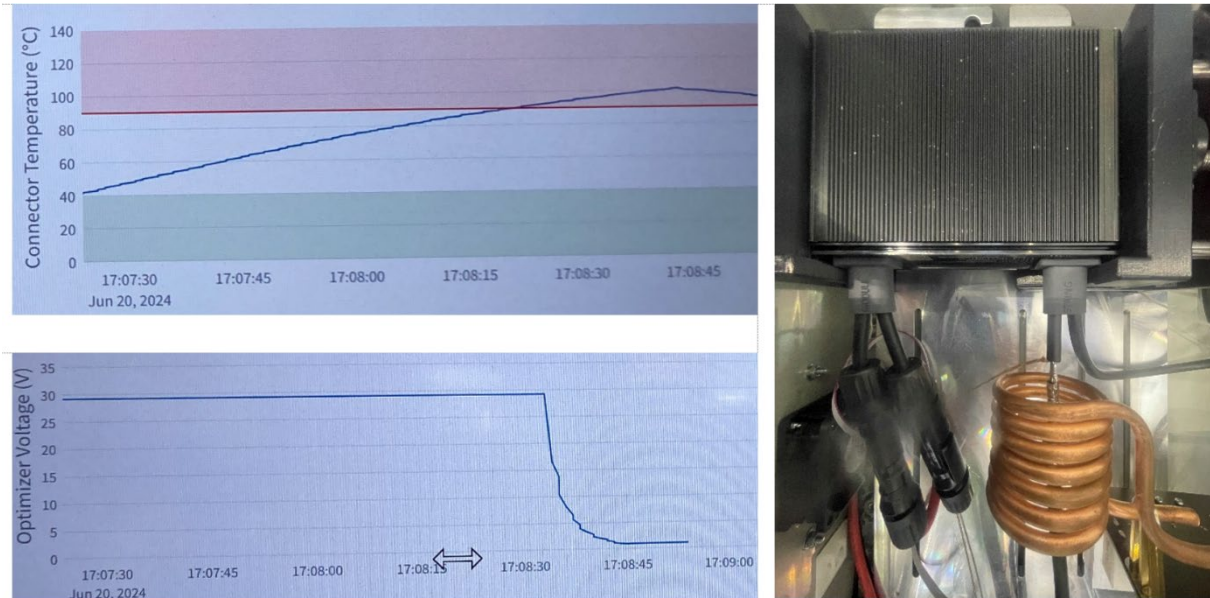


Figure 49: Sense Connect – Live Demo at the booth of SolarEdge at Intersolar Munich, 2024-06-20 showing the safety shutdown of the optimiser voltage at optimiser connector temperature above 90°C. (Foto F. Baumgartner)

Measurements at the BFH PV laboratory show that when the string is disconnected, the optimisers switch individually to SafeDC mode, but the bus voltage is still maintained by the AC mains side. Even the simulated contact of the string cables does not lead to an interruption of the inverter-side power supply to the string cables. The bus voltage is only reduced a few percent and basically kept at 750 VDC (Figure 50).

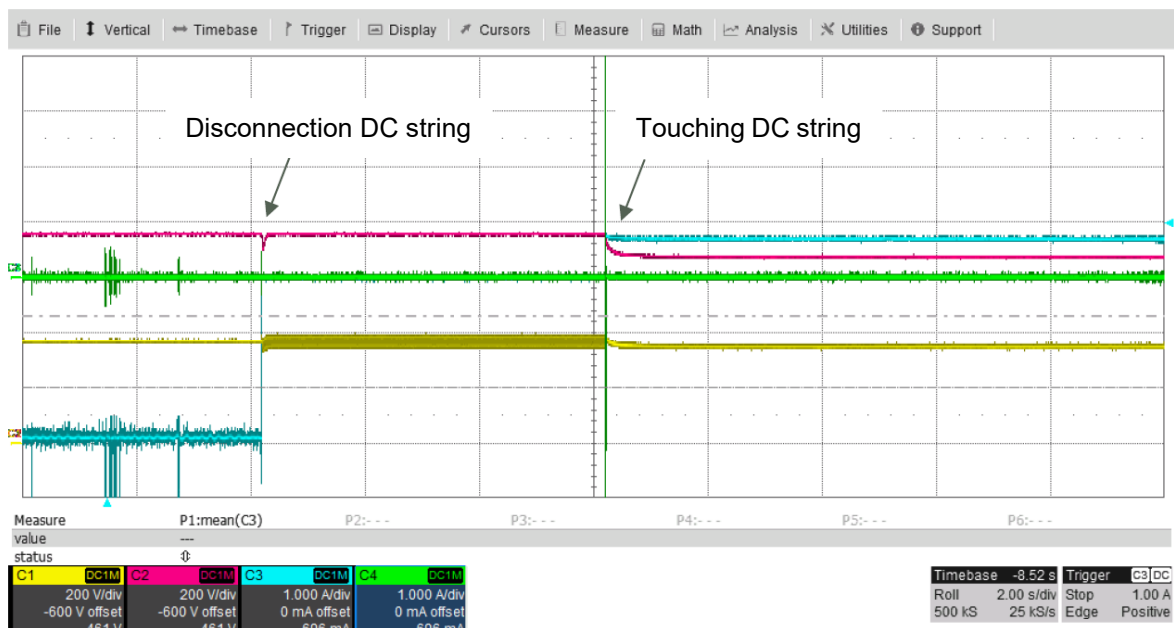


Figure 50: Contact of both active conductors after disconnection of the string with the feet touching the ground. The inverter appears to continue to feed the string from the AC grid side and maintains the system voltage (purple: 750 V).



6.4.3 Arc-fault Detection

In an anonymized comparison test of Arc-Fault Detection (AFCI) [66], the BFH was able to show that a high inductance of the DC lines potentially poses a challenge for the inverter-integrated arc detectors of some test devices. However, up to cable lengths of 200 m, practically all tested inverters, if correctly configured by the manufacturer, recognized, extinguished, and reported most arcs. Basically, the arc detectors of the test devices function satisfactorily and can contribute to an increase in safety in PV systems.

In one device family, however, the AFCI did not work on two out of three inverters with optimisers, despite software activation, until the manufacturer's support team remotely adjusted certain parameters.

6.4.4 Optimiser on Fire

Indicative measurements on three individual power optimisers show a fundamentally robust operating behaviour of the overall system under thermal load of an optimiser. The optimisers measured feed current from the connected PV module into the string up to a certain temperature before switching to idle mode on the primary side after exceeding the temperature. If the temperature in the device is lowered and falls below a lower temperature threshold for a longer period, the heated optimisers contribute to energy generation again – provided they have not become defective due to overheating. The threshold values determined based on the few measurements are presumably 100°C for switching back on after cooling down and 170°C for switching off in the event of overheating. All three optimisers failed after 30 minutes at most and several switch-off/switch-on cycles at temperatures above 200°C. In the defective state, the optimisers under investigation went into idle mode on the primary side and into power consumption (approx. 2.5 W) from the string on the secondary side.

During all tests, the entire system remained in feed-in mode and did not report any faults. This behaviour was also observed when the optimiser was set on fire with a gas burner for a few minutes in the last test. The system was switched off manually after it had been running for two hours without an error message.

6.5 Electromagnetic Emissions and Compatibility

PV systems, like all electronics, generate electromagnetic emissions which can interfere with radio communications and sensitive equipment in their surroundings. EMC, electromagnetic compatibility, is a device's ability to operate within an acceptable limit of electromagnetic emissions for its surroundings. For wide adoption of PV in the built environment, it needs to comply with EMC limits.

A PV system's wiring, loop surface, functional equipotential earthing, choice of module and inverter all affect electromagnetic interference and EMC. A Swedish case-study comparing MLPE, and string inverter systems showed that an MLPE system emitted more electromagnetic interference than a string inverter system [67]. In these tests a SolarEdge MLPE system using an SE-5k-N4 inverter and P505-4RM4MBM optimisers was compared to a Kostal Planticore 5.5 Hybrid string inverter. Both inverter systems used the same experimental setup of 14 PV modules, either unifacial half-cut with an aluminium frame, or bifacial and frameless. It should be noted that after these tests the P505 optimiser was one of several optimiser models that in December of 2021 were banned from further sales and recalled in Sweden by the National Electrical Safety Board (Elsäkerhetsverket) due to their emissions of electromagnetic interference [68].

Currently published results from the study are for a best-case comparison between the systems, they were wired with positive and negative leads as close to each other as possible to minimize the loop surface and the systems were under functional equipotential earthing. Electromagnetic interference was



measured at different positions 10 m away from the systems with an antenna in three different orientation planes: X, Y, and Z. A statistical model was used for analysis using measured peak-values compared to the background interference, and the limit for EMC.

Figure 51 shows the measured interference peaks for both inverters with unifacial PV-modules as a function of frequency. The optimiser systems emitted more electromagnetic interference peaks and exceeded the EMC limit more frequently. Note that both cases exhibited some measurements outside the EMC limit. The study deemed it unlikely that string inverter systems would interfere with radiocommunications, whereas the MLPE inverter system tended to have more emissions and was thus deemed more likely to interfere. It was also observed that the choice of module noticeably impacted emissions, where frameless glass/glass modules had higher emissions than framed glass/back sheet modules.

Further results on MLPE still on the Swedish market and other system configurations are planned for publishing in late 2024.

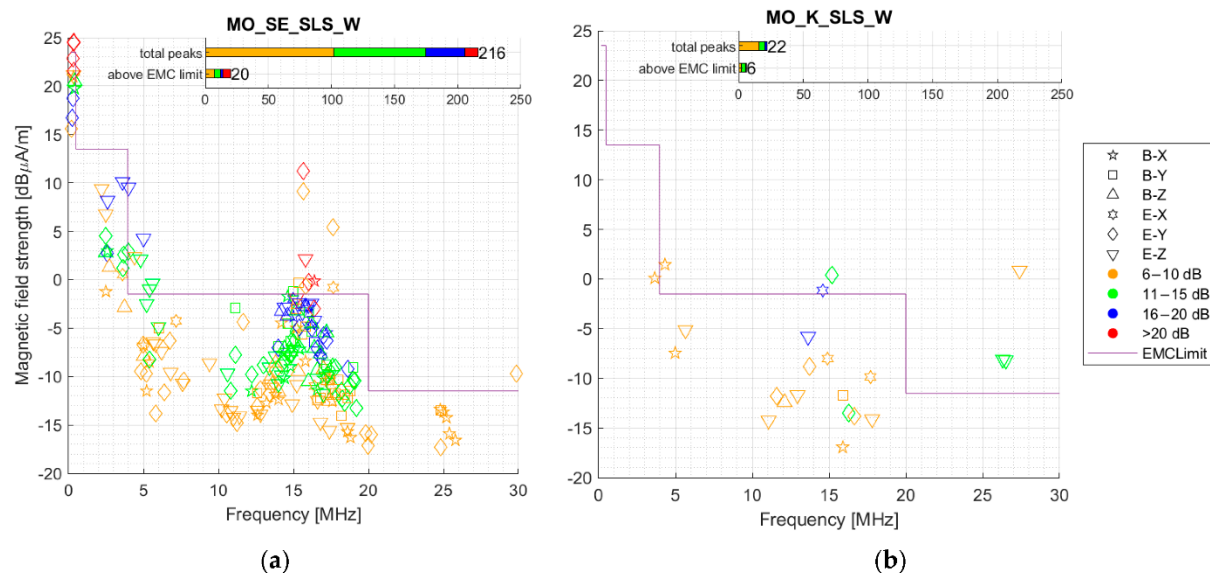


Figure 51: A comparison between two inverter concepts for unifacial and framed PV-modules. (a) MLPE Inverter, (b) String inverter. The colour scale depicts how much the peak interference exceeded the background interference, different symbols depict different measurement locations and antenna orientations [67].



7 Recommendations for PV Installers

7.1 Systems by Severity of Shading

The PV generator should ideally receive unobstructed sunlight to maximize electricity yield. However, this is not always possible on real roofs in built-up areas. Therefore, the PV planner must carefully consider where to place each PV module, especially if there are nearby structures like chimneys or dormers.

Figure 52 shows the simulation results of the annual PV production for 30 cm and 50 cm distance to the module behind the chimney, which is reached by the shade at midday. The results show that the MLPE solution delivers a higher yield in the chimney near position, but at 50 cm distance the SINV is 3% ahead of the MLPE solution with the 30 cm. In practice, it is not sufficient to differentiate only between MLPE and SINV for shading. It is crucial to include the actual losses of the power electronics components used in the calculation, as this can result in differences of 1 to 2% for the same system variant.

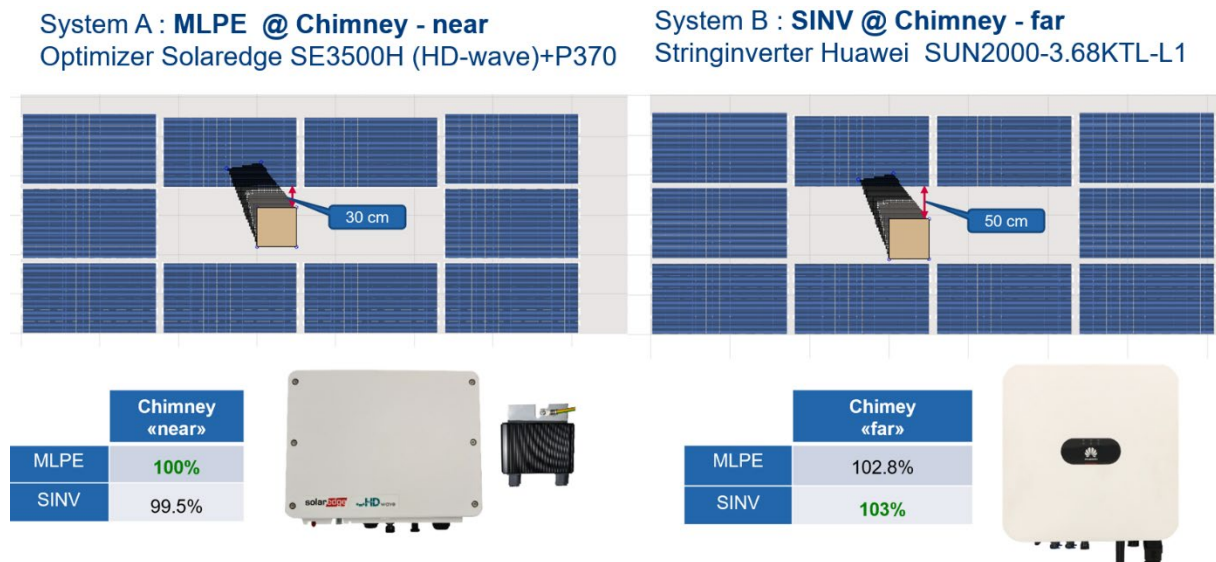


Figure 52: The distance of the shading object to the shaded PV module at high irradiance, for example, a chimney at noon is dominating the annual performance either in advantage for the SINV or the MLPE approach, additionally dependent on the actual effectiveness of the individual conditioner of the used power electronic power conditioner using the ZHAW PVshade tool [48].

The same two SINV and allMLPE components as above in Figure 52 were systematically examined for the position of the chimney in a slightly different module arrangement in Figure 53 at lower shade index; the module on the north side, which could be shaded at midday, is missing. The highest yield advantage of 0.79% is achieved for this allMLPE solution if the chimney is placed in the corner positions of the array. However, a clever positioning of the chimney in the middle can achieve the lowest shading, which then gives the SINV a yield advantage of 0.2%, as the conversion losses of all those MLPEs that never operate shaded modules then lead to annual losses in performance [14]. Another example of performance versus position of a smaller ventilation pipe as a shading object is presented in Figure 54 and the south position of chimney at elevated distance to the small PV generator is given in Figure 55.

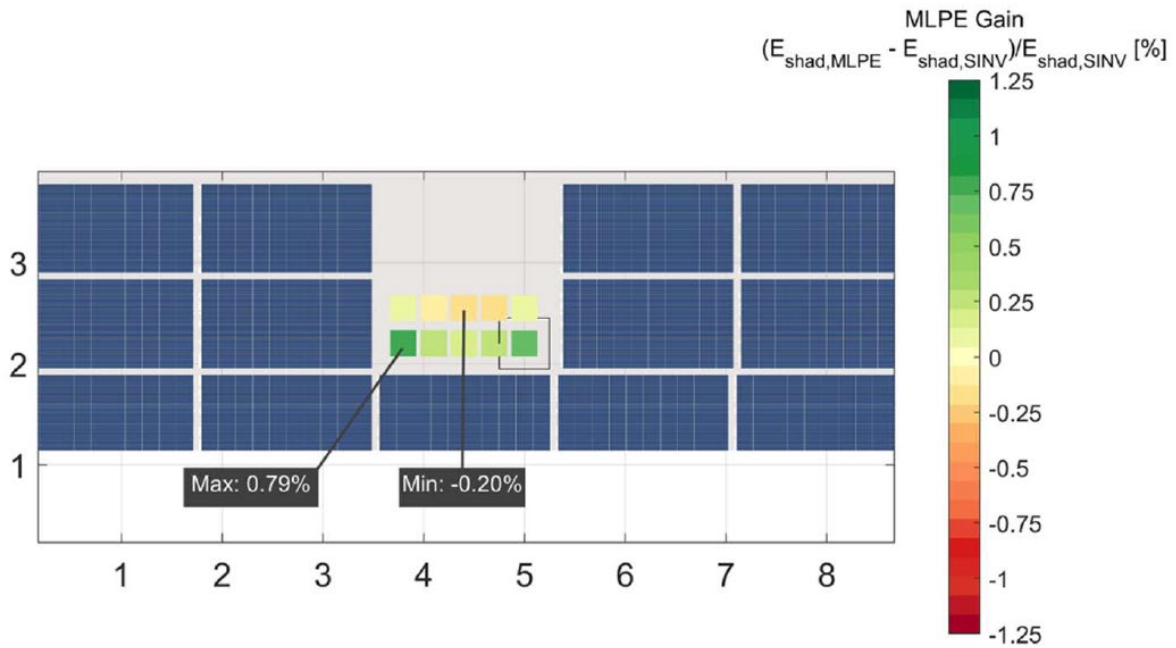


Figure 53: Sensitivity analyses of the position of the chimney to increase the gain in annual performance of allMLPE versus SINV for ten different positions at a horizontal interval 30 cm and vertical 35 cm on the 30° inclined roof. The same commercial components used in the ZHAW PVshade tool like in Figure 51 [14].

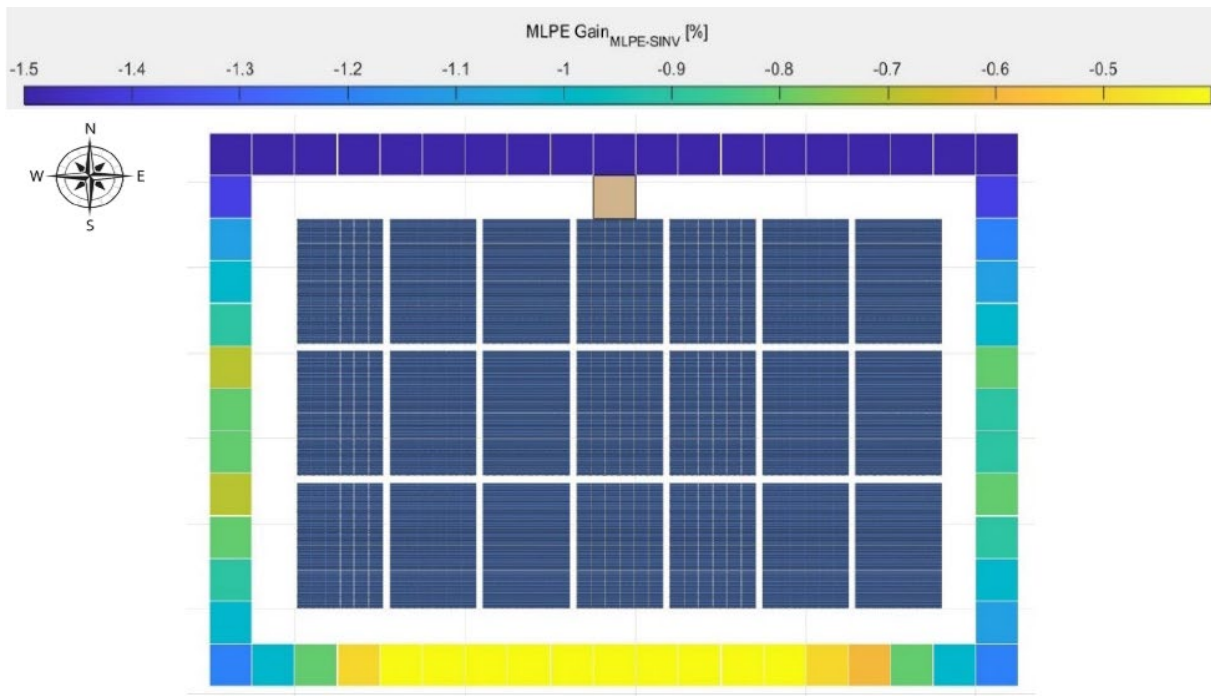


Figure 54: Sensitivity analyses of the position of the ventilation pipe to increase the gain in annual performance of allMLPE versus SINV for different positions close to the PV generator which is never beneficial so that the SINV always shows highest yield, especially if it is placed to the north of the PV modules with a 1.5% higher yield for SINV. ZHAW PVshade tool used [51].

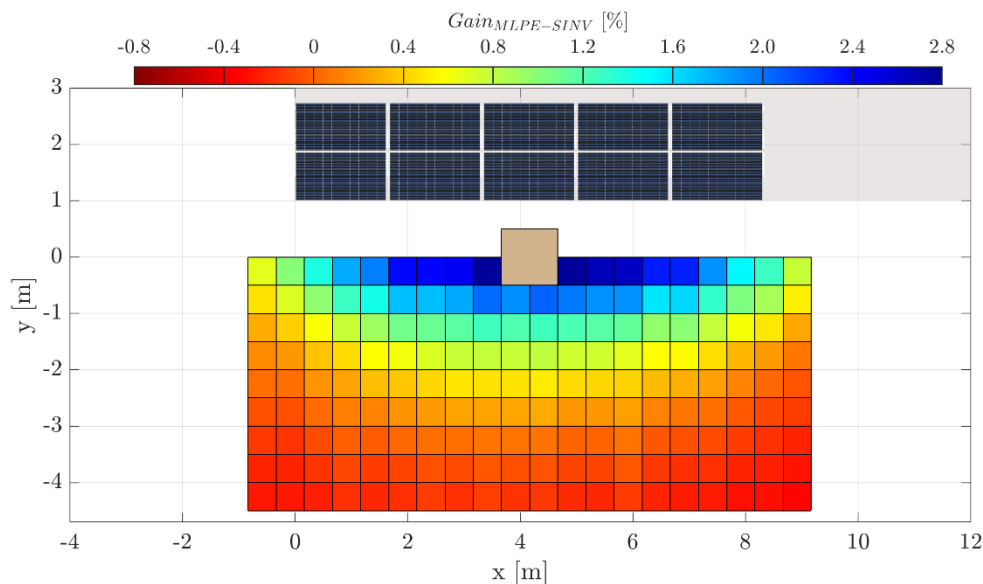


Figure 55: Sensitivity analyses of the south position of the chimney on a 30° inclined PV roof to increase the gain in annual performance of allMLPE versus SINV for different south positions in various distance to the PV generator. ZHAW PVshade tool used [16].

The following simulations of PV yield losses when shading with a dormer (see also roof top examples in Figure 14) are intended to give PV system planners a quantitative indication of how important the distance between the modules and the shading object is [49]. With a moderate spacing of 30 cm in Figure 56, the shading index is 5.3% and the conventional string inverter SINV delivers 1.8% less AC annual yield. In the SINV simulation the Huawei-SUN2000-3.68KTL-L1 was implemented.

The most efficient solution is allMLPE and 1% worse is the use of two buck converters at module numbers 2 and 5 for indMLPE for the products given below. The detailed analysis shows that the indMLPE with SAE efficiency (DC) generates less losses at the DC level, as the number of MLPEs is lower than allMLPE, but the subsequent DC/AC conversion is more efficient. The commercial product Huawei SUN2000-450W-P was used for the indMLPE and the SolarEdge P370 as allMLPE together with the SolarEdge DC/AC inverter SE3500H.

As shown in Figure 57, if the shading increases to a shading index of 8.9% due to a PV system design that does not maintain any distance between the PV module and the dormer, the ranking of the three electrical system concepts remains the same. However, the SINV now experiences twice as many losses compared to the previous case with a 30 cm distance.



	Dormer south-facing with spacing (30 cm) Shading-index 5.33%	SINV	indMLPE	aIMLPE
	AC-out [kWh]	4,383	4,421	4,465
	Loss to best case (AC)	-1.83%	-0.99%	-
	SA efficiency (AC)	94.73%	95.54%	96.49%
	SA efficiency (DC)	97.05%	97.85 %	97.75 %
	Total energy loss (to DC max.)	-5.27%	-4.46%	-3.51%

Figure 56: PV system annual performance analysis results with a dormer as a shading object consists of PV full-cell modules with a south-facing orientation and an inclination angle of 35° placed portrait at a distance of approx. 30 cm from the dormer. The simulation of the three topologies carried out by ZHAW PVshade tool. SINV: Huawei-SUN2000-3.68KTL-L1; indMLPE: same inverter together with two Huawei SUN2000-450W-P; aIMLPE: SolarEdge DC/AC inverter SE3500H together with SolarEdge P370 [49].[50]

	Dormer south-facing without spacing Shading-index 8.85%	SINV	indMLPE	aIMLPE
	AC-out [kWh]	3,813	3,871	3,957
	Loss to best case (AC)	-3.63%	-2.16%	-
	SA efficiency (AC)	92.72%	94.13%	96.21%
	SA efficiency (DC)	95.31%	96.7%	97.5%
	Total energy loss (to DC max.)	-7.28%	-5.87%	-3.79%

Figure 57: PV system annual performance analysis results with a dormer as a shading object consists of PV full-cell modules with a south-facing orientation and an inclination angle of 35° placed portrait without any distance from the dormer. The simulation of the three topologies carried out by ZHAW PVshade tool, same components as in the previous Figure [49].

	Dormer south-facing with spacing (90 cm) Shading-index 4.56%	SINV	indMLPE	aIMLPE
	AC-out [kWh]	5,120	5,152	5,192
	Loss to best case (AC)	-1.38%	-0.78%	-
	SA efficiency (AC)	95.12%	95.7%	96.46%
	SA efficiency (DC)	97.47%	98.04%	97.68%
	Total energy loss (to DC max.)	-4.88%	-4.30%	-3.54%

Figure 58: PV system annual performance analysis results with a dormer as a shading object consists of PV full-cell modules with a south-facing orientation and an inclination angle of 35° placed landscape at a distance of approx. 30 cm from the dormer. The simulation of the three topologies carried out by ZHAW PVshade tool, same components as in the previous Figure [49].



However, if the distance is increased to 90 cm, as shown in Figure 58, the shadow index drops to 4.6% and the yield disadvantage of the conventional SINV solution also shrinks to 1.4%. The shadow conditions and thus the losses also change if a roof is considered that faces east (as shown in Figure 59) and therefore less yield is to be expected from the modules with the numbers 3 and 6. In this case, the SINV solution would generate 2.9% less annual yield with a shade index of 6.3%.

When comparing Figure 56 to Figure 59, it should be noted that the number of PV modules connected in series has also been adjusted in order to achieve an attractive PV roof design. However, this also changes the losses in the power electronics components, as the SINV is dependent on the DC input voltage (Figure 18 and Figure 19) and in the DC/DC MLPE the operating point varies with the voltage ratio, optimiser input to output and the number of optimisers in the string (Figure 20 to Figure 25) [73].

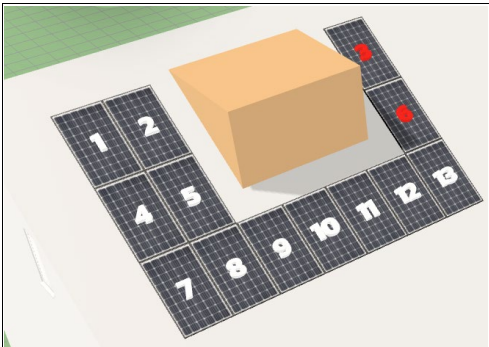
	Dormer east-facing with spacing (30 cm) Shading-index 6.25 %		
	SINV	indMLPE	allMLPE
AC-out [kWh]	3,257.3	3,324.6	3,355.4
Loss to best case (AC)	-2.93 %	-0.92 %	-
SA efficiency (AC)	93.75 %	95.69 %	96.58 %
SA efficiency (DC)	96.12 %	98.05 %	97.86 %
Total energy loss (to DC max.)	-6.25 %	-4.31 %	-3.42 %

Figure 59: PV system annual performance analysis results with a dormer as a shading object consists of PV full-cell modules with an east-facing orientation and an inclination angle of 35° placed landscape at a distance of approx. 30 cm from the dormer. The simulation of the three topologies carried out by ZHAW PVshade tool, same components as in the previous Figure [49].

ZHAW webPVshade website gives the results of annual performance simulations of different PV shading examples as shown in Figure 60 and Figure 61 [52]. Three different power electronics system variants are always calculated, each based on commercial components but using realistic loss models for MLPEs and SINV. This data corresponds very well with the special efficiency values listed in the manufacturer data sheets for the SINV but currently not yet with the sparse manufacturer data from MLPE.

Beside the total annual energy results of the three system variants also the annual performance of each module is given, to qualify the contribution of each partial shaded components (Figure 61).

These shading examples will be extended on the website with new typical shading cases and other commercial power electronics components when their exact loss factors are known over the entire operating range.

Shading-tolerant PV Modules

If the optimisation of the module positions and geometries has been exhausted, it can be advantageous to use shading-tolerant modules that have more bypass diodes, as shown in Figure 4 to Figure 6, and only render a small part of the PV module ineffective when shaded. Especially at trade fairs or in promotional videos, these new types of modules are often presented at a moment in a special shadow scenario, where they have great advantages over the standard module. How this affects the annual yield in combination with the available power electronics systems was analysed and presented in [8].

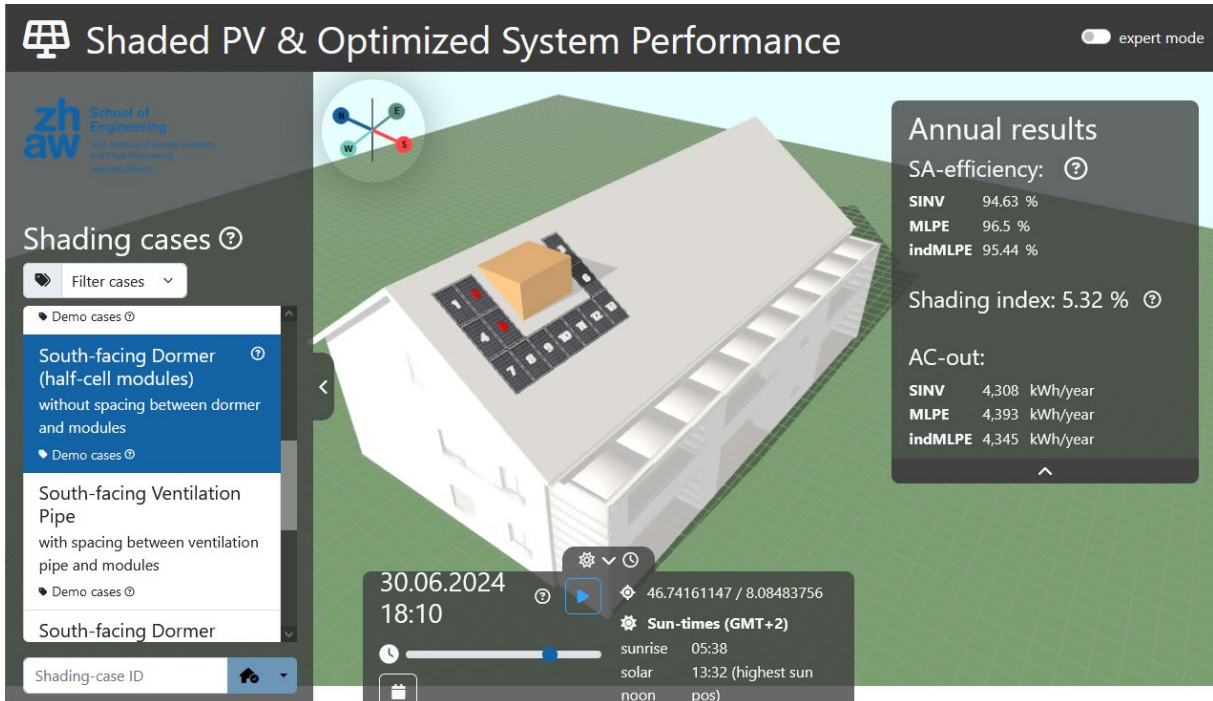


Figure 60: Public website to present selected typical shaded PV systems always with the annual performance analysis results of ZHAW PVshade and always with the three system configurations SINV, indMLPE and allMLPE with commercial product losses. The user will turn the object and is able to watch the shade hiding the PV modules for different times in the year – link <https://srv-lab-t-579.zhaw.ch/> [52].

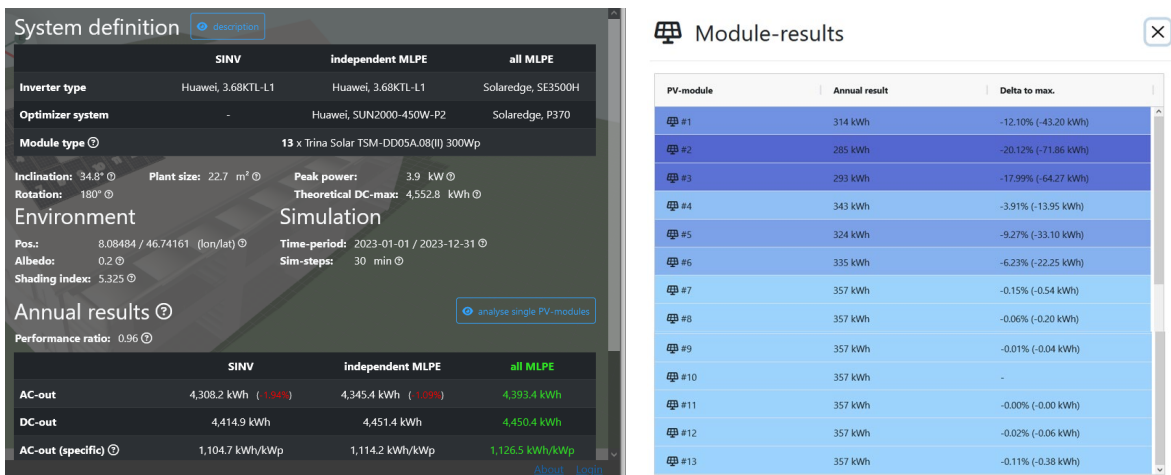
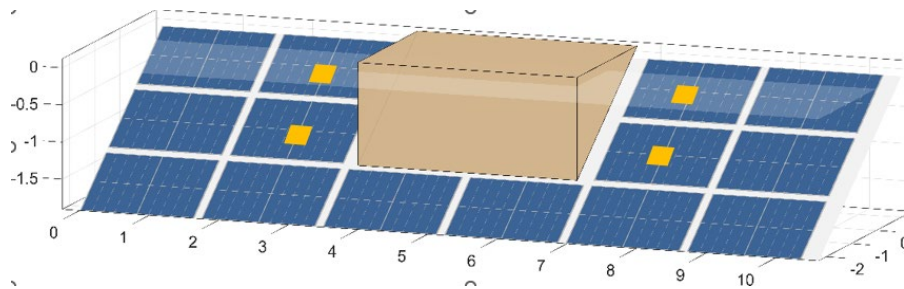
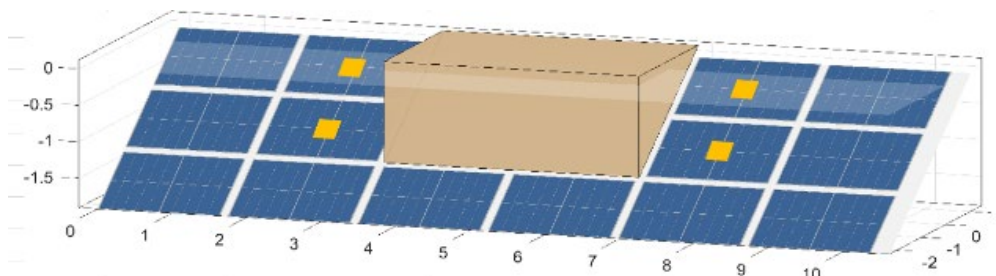


Figure 61: Public website ZHAW PVshade shows detailed information in the expert mode of the used commercial products SINV, indMLPE and allMLP and table of annual yield of the different shaded PV Modules [52].



		Full Cell PV Module	Half-cut cell PV Module	Third-cut cell PV Module	Shading-resistant 4 quadrant	Shading-resistant All Cells + Diode	
Relative Annual Energy							
Unshaded + no losses				100			%
shaded + no losses		95.2	94.4	94.6	97.3	97.1	%
SINV	Relative Energy	90.1	89.1	88.9	92.1	92.9	%
	MLPE Gain	1.0	1.1	1.4	0.6	0.3	%
indMLPE	Relative Energy	91.0	90.0	90.1	92.6	93.1	%
	MLPE Gain	1.0	1.1	1.4	0.6	0.3	%
allMLPE	Relative Energy	91.4	90.4	90.8	93.2	93.1	%
	MLPE Gain	1.5	1.5	2.1	1.2	0.3	%
Average Rel. Energy		90.8	89.8	90.0	92.6	93.0	%

Figure 62: PV simulation cases with shading tolerant PV modules (chap. 2.2) with 15 cm larger distance to dormer as next Figure which were simulated with the same meteorological data, PV modules, as well as power electronic components in ZHAW PVshade tool ([8] and [13]).



		Full Cell PV Module	Half-cut cell PV Module	Third-cut cell PV Module	Shading-resistant 4 quadrant	Shading-resistant All Cells + Diode	
Relative Annual Energy							
Unshaded + no losses				100			%
shaded + no losses		94.3	93.3	93.5	96.5	96.6	%
SINV	Relative Energy	88.4	87.4	87.1	90.8	92.3	%
	MLPE Gain	1.4	1.4	1.7	0.8	0.3	%
indMLPE	Relative Energy	90.6	88.7	88.7	91.6	92.7	%
	MLPE Gain	1.4	1.4	1.7	0.8	0.3	%
allMLPE	Relative Energy	89.6	89.4	89.7	92.5	92.7	%
	MLPE Gain	2.4	2.2	2.9	1.8	0.4	%
Average Rel. Energy		89.5	88.5	88.5	91.7	92.5	%

Figure 63: PV simulation cases with shading tolerant PV modules (chap. 2.2) for a higher shading index due to shorter distance of the modules to the dormer components are the same than the previous Figure [8, 22].

In Figure 62 the annual increase of AC yield of 2% by using shading-tolerant PV modules equipped with four bypass diodes (Figure 4) is documented using only a SINV. This more robust design does not need complex electronics on the heated roof and thus this type of PV modules could reach a higher market price. On top of that the combination of this module with an allMLPE solution will add another 1.1% or 3.1% to the full cell SINV solution without an optimiser.

It is worth noting that the module in the right-hand column, which has a bypass diode (BD) behind each solar cell (see Figure 6), does not deliver the maximum annual yield. This is because if several cells are shaded, each additional BD with its forward voltage causes losses with the module current. Fewer BD



in total per module or adding additional parallel BD per sector is more beneficial in terms of maximum annual yield.

With a higher degree of shading from Figure 62 to Figure 63, due to the smaller distance of the lateral modules to the dormer, MLPE will increase gain relative to SINV. If standard full-cell modules are used, see the left column of the annual yield using the SINV that can be increased by 2.2% using four indMLPEs. With this shading by the dormer, this is 9.4% less electricity compared to if there were no dormer, which is also noted in the table above.

Moreover, if the module is pressed very close to the side of the dormer, only the solution with MLPE can provide the maximum yield, which is then only 0.5% lower, as is the case in Figure 62 above with more lateral distance. Further noteworthy results for the PV planner have also been analysed in [8], such as the increase in yield due to an additional 14th module behind the chimney, in addition to the arrangement according to Figure 53. The annual yield increases by 1/13, i.e. by 7.6%, with a slight decrease in yield of 0.9% when kWh/kWp is considered.

7.2 Orientation and String-length Considerations

Small PV roof surfaces, which are orientated differently, are often found in typical European historic old towns, but also on larger new villas in the USA. A manufacturer of SINV power electronics favoured in 2022 shorter module strings as an alternative to MLPs for these applications and a technology development by SINV that can also efficiently convert lower string voltages [75].

As they do not have to be installed on the roof, reduced costs for service personnel on site and higher mean time between failure rates can be expected in the event of a service call.

7.3 Improvement of One-axis Tracking

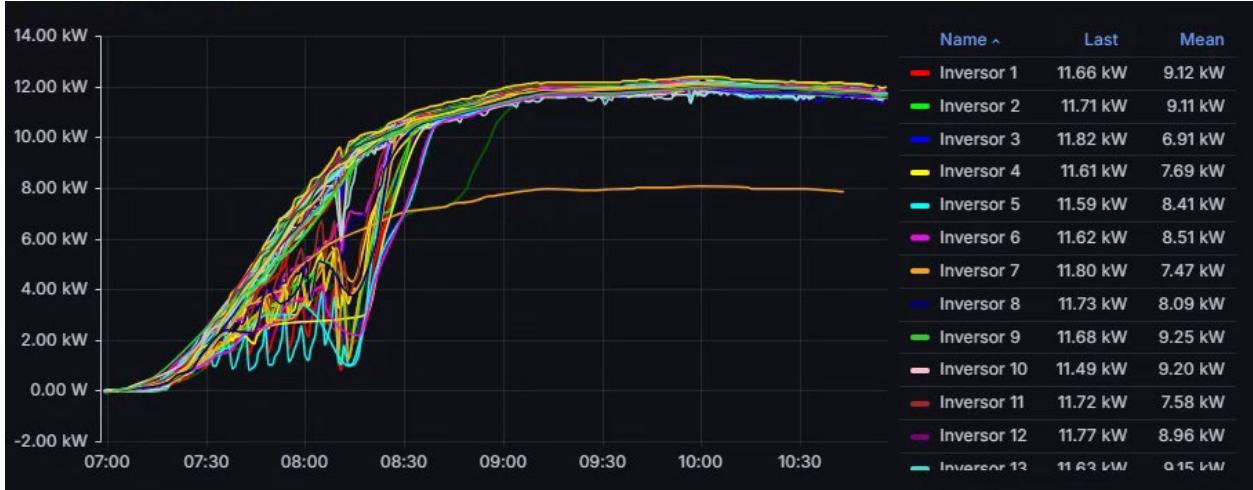
The single axis tracking 1 MW PV power plant presented in chap. 4.3 caused yield losses during mechanical tracking due to partial shading of the individual rows next to each other. Figure 63 shows the differences in the power produced by each inverter during the morning hours due to partial shading conditions. As shown, the power/energy injected by each inverter in the plant is not homogeneous, i.e., there are noticeable differences among the power/energy injected by the Refusol inverters. The inverters injecting less power/energy corresponds to the ones that are installed in the power blocks at the top of Figure 37b (32 of the total string inverters in the plant). This operating condition represents an energy loss of about 20% in the period from 7:00 to 10:30 with respect to the ideal power that Lalcktur is able to generate, considering that this phenomenon also appears during the evening hours when the sun begins to set.

Figure 65 presents the improvements in power generation achieved with the new algorithm that has optimised backtracking. As evident, now the power production of all inverters is almost the same, which indicates that the partial shading effect was removed. Accordingly, the energy production of the Lalcktur plant rose, allowing to reach plant factors of about 40% to 44%. The plant factor is defined here as the ratio of the nominal operating hours achieved to the total number of hours in a month, for example. This is a significant improvement with respect to the situation before shown in Figure 64, since with the partial shading taking place during the morning and afternoon hours with losses of approx. half of the possible power in these sixty minutes for some affected inverters.

Recently, the IEA PVPS T13 published a detailed report on the market-dominant single-axis trackers with bifacial PV modules, in which the reduction of row-to-row partial shading, e.g. through

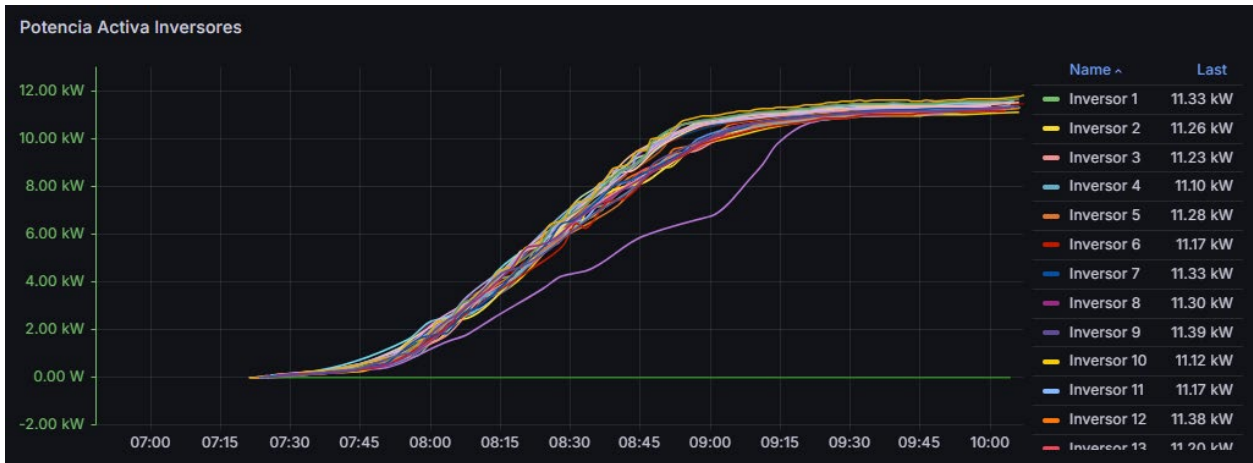


improvements to the backtracking algorithm, was discussed in detail in Chap. 2.4 [77]. **Figure 64: Ef-**



fect of partial shading in the power production of Lalcktur power plant during the morning hours.

Figure 65: Power production of Lalcktur power plant during the morning hours once the new tracking algorithm was implemented.





8 Conclusion

Since the early days of photovoltaics, simple bypass diodes have been used as a very efficient solution to the problem of different operating points when the PV generator is partially shaded. Today, these are still favoured if they are powered by conventional string inverters for the majority of PV applications when only slight to medium shading occurs.

In the literature, a few measurements have been discussed to verify the efficiency or annual yield of different power electronics systems using outdoor and indoor methods in the case of partial shading. However, an outdoor test of pole shading in Denmark powered by SINV versus MLPE clearly shows that the difference between the annual AC yield of the different system variants is not greater than 3%.

More detailed analysis of the performance of conventional SINVs by complex simulation tools, which are not yet implemented in commercial planning tools, has shown SINV to be the performance winner over MLPEs for slightly shaded PV generators, e.g. with a chimney ventilation pipe or a dormer, if the modules are not placed very close to the respective object. The reason lies in the relevant losses when an MLPE operates a module that is never shaded and there are many of them in the string dissipation PV power.

But MLPE and indMLPE systems can improve the DC/DC power of the heavily shaded PV plants, with a shading index of about 5% or more, respectively. This occurs if the modules are placed too close to the dormer or if several shading objects affect the yield of more than one module at midday, or if several modules are shaded by a neighbouring building or a large tree.

However, due to the additional losses by the conversion of the MLPE devices, the performance increase is finally thinned out for medium shaded conditions with a shading index typical below 5%. MLPEs show clear performance advantages with a few modules that are mounted in different directions, e.g. on different roof surfaces, and are too few to be able to operate the different inputs of a multi-string SINV because the string voltages are too low – see Appendix Figure 67. Nonetheless, the conditions, at which the power optimiser can improve the performance of the PV systems are limited for all PV roof markets [22].

A price comparison during the construction of the PV power plant shows that the slightly higher costs of the MLPEs compared to the simpler SINVs are compensated for if the yield advantage of the MLPEs is over 5%. However, this does not consider the possible costs of replacing an MLPE on the roof of a detached house, for example, the higher risk of the replacement itself due to the larger number of parts in series connection and the higher operating temperature on the roof, or the costs of possible fall protection for workers.

Since the additional MLPE losses can be up to 2%, depending on the number of MLPEs in the string and the resulting operating point, it is not recommended to use them for the detection of modules to recognize slightly different degradations, e.g. of the module MPP current, over many years. This is because these differences in degradation are associated with lower losses in simple series connection over the service life compared to the higher losses of the distributed DC/DC converters themselves.

As the annual yield differences of the known PV system variants SINV versus MLPE are usually around 3% or less for the majority of PV roofs on the base of professional PV modules positioning, the manufacturers of MLPE components are challenged. They must finally provide precise data on the efficiencies of their products across the entire working field, as these differences from the 99% in the data sheet can



typically amount to 2%. Even two decades ago, string inverter manufacturers took some time to make this available in the data sheets.

In the future, the market is expected to see an increase in small PV roof surfaces operated by new multi-string SINVs, which are also capable of lower DC voltages. They are therefore in the performance class between module inverters and classic SINVs and have outputs well above one kW per string, which is above the rated output of commercially available DC/DC MLPEs.

Shade-tolerant modules, also known as hotspot-free modules, are now also available on the market. Different module design solutions will prove to be efficient if they have significantly less than the typical twenty silicon solar cells per bypass diode used in standard modules today. If half-cell modules are used, as it is the standard today, the smaller cell current, provides reduced heating power in the hotspot case on small surfaces in the mm² range and thus prevents the classic hotspot case with its negative effects. These shade-tolerant modules will be a perfect symbiosis with SINV at reduced risk for replacement of several components of complex power electronics on the roof at high annual performance.

Consequently, the MLPEs should have the option to switch off the MPP operation mode to avoid hotspot operating points for this half-cell modules to be able to generate the maximum PV power over the year, without any risks of harmful hotspot effect.



REFERENCES

- [1] R. Bründlinger, N. Henze, G. Lauss and J. Liu, "Module Integrated Power Converters - A Comparison of State-Of-The-Art Concepts and Performance Test Results," in *26th European Photovoltaic Solar Energy Conference and Exhibition (EUPVSEC)*, Hamburg, 2011.
- [2] C. Deline, B. Marion, J. Granata, S. Gonzalez, A performance and economic analysis of distributed power electronics in photovoltaic systems, Technical report, National Renewable Energy Laboratory (NREL) and Sandia National Laboratories, 2011.
- [3] C. Allenspach, V. G. de Echavarri Castro, S. Richter, C. Meier, F. Carigiet, F. Baumgartner, "Module level power electronics under indoor performance tests," in *37th European Photovoltaic Solar Energy Conference and Exhibition (EUPVSEC)*, , 2020.
- [4] N. Pearsall, F. P. Baumgartner et. al, "chap. 5 - Photovoltaic (PV) balance of system components: Basics, performance," in *The Performance of Photovoltaic (PV) Systems - Modelling, Measurement and Assessment*, ISBN: 9781782423546, Woodhead Publishing, Elsevier, 2016.
- [5] Li C. Rendler, C. Reichel, M. F. Berwind, A. Heimsath, D. H. Neuhaus, "*Innovative Layouts for Utility-Scale PV Modules: Module Characteristics, Shading Tolerance, and Electricity Costs*", IEEE US PVSC June 2023
- [6] Viera, R.G. et al.. A Comprehensive Review on Bypass Diode Application on Photovoltaic Modules. *Energies* 2020, 13(10), 2472, <https://doi.org/10.3390/en13102472>
- [7] Patents on bypass devices, G. Wolff et al., 1973, US 3 952 324; R. Hollaus et. al., 1986, US 4 567 316; L. Rubin et al., 2009, WO 2009/012567 A1
- [8] F. Baumgartner, C. Allenspach, "Performance gain of shading tolerant PV modules in different electrical PV system setups" in 40st European Photovoltaic Solar Energy Conference and Exhibition (EUPVSEC), Lisbon, 2023
- [9] W.R. Baron, P.F. Virobik,. Effect of shadows on solar array output. In Proceedings of the IEEE 4th Photovoltaic Specialists Conference, Cleveland, OH, USA, 2–3 June 1964
- [10] Manufactures websites of shading tolerant PV module claiming very high yields <https://www.solaria.com/powerxt-400-solar-panels>; TSC PowerXT 365Wp, parallel cells + 4diodes; [Online: accessible in Sept. 2023]
- [11] SolarEdge Technologies Inc., Solaredge Fact Sheet, www.solaredge.com/sites/default/files/se-fact-sheet-na.pdf, [Online: accessed 15.05.2022].
- [12] C. Allenspach, F. Baumgartner, *Lab measurements of power optimiser efficiency and performance simulation*, In Proceedings of the 40th European Photovoltaic Solar Energy Conference and Exhibition (EUPVSEC), Online. WIP Renewable Energies, Lisbon, Portugal, 2023
- [13] F. Baumgartner, C. Allenspach in Chapter 3.1.4 of the IEA Report, *Performance of New Photovoltaic System Designs*, Report IEA-PVPS T13-15:2021, April 2021, ISBN 978-3-907281-04
- [14] C. Allenspach, F. Carigiet, A. Bänziger, A. Schneider, F. Baumgartner; *Power Conditioner Efficiencies and Annual Performance Analyses with Partially Shaded Photovoltaic Generators Using Indoor Measurements and Shading Simulations*; Sol. RRL 2022, 2200596



- [15] web presentation of ZHAW WebPVshade performance analyses of shaded PV plants, <https://pvshade.engineering.zhaw.ch/>; run by ZHAW School of Engineering (ZHAW), Institute of Energy systems and Fluid-Engineering (IEFE); [Online: accessible in Jan 2024].
- [16] C. Allenspach, "Performance of Power Optimiser versus String Inverter Systems," in *21st Swiss PV Conference*, Bern, Switzerland, 2023.
- [17] manufactures websites of shading tolerant PV module; ShadeStar products AE400HM6-60 product with 60 by-pass diodes, <https://www.ae-solar.com/de> [Online: accessible in Jan 2024].
- [18] Calcabrini et al., Low-breakdown-voltage solar cells for shading-tolerant photovoltaic modules, *Cell Reports Physical Science* (2022), <https://doi.org/10.1016/j.xcrp.2022.101155>; compare datasheet of commercial IBC module Neostar 3S54 using similar concepts introduced in Calcabrini publication <https://aikosolar.com/> [Online: accessible in June 2024].
- [19] F. Baumgartner, R. Vogt, C. Allenspach, F. Carigiet, *Performance of shaded PV module power electronic systems*, In Proceedings of the 38th European Photovoltaic Solar Energy Conference and Exhibition (EUPVSEC), 2021, [Online: accessible in 2021], WIP and video of the talk <https://youtu.be/NILg1MOyvWg>
- [20] E.T. Schoenholzer, S. Roth, Bulletin SEV/VSE 10/1996, page 23 – 29; as reference in Patent DE10136147B4, Hendrik Kolm et. al. applied 2001
- [21] A. Nazer, P. Manganiello and O. Isabella, A virtual bus parallel differential power processing configuration for photovoltaic applications, *Mathematics and Computers in Simulation* (2023), <https://doi.org/10.1016/j.matcom.2023.06.001>
- [22] C. Allenspach, "Module Level Power Electronics Dynamic and Static Performance in Partial Shaded Photovoltaic Systems, Master Thesis," ZHAW School of Engineering, Winterthur, Switzerland, 2022; https://digitalcollection.zhaw.ch/bitstream/11475/27358/3/2023_Allenspach_Cyril_MSc_SoE.pdf [Online: accessible in Jan 2024]
- [23] T. Eskilson, A. Jehle, P. Schmidt, M. Makoschitz and F. Baumgartner, "Identifying the potential of SiC technology for PV inverters," 2023 25th European Conference on Power Electronics and Applications (EPE'23 ECCE Europe), Aalborg, Denmark, 2023, pp. 1-7, doi: 10.23919/EPE23ECCEurope58414.2023.10264500
- [24] Data sheet of the SP-350K-H1 350kW multistring PV inverter, <https://en.si-neng.com/> [Online: accessible in June 2024].
- [25] SUN2000-150K-MG0, DC/DC conditioner MERC 1100W, detailed efficiency information is missing on the data sheet <https://support.huawei.com/>; visit at booth at Intersolar Munich, 20th June, 2024, www.intersolar.de, In their exhibition documents, they claim an annual failure rate of below 0.5% for millions of such units.
- [26] F. Lu, S. Guo, T. M. Walsh, and A. G. Aberle, "Improved PV module performance under partial shading conditions," in *Energy Procedia*, Elsevier Ltd, 2013, pp. 248–255. doi: 10.1016/j.egypro.2013.05.065.
- [27] A. Dolara, G. C. Lazaroiu, S. Leva, and G. Manzolini, "Experimental investigation of partial shading scenarios on PV (photovoltaic) modules," *Energy*, vol. 55, pp. 466–475, Jun. 2013, doi: 10.1016/j.energy.2013.04.009.
- [28] A. G. Galeano, M. Bressan, F. J. Vargas, and C. Alonso, "Shading ratio impact on photovoltaic modules and correlation with shading patterns," *Energies (Basel)*, vol. 11, no. 4, Apr. 2018, doi: 10.3390/en11040852.



- [29] Q. Li, L. Zhu, Y. Sun, L. Lu, and Y. Yang, "Performance prediction of Building Integrated Photovoltaics under no-shading, shading and masking conditions using a multi-physics model," *Energy*, vol. 213, Dec. 2020, doi: 10.1016/j.energy.2020.118795.
- [30] H. Sträter and S. Riechelmann, "An approach for a shading resistance classification of PV modules," in *8th World Conference on Photovoltaic Energy Conversion*, Milano, 2022.
- [31] Y. Sun, X. Li, R. Hong, and H. Shen, "Analysis on the Effect of Shading on the Characteristics of Large-scale on-grid PV System in China," *Energy Power Eng*, vol. 05, no. 04, pp. 215–218, 2013, doi: 10.4236/epe.2013.54b042.
- [32] IEA PVPS Task 13, "Soiling Losses – Impact on the Performance of Photovoltaic Power Plants," 2022.
- [33] A. Fairbrother *et al.*, "Long-Term Performance and Shade Detection in Building Integrated Photovoltaic Systems," *Solar RRL*, vol. 6, no. 5, May 2022, doi: 10.1002/solr.202100583.
- [34] D. Chianese and M. Caccivio, "Investigation on the main causes for reduced performances during the early stage of life of rooftop PV systems," in *37th European Photovoltaic Solar Energy Conference and Exhibition*, 2020.
- [35] F. Frontini, S. M. Bouziri, G. Corbellini, and V. Medici, "S.M.O Solution: An Innovative Design Approach to Optimize the Output of BIPV Systems Located in Dense Urban Environments," in *Energy Procedia*, Elsevier Ltd, 2016, pp. 945–953. doi: 10.1016/j.egypro.2016.06.261.
- [36] International Electrotechnical Commission (IEC) - TC 82, "IEC 61683:1999 Photovoltaic systems - Power conditioners - Procedure for measuring efficiency," IEC, Geneva, 1999.
- [37] International Electrotechnical Commission (IEC) - TC 82, "International Electrotechnical Commission - IEC 61683:1999," IEC, 2023.. Available: <https://webstore.iec.ch/publication/5720> [Online: accessible in in June 2023]
- [38] International Electrotechnical Commission (IEC) - TC 82, "IEC 62894:2014+AMD1:2016 CSV Photovoltaic inverters - Data sheet and name plate," IEC, Geneva, 2016.
- [39] International Electrotechnical Commission (IEC) - TC 82, "IEC 62891:2020 Maximum power point tracking efficiency of grid connected photovoltaic inverters," IEC, Geneva, 2020.
- [40] International Electrotechnical Commission (IEC) - TC 82, "IEC TS 63156:2021 Photovoltaic systems - Power conversion equipment performance - Energy evaluation method," IEC, Geneva, 2021.
- [41] International Electrotechnical Commission (IEC) - TC 82, "IEC TS 63106-1:2020 Simulators used for testing of photovoltaic power conversion equipment - Recommendations - Part 1: AC power simulators," IEC, Geneva, 2020.
- [42] International Electrotechnical Commission (IEC) - TC 82, "IEC TS 63106-2:2022 Simulators used for testing of photovoltaic power conversion equipment - Recommendations - Part 2: DC power simulators," IEC, Geneva, 2022.
- [43] F. P. Baumgartner, "Euro Realo Inverter Efficiency: DC-Voltage Dependency," in *20th European Photovoltaic Solar Energy Conference (EUPVSEC)*, Barcelona, 2005.
- [44] W. Bower, C. Whitaker, W. Erdman, M. Behnke and M. Fitzgerald, "Performance Test Protocol for Evaluating Inverters Used in Grid-Connected Photovoltaic Systems," Sandia National Laboratories, Endecon Engineering, BEW Engineering, Inc., Institute for Sustainable Technology, Albuquerque, 2004.



- [45] A. Mershami and J. Omoletski, "Guidelines for California's Solar Electric Incentive Programs (Senate Bill I) - 7th Edition - Chapter III: Solar Energy System Component Standards - C. Inverters," California Energy Commission (CEC), Sacramento, 2018.
- [46] C. Allenspach, F. Carigiet, A. Bänziger, A. Schneider and F. Baumgartner, "Performance Analysis of Power Optimisers by Indoor Lab Testing and Shading Simulation," in *8th World Conference on Photovoltaic Energy Conversion (WCPEC-8)*, Milano, Italy, 2022.
- [47] International Electrotechnical Commission (IEC) - TC 82, "IEC 62920:2017+AMD1:2021 CSV - Photovoltaic power generating systems - EMC requirements and test methods for power conversion equipment," IEC, Geneva, 2017.
- [48] F. Baumgartner, "Will PV optimiser lead to optimum solar output at light shading", presentation at the IEA side event in *8th World Conference on Photovoltaic Energy Conversion (WCPEC-8)*, Milano, Italy, 2022, https://www.wcpec-8.com/images/2022/-parallelevents/presentations/Franz_P_BAUMGARTNER.pdf [Online: accessible in June 2024]
- [49] A. Widler, L. Baumann, "Optimum PV System Designe with Optimiser and String Inverter, Bachelor Thesis," ZHAW School of Engineering, IEFÉ, Winterthur, Switzerland, 2024;
- [50] Wulf-Toke Franke, "The Impact of Optimisers for PV-Modules – A comparative outdoor study report", University of Southern Denmark, May 2019 https://www.sdu.dk/-/media/files/om_sdu/centre/cie/optimizer+for+pv+modules+ver11_final.pdf [Online: accessible in June 2024]
- [51] A. Bänziger, A. Schneider; Economical and technical performance analysis of photovoltaic power optimiser systems under partial shading conditions, Bachelor Thesis, ZHAW SoE, 2022; and final SFOE 2022 project report EFPVShade under contract no. SI/502247-01 2021 to 2022 <https://www.aramis.admin.ch/Default?DocumentID=71181&Load=true> [Online: accessible in June 2024]
- [52] ZHAW webPVshade website presenting simulation results of performance analyses of shaded PV systems powered by different commercial power electronic systems; <https://srv-lab-t-579.zhaw.ch/> [Online: accessible in June 2024]
- [53] S. M. Golroodbari, A. d. Waal and W. van Sark, "Improvement of Shade Resilience in Photovoltaic Modules Using Buck Converters in a Smart Module Architecture", *Energies*, vol. 11, p. p. 250, 2018.
- [54] S. M. Golroodbari, A. d. Waal and W.G.J.H.M. van Sark, "Proof of concept for a novel and smart shade resilient photovoltaic module," *IET-Renewable Power Generation*, Vols. vol. 13,, pp. 2184-2194, 2019.
- [55] K. Sinapis, C. Tzikas, G. Litjens, M. v. d. Donker, W. Folkerts, W. v. Sark and A. Smets, "A comprehensive study on partial shading response of c-Si modules and yield modeling of string inverter and module level power electronics,," *Solar Energy*, vol. 135, pp. 731-741, 2016.
- [56] A. Hanson, C. Deline, S. MacAlpine, J. Stauth and C. R. Sullivan, "Partial-Shading Assessment of Photovoltaic Installations via Module-Level Monitoring," in *40th Photovoltaic Specialist Conference (PVSC)*, Colorado, USA, 2014.
- [57] Mathworks Inc., "Products: Matlab R2022a," 2023. [Online]. Available: mathworks.com/products/matlab.html. [Accessed 05 07 2023].
- [58] F. Carigiet, *Influence of diffuse irradiation on the performance of crystalline solar cells, Master Thesis (in German)*, Winterthur: ZHAW School of Engineering, 2015.



- [59] Swiss Federal Office of Meteorology and Climatology (MeteoSwiss), "IDAwab: Data portal of ground station measurements for education and research," 2023. [Online]. Available: gate.meteoswiss.ch/idaweb/. [Accessed 01 07 2023].
- [60] P. Ineichen, R. R. Perez and e. al., "Dynamic global-to-direct irradiance conversion models", *ASHRAE transactions*, vol. 98, no. 1, pp. 354-369, 1992.
- [61] B. Müller*, L. Hardt, A. Armbruster, K. Kiefer and C. Reise, "Yield predictions for photovoltaic power plants: empirical validation, recent advances and remaining uncertainties", *Prog. Photovolt: Res. Appl.* 2016; 24:570–583, DOI: 10.1002/pip <https://www.ise.fraunhofer.de/de/geschaeftsfelder/solkraftwerke-und-integrierte-photovoltaik/photovoltaische-kraftwerke/pv-systemsimulation.html> [Online: accessible in June 2024]
- [62] C. Bucher, J. Wandel and D. Joss, "Life Expectancy of PV Inverter and Optimizers in Residential PV Systems," in *8th World Conference on Photovoltaic Energy Conversion (WCPEC-8)*, Milano, Italy, 2022.
- [63] IEA PVPS Task 13, "Quantification of Technical Risks in PV Power Systems", Report IEA-PVPS T13-23:2021; ISBN 978-3-907281-11-6
- [64] MPP tracking Shadefix from SMA described in a white paper 2021, https://files.sma.de/downloads/SHADEFIX_WHITEPAPER-de_210127.pdf [Online: accessible in June 2024]
- [65] SolarEdge, "SolarEdge Whitepaper: Brandbekämpfung in Gegenwart einer PV-Anlage - Sicherheitsrisiken und Lösungsansätze," 06 2010. [Online]. Available: https://knowledge-center.solaredge.com/sites/kc/files/fire_safety_white_paper_de.pdf. [Accessed 04 12 2023].
- [66] D. Joss, P. Wüthrich and S. Koch, "Lichtbogendetektoren in PV-Anlagen," Burgdorf, Switzerland, 2023.
- [67] D. Kroner, U. Lundgren, A. Augusto and M. Bollen, "Radiated Electromagnetic Emission from Photovoltaic Systems – Measurement Results: Inverters and Modules," *Energies*, vol. 17, p. 1893, 2024.
- [68] Elsäkerhetsverket, "SolarEdge tvingas säljstoppa optimerare," 06 12 2021. [Online]. Available: <https://www.elsakerhetsverket.se/privatpersoner/dinadelprodukter/forsaljningsforbud/solaredge-tvingas-saljstoppa-vaxelriktare/>. [Accessed 13 05 2024].
- [69] IEA PVPS Task 13, "Service Life Estimation for Photovoltaic", Modules Report IEA-PVPS T13-16:2021, June 2021. ISBN 978-3-907281-05-5.
- [70] Helioplant in Sölden Austria, solar trees in the alps, Photo Baumgartner, system concept see Jan 2014 <https://www.sonnenseite.com/> [Online: accessible in Dec 2023].
- [71] J. Quian, "Comparison of Half-Cell and Full-Cell Module Hotspot-Induced Temperature by Simulation", *IEEE JOURNAL OF PHOTOVOLTAICS*, VOL. 8, NO. 3, May 2018
- [72] S. Suarez et. al, "THERMAL ISSUES ON HALF- CELL BIFACIAL MODULES. A WAY THROUGH ALBEDO AND MISMATCH VOLTAGE", in *40st European Photovoltaic Solar Energy Conference and Exhibition (EUPVSEC)*, Lisbon, 2023; DOI 10.4229/EUPVSEC2023/3AV.3.19.
- [73] F. Baumgartner, M. Golgoodbari, C. Bucher, B. Matthew, F. Valencia, U. Jahn, "Performance of partial shaded PV generators operated by optimized power electronics review - an IEA PVPS T13 activity", in *41st European Photovoltaic Solar Energy Conference and Exhibition (EUPVSEC)*, Vienna, 2024, see also WIP publication of plenary talk 4CP.2.3 slides.



- [74] F. Baumgartner, M. Klenk, A. Widler, L. Baumann, "MPP Tracking Losses of Module Level Power Electronics at Partial Module Shading", in *41st European Photovoltaic Solar Energy Conference and Exhibition (EUPVSEC)*, Vienna, 2024, see also proceedings of paper and slides of talk 3EO.1.5
- [75] Tesla Solar Inverter Architecture White Paper NA-EN-12212022, Dec 2022;
https://digitalassets.tesla.com/tesla-contents/image/upload/Tesla_Solar_Inverter_Architecture_White_Paper_NA-EN_12212022
[Online: accessible in June 2024]
- [76] C. Olalla, D. Clement, M. Rodriguez and D. Maksimovic, "Architectures and Control of Submodule Integrated DC–DC Converters for Photovoltaic Applications," *IEEE Trans. Power Electron.*, vol. 28, p. 2980–2997, 2013.
- [77] J.S. Stein et.al, IEA Report, *Best Practices for the Optimization of Bifacial Photovoltaic Tracking Systems*, Report IEA-PVPS T13-26:2024, Aug 2024, ISBN 978-3-907281-62-8



Appendix

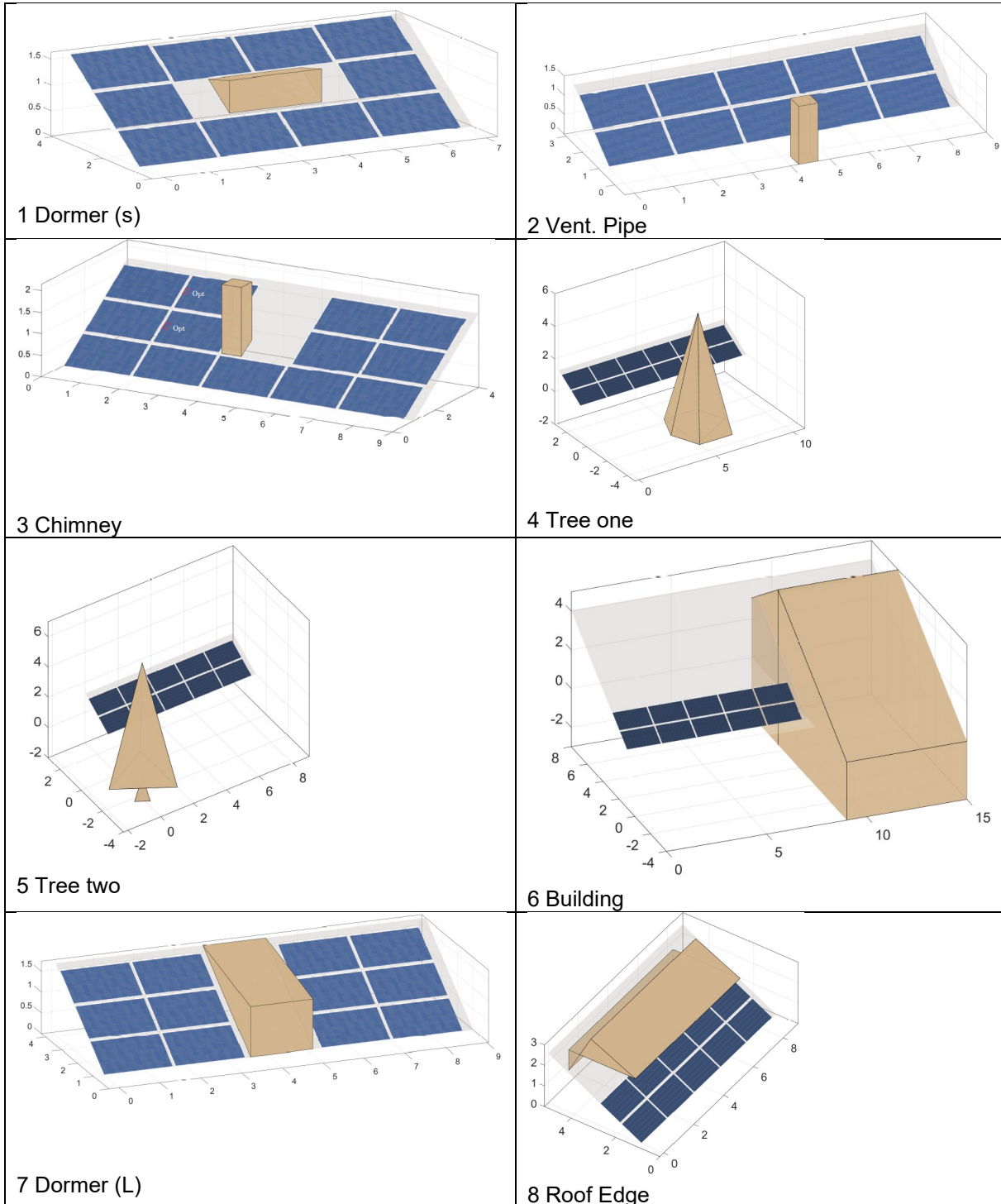


Figure 66: PV Shading cases given in Table 4 according to the proposal of an IEC standard discussion for power electronic components performance to be used in partial shaded PV plants. Dimensions in the drawings are shown in meters [22].

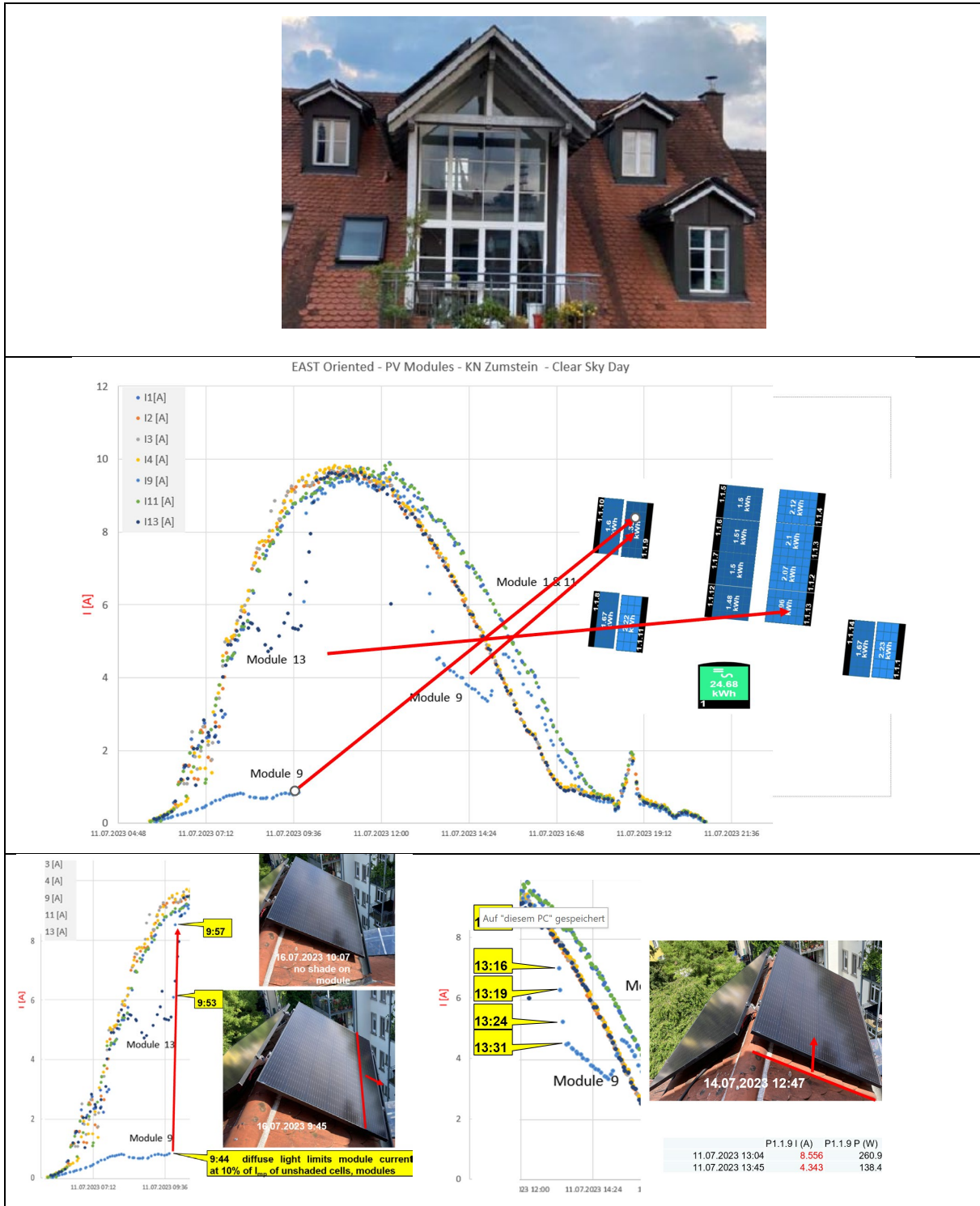


Figure 67: Typical PV rooftop installation on the lake of Constance operated with an allMLPE solution where only the four different dormers on the north side were allowed to be equipped with a total of only fourteen PV modules due to the requirements of the preservation orders of the local town [73]. The different module orientations, east and west, with a very small number of modules with the same orientation and the same shading situation favour the use of power optimisers over standard SINVs – Foto Franz Baumgartner.

